Czech Technical University in Prague
Faculty of Nuclear Sciences and Physical Engineering
Department of Physical Electronics

Modelování nelokálního transportu energie v plazmatu

Modelling of non-local energy transport in plasma

Dissertation study

Author: **Ing. Jan Nikl**
Supervisor: **Doc. Ing. Milan Kuchařík, Ph.D.**
Consultant: **Dr. Stefan Andreas Weber**
Academic year: **2020**

Prohlášení

Prohlašuji, že jsem předloženou práci vypracoval samostatně a že jsem uvedl veškerou použitou literaturu.

V Praze dne 15. června 2020 Ing. Jan Nikl

Acknowledgements

I would like to express my deep gratitude to my supervisor, Doc. M. Kuchařík, for his boundless support and countless hours spent on corrections of all my academic and scientific works. It is not an overstatement that this work would not exist in this form without him. My thanks also belong to my consultant, Dr. S. Weber, for his stimulating inputs based on his broad expertise in the field. Finally, I would like to thank my collaborator M. Holec, Ph.D. for the common work on the methods of non-local transport and bringing me to this interesting topic.

Ing. Jan Nikl

Název práce:

Modelování nelokálního transportu energie v plazmatu

Autor: Ing. Jan Nikl

Obor: Fyzikální inženýrství
Druh práce: Studie k dizertační práci

Vedoucí práce: Doc. Ing. Milan Kuchařík, Ph.D.
Konzultant: Dr. Stefan Andreas Weber

Abstrakt: Numerické modelování transportních dějů v plazmatu typicky následuje klasickou difúzní teorii. Existuje však rozpor mezi výsledky simulací a experimentálními daty v případě intezivních laserových impulzů, jelikož energetické elektrony a fotony pronikají hluboko do terče. Musí být proto tato nelokalita transportu modelována, což má zásadní důležitost pro aplikace jako je inerciální fúze, předpulzy laserů o ultravysoké intenzitě, magneticky držená fúze nebo studie teplé husté hmoty. Tato práce shrnuje podkladovou teorii a příspěvky k výzkumu tohoto komplexního jevu. Je následováno několik přístupů, jednak kinetické simulace problému v rámci Vlasov–Fokker–Planck–Maxwell modelu a stejně tak hydrodynamický model opatřený doplňujícími modely pro nelokální transport elektronového tepla a radiace. Jsou navrhnuty nové fyzikální modely a numerické metody, které jsou demonstrovány na fyzikálně relevantních simulacích.

Klíčová slova: nelokální transport, laserové plazma, kinetické modelování, Fokker–Planck, lagrangeovská hydrodynamika, transport tepla, absorpce laseru, radiační transport

Title:

Modelling of non-local energy transport in plasma

Abstract: Numerical modelling of transport processes in plasma follows the classical diffusion theory typically. However, a discrepancy between the simulation results and the experimental data exists in the case of intense laser pulses, since the energetic electrons and photons penetrate deep into the target. Hence, non-locality of the transport must be modelled, which holds a significant importance for applications like inertial fusion, prepulses of ultra-high intensity lasers, magnetic confinement fusion or warm dense matter studies. This work summarizes the background theory and contributions to the research of this complex phenomenon. Multiple approaches are followed, it is the kinetic treatment of the problem in terms of Vlasov–Fokker–Planck–Maxwell simulations as well as the hydrodynamic model equipped with additional closure models for the electron heat and radiation non-local transport. New physical models and numerical methods are proposed and demonstrated in physically relevant simulations.

Key words: non-local transport, laser plasma, kinetic modelling, Fokker–Planck, Lagrangian hydrodynamic, heat transport, laser absorption, radiation transport

Contents

1 Introduction

Plasma, the fourth state of matter, is the primordial origin of all matter, as the quark–gluon plasma dominated the early stage of the universe, and maybe its ultimate end at the same time, when becomes trapped on the accretion disk of a quasar. Plasma also accompanied our kind from its very beginning, as our civilization would not exist probably, when fire, a form of plasma, was not discovered. And it may also define its future, as it provides a nearly unlimited source of energy due to the thermonuclear fusion. Hence, its mysterious nature has attracted attention of scientists for long time.

Unless being absolutely still and homogeneous, plasma exhibits transport processes. Therefore, their understanding is a cardinal discipline of the plasma research from its beginning. Actually, it can be tracked even before its foundation to the studies of gases. It was as early as 1905, when Lorentz described the transport processes in metals in a simple collisional manner by what is hence known as the Lorentz gas [1]. Another landmark is then the formulation of the theory of gases by Chapman in 1916 [2]. However, plasma is not a neutral gas, even though it behaves like that in certain aspects. The important distinction is that long range forces are involved unlike the close encounters in a gas. A fundamental yet incomplete description was then given by Landau for the Coulombic interaction [3]. Later, the notion of dynamic friction in the astrophysical context originally was formulated by Chandrasekhar [4], but its statistical basis predetermined it to be generalized to other fields. However, the effect of electron–electron collisions was not clear and a strong belief existed that the theory of gases should be simply extended for plasma as done by Cowling [5]. The influential paper of Cohen, Spitzer and Routly then described the collisions in a consistent manner as the dynamic friction and diffusion [6]. The theory was then further improved in the work of Spitzer and Härm [7], which defines what is till today referred to as the classical diffusion theory of plasma. In the context of magnetized plasmas, it was rather the work of Braginskii [8] based on the earlier formulation of Landau, which presents the cornerstone of the description. However, the models relied only on the small anisotropy approximations, limiting their accuracy. A systematic formulation was then provided by Rosenbluth [9].

In parallel, the research of lasers started. However, it was recognized with their increasing power [10] that the diffusion theory does not reflect the phenomenon of heat flux saturation for steep gradients in plasma and the heat flux limiting technique was proposed for the numerical solution [11]. The physical findings were then confirmed by the dedicated experiments [12]. Kinetic simulations suggested that there may exist such a limitation [13, 14], but it was believed that the diffusion description can be just simply corrected. The flux limiting techniques could solve with a partial success the problem of the excessive heat flow, but they could not describe the pre-heating effect occurring on the downstream of the gradient. Empirical methods were proposed then [15], delocalizing the electron heat flux and introducing the notion of non-locality to the hydrodynamic simulations. However, the ground-shaking mathematical analysis of the problem showed that such treatment may produce severe non-physical effects [16]. From that time, various models of non-local transport have been proposed [17, 18, 19], but all possessing their own inherent advantages and disadvantages.

This defines the starting point of our research, which focuses on the phenomenon of non-local energy transport in plasma. This topic has a great importance for multiple fields of applications like the inertial fusion research [20], pre-pulse physics of ultra-high intensity lasers [21, 22, 23], magnetic confinement fusion [24] or warm dense matter research [25]. The complex nature of the non-local energy transport is given by the fact that it originates from the microscopic phenomena in the plasma, but becomes manifested on the macroscopic level. Therefore, also the numerical modelling must be reformed to reflect this multi-scale problem adequately. This text addresses several aspects of the non-local transport in the context of laser–target interaction, which cannot be attributed to the electrons solely as discussed so far, but also to the radiative transfer, where energetic photons may penetrate deep into the target. Moreover, the laser absorption methods are deeply connected to both phenomena, when an intense laser beam impinges a solid target and its power drives both effects. Finally, it is the hydrodynamic modelling which provides the vessel for integration of all mentioned methods together and simulation of plasma formation and expansion, which must be also improved to accommodate the new models and follow the shift of paradigm in the modelled detail.

The text is organized as follows. The introduction to the basic kinetic theory is given in chapter 2, which is reduced to the hydrodynamic description in chapter 3. However, the hydrodynamic model is incomplete as it misses exactly the transport processes we are mostly interested in. This is addressed by chapter 4, which reintroduces the phenomenon of heat transport, followed by chapter 5 dedicated to the radiative transfer. Finally, a brief overview of the methods for laser absorption is given in chapter 6. When the theory and the status of the current research are summarized, our contributions to the them can be put into the right context as done in chapter 7.

2 Kinetic theory

Kinetic description of plasma originates from the statistical picture, where the exact population of species is replaced by the distribution function through the averaging process. It is assumed that there exists sufficiently high number of species on every observable scale, so the statistics of such ensemble converge to the average values and the continuous description is valid. The distribution function $f_\alpha = f_\alpha(\vec{x}, \vec{v}, t)$ is then function of the phase space coordinates and describes the number of particles α in the differential volume $\mathrm{d}\vec{x}$, $\mathrm{d}\vec{v}$, where $\vec{x}$ is the spatial coordinate and $\vec{v}$ is the velocity space coordinate and t is time. Following Liouville's theorem, the total derivative $\frac{\mathrm{d}f_\alpha}{\mathrm{d}t}$ can be expanded to form the Boltzmann equation:

$$\frac{\partial f_\alpha}{\partial t} + \vec{v} \cdot \nabla_{\vec{x}} f_\alpha - \frac{\vec{F}_\alpha}{m_\alpha} \cdot \nabla_{\vec{v}} f_\alpha = \left(\frac{\partial f_\alpha}{\partial t} \right)_{\mathrm{coll}} . \tag{1}$$

The symbol $\vec{F} = F(\vec{x}, \vec{v}, t)$ represents the generalized force exerted on the α species and m_α is their mass. The term on the right-hand-side represents the collision operator, where it is assumed that the collisions involve only strongly localized transient fields. Therefore, they can be separated in the averaging process and $\vec{F}$ does not include these microscopic contributions.

In the context of plasma dynamics, the electron distribution f_e is of a significant interest as it is responsible for the most transport phenomena described in later chapters. Because its frequent occurrence in the text, the lower index is omitted henceforth. The collective behaviour of the plasma is intermediated by the macroscopic electric field $\vec{E} = \vec{E}(\vec{x}, t)$ and magnetic field $\vec{B} = \vec{B}(\vec{x}, t)$ acting on the electrons through the Lorenz force. Inserting it to (1), yields the kinetic equation:

$$\frac{\partial f}{\partial t} + \vec{v} \cdot \nabla_{\vec{x}} f - \frac{e}{m_e} (\vec{E} + \vec{v} \times \vec{B}) \cdot \nabla_{\vec{v}} f = \left(\frac{\partial f}{\partial t} \right)_{\mathrm{coll}} , \tag{2}$$

where e is the elementary charge.

The description is enclosed by the Maxwell's equations for the macroscopic fields, which are composed of Ampère's law and Faraday's law taking the following forms respectively:

$$-\frac{1}{c^2} \frac{\partial \vec{E}}{\partial t} + \nabla \times \vec{B} = \mu_0 \vec{j}, \tag{3}$$

$$\frac{\partial \vec{B}}{\partial t} + \nabla \times \vec{E} = 0. \tag{4}$$

The quantity $\vec{j} = \vec{j}(\vec{x}, t)$ is the electric current and its relation to the distribution function is defined in chapter 2.2. The symbol μ_0 represents the vacuum permeability.

2.1 Collision operator

The kinetic description cannot be complete without a particular definition of the collision operator operating on the right-hand-side of the kinetic equation (2). In the simplest case, when the plasma is ideal in the sense that the collective phenomena completely dominate over the close range interactions, it can be modelled as nearly collision-less and the collision operator is set $(\partial f/\partial)_{\text{coll}} \equiv 0$. This form of the equation is known as the Vlasov equation.

However, the collisions cannot be neglected in the applications of the primary interest here. In order to reduce complexity of the collision term, it is expanded to the BBGKY hierarchy in the number of interacting particles [26, 27]. This expansion is then truncated after the first term, i.e. the binary interaction between the species. This approximation is related to the Debye-Hückel theory of shielding, where potential of a single particle over the distances longer than the Debye length λ_{De} is effectively shielded and decays exponentially. Therefore, even in the case of long range inverse square forces like the Coulomb interaction between the particles, only the close range interaction on the distances $< \lambda_{De}$ must be modelled within the collision term and the long range interaction is intermediated by the macroscopic fields. The collisions then present local fluctuations and do not contribute to the mean values of the fields. This kind of wavelength splitting is applicable only when the electrons are weakly coupled, i.e. the kinetic energy of the species is significantly higher than the potential energy.

2.1.1 Fokker–Planck operator

In order to simplify the collision operator, several additional assumptions are made. First, the observed time scales are relatively short compared to the collision time that it takes an average particle to be deflected to the perpendicular direction. However, the number of single events is high per that time, implying that the deflection can be considered as a series of small angle collisions. It is in an agreement with the fact the plasma parameter $N_D = \frac{4\pi}{3} n_e \lambda_{De}^3 \gg 1$, so there is a high number of particles in the Debye sphere and the statistical treatment on this scale is meaningful. Moreover, the binary collisions are also elastic, conserving the relative velocity during the encounter. Finally, they can be superposed within the Debye sphere (i.e. distances $\leq \lambda_{De}$), as they are not correlated, and form a Markovian chain, where the event can be modelled by the probability ψ. In particular, the probability $\psi = \psi(\vec{v}, \Delta\vec{v})$ is introduced for the transition of the distribution function from velocity $\vec{v}$ to $\vec{v} + \Delta\vec{v}$. The distribution function then can be expressed as [28]:

$$f(\vec{x}, \vec{v}, t) = \int \psi(\vec{v} - \Delta\vec{v}, \Delta\vec{v}) f(\vec{x}, \vec{v} - \Delta\vec{v}, t - \Delta t)\, \mathrm{d}\Delta\vec{v}. \tag{5}$$

These considerations enable to expand the collision term to the Taylor series in the velocity increments. When this procedure is ceased after the second term following

the assumption on short time increment Δt, the Fokker–Planck operator is obtained:

$$\left(\frac{\partial f}{\partial t}\right)_{\text{coll}} = -\nabla_{\vec{v}} \cdot \left\{ f \left\langle \frac{\Delta \vec{v}}{\Delta t} \right\rangle \right\} + \frac{1}{2} \nabla_{\vec{v}} \nabla_{\vec{v}} : \left\{ f \left\langle \frac{\Delta \vec{v} \Delta \vec{v}}{\Delta t} \right\rangle \right\}. \tag{6}$$

The physical meaning of the terms can be identified. The first term is known as the dynamic friction and describes the slowing down process, while the second term of diffusion is responsible for spreading of the distribution function and increase of entropy. The averaged collision coefficients appearing in (6) are defined as follows [9]:

$$\left\langle \frac{\Delta \vec{v}}{\Delta t} \right\rangle = \frac{1}{\Delta t} \int \psi(\vec{v}, \Delta \vec{v}) \Delta \vec{v} \, \mathrm{d}\vec{v}, \tag{7}$$

$$\left\langle \frac{\Delta \vec{v} \Delta \vec{v}}{\Delta t} \right\rangle = \frac{1}{\Delta t} \int \psi(\vec{v}, \Delta \vec{v}) \Delta \vec{v} \Delta \vec{v} \, \mathrm{d}\Delta v. \tag{8}$$

Then, transition to the center of mass system for the colliding particles α and β is performed, where the relative velocity $\vec{g} = \vec{v}_\beta - \vec{v}_\alpha$ is introduced ($g = |\vec{g}|$). For an interaction with the differential cross-section σ, the probability is given by the volume of the collision cylinder $\psi \, \mathrm{d}\Delta \vec{v} = \Delta t f_\beta g \sigma \, \mathrm{d}\vec{v}_\beta$. Substitution to (7–8) yields [29]:

$$\left\langle \frac{\Delta \vec{v}}{\Delta t} \right\rangle = \sum_\beta \frac{m_\beta}{m_\alpha + m_\beta} \int \Delta \vec{g} g f_\beta \sigma \, \mathrm{d}\vec{v}_\beta, \tag{9}$$

$$\left\langle \frac{\Delta \vec{v} \Delta \vec{v}}{\Delta t} \right\rangle = \sum_\beta \left(\frac{m_\beta}{m_\alpha + m_\beta} \right)^2 \int \Delta \vec{g} \Delta \vec{g} g f_\beta \sigma \, \mathrm{d}\vec{v}_\beta. \tag{10}$$

The derivation is continued by insertion of the Coulomb cross-section, which takes form [28]:

$$\sigma(\chi, \theta) = \frac{b_0^2}{4 \sin^4 \frac{\chi}{2}}, \qquad b_0 = \frac{q_\alpha^2 q_\beta^2}{4 \pi \varepsilon_0 \mu_{\alpha\beta} g^2}, \qquad \mu_{\alpha\beta} = \frac{m_\alpha m_\beta}{m_\alpha + m_\beta}, \tag{11}$$

where χ is the deflection angle, θ azimuthal angle, ε_0 vacuum permittivity, q_α charge of the α species and $\mu_{\alpha\beta}$ reduced mass in the center of mass system. The integration is elaborated, while the divergence of the collision integral is overcome by limiting the impact parameter of the collisions to only the Debye length $\lambda_{D\alpha}$ following the assumptions [30]. Finally, the form with the Rosenbluth potentials are obtained after some manipulations:

$$\left\langle \frac{\Delta \vec{v}}{\Delta t} \right\rangle = \sum_\beta \frac{m_\beta}{m_\alpha + m_\beta} Y_{\alpha\beta} \nabla_{\vec{v}_\alpha} \cdot H_{\alpha\beta}, \tag{12}$$

$$\left\langle \frac{\Delta \vec{v} \Delta \vec{v}}{\Delta t} \right\rangle = \sum_\beta \left(\frac{m_\beta}{m_\alpha + m_\beta} \right)^2 Y_{\alpha\beta} \nabla_{\vec{v}_\alpha} \nabla_{\vec{v}_\alpha} : G_{\alpha\beta}, \tag{13}$$

where the potentials themselves are defined as:

$$H_{\alpha\beta} = \int f_\beta \left|\vec{v}_\alpha - \vec{v}_\beta\right|^{-1} \mathrm{d}\vec{v}_\beta, \tag{14}$$

$$G_{\alpha\beta} = \int f_\beta \left|\vec{v}_\alpha - \vec{v}_\beta\right| \mathrm{d}\vec{v}_\beta. \tag{15}$$

The name potentials stems from the fact that they satisfy the Poisson equation in the form:

$$\nabla^2_{\vec{v}} H_{\alpha\beta} = -4\pi f_\beta, \qquad \nabla^2_{\vec{v}} G_{\alpha\beta} = 2H_{\alpha\beta}. \tag{16}$$

In the previous, it is assumed that $Y_{\alpha\beta}$ is slowly spatially variable and is given by:

$$Y_{\alpha\beta} = \frac{q_\alpha^2 q_\beta^2}{4\pi\varepsilon_0^2 \mu_{\alpha\beta}^2} \ln\Lambda_{\alpha\beta}, \qquad \Lambda_{\alpha\beta} = \frac{\lambda_{D\alpha}}{b_0}, \tag{17}$$

The term $\ln\Lambda_{\alpha\beta}$ is known as the Coulomb logarithm. The relative velocity g in the definition of the impact parameter b_0 (11) is approximated by the thermal velocity of the species usually. It is worth noting that $\Lambda_{\alpha\beta} \sim N_D$, so the Coulomb logarithm attains high values in ideal plasma, where $N_D \gg 1$. This correlates again with the fact that the small angle deflections are more frequent in the plasma as it can be shown that the ratio between the contribution from subsequent small deflections a single $\pi/2$ scattering is $\sim \ln\Lambda$ [31].

The Coulomb logarithm can be interpreted as a ratio between the maximal impact parameter b_{max} and "minimal" impact parameter b_{min}. The maximum cut-off is given by the Debye length, conforming with the assumptions made. The "minimal" value is given by b_0, which can be interpreted as the impact parameter of the $\pi/2$ deflection. However, this parameter does not present a true cut-off in the physical sense. It can be viewed as a mere convenient approximation of a more exact treatment [32]. Moreover, the definition is usually modified in case of dense plasmas, where electrons undergo partial degeneracy [33]. In the first approximation, the quantum treatment of highly energetic encounters can be reduced to limiting the value by the reduced thermal de Broglie wavelength $\lambda_\hbar$ [28]. The impact parameters are then defined as:

$$b_{max} = \lambda_{De} = \sqrt{\frac{\varepsilon_0 k_B T_e}{n_e e^2}}, \qquad b_{min} = \max(b_0, \lambda_\hbar), \qquad \lambda_\hbar = \frac{\hbar}{\sqrt{m_e k_B T_e}}, \tag{18}$$

where k_B is the Boltzmann constant, $\hbar$ reduced Planck constant, n_e electron density, T_e electron kinetic temperature.

In addition to the Rosenbluth formalism used here, there exists a different approach based on the work of Landau [3], which treats the collisions as an anisotropic diffusion process in phase space. However, both formulations are equivalent and the Landau form of the operator can be derived from (6) by using the differential identity $\nabla_{\vec{v}_\alpha}\nabla_{\vec{v}_\alpha} g = \underline{\underline{I}}/g - \vec{g}\vec{g}/g^3$, where $\underline{\underline{I}}$ is the identity tensor. After some manipulations, the

Landau form of the Fokker–Planck operator is obtained:

$$\left(\frac{\partial f_\alpha}{\partial t}\right)_{coll} = \sum_\beta \frac{1}{2} Y_{\alpha\beta} \frac{\mu_{\alpha\beta}^2}{m_\alpha} \nabla_{\vec{v}_\alpha} \cdot \int \frac{g^2 \underline{\underline{I}} - \vec{g}\vec{g}}{g^3} \cdot \left(\nabla_{\vec{v}_\alpha} \frac{f_\alpha}{m_\alpha} f_\beta - f_\alpha \nabla_{\vec{v}_\beta} \frac{f_\beta}{m_\beta}\right) \mathrm{d}\vec{v}_\beta. \tag{19}$$

The operator holds many convenient properties like full symmetry of the integral part in the index of the species and other, which are further explored in the subsequent chapters.

It is also of an interest to investigate the limit $m_\alpha \ll m_\beta$, which will be the case for the electron–ion scattering for example. Under these conditions, the second term in the Fokker–Planck–Landau operator (19) can be neglected compared to the first one. Furthermore, approximation of the relative velocities as $\vec{g} \approx \vec{v}_\alpha$ for nearly static scatterers yields the simplified form of the operator:

$$\left(\frac{\partial f_\alpha}{\partial t}\right)_{coll} = \sum_\beta \frac{1}{2} Y_{\alpha\beta} \frac{\mu_{\alpha\beta}^2}{m_\alpha^2} n_\beta \nabla_{\vec{v}_\alpha} \cdot \left(\frac{\vec{v}_\alpha^2 \underline{\underline{I}} - \vec{v}_\alpha \vec{v}_\alpha}{v_\alpha^3} \cdot \nabla_{\vec{v}_\alpha} f_\alpha\right), \tag{20}$$

where $n_\beta = \int f_\beta \, \mathrm{d}\vec{v}_\beta$ is the density of the β species.

2.1.2 Bhatnagar–Gross–Krook operator

The Fokker-Planck operator presented in chapter 2.1.1 has inherently non-linear structure. Its numerical solution is demanding consequently. However, when the physical system is close to the collisional equilibrium, even only a linearized form can be sufficient for the description of the relaxation processes. A linear operator of this kind was constructed by Bhatnagar, Gross and Krook [34]. It can be written as:

$$\left(\frac{\partial f_\alpha}{\partial t}\right)_{coll} = -\sum_\beta \nu_{\alpha\beta}(f_\alpha - f_{\beta 0}), \tag{21}$$

where $\nu_{\alpha\beta}$ is the collision frequency between α and β species. This kind of operator is called empirical, as the a priori known equilibrium distribution functions $f_{\alpha 0}$ for a single specie plasma appear in the definition. In addition, an apparent drawback of this approach is violation of the conservation laws. Unless the collision frequency is independent of velocity, it does not conserve neither of mass, momentum nor energy [35]. On the other hand, convergence to the equilibrium is guaranteed and the distribution function remains positive.

This can be compared to the Fokker–Planck operator from chapter 2.1.1, which conserves all three mentioned collisional invariants as shown in chapter 2.2. Moreover, it satisfies the H-theorem, so the entropy $S = -\int f \log f \, \mathrm{d}\vec{v}$ increases in time. In order to prove this, (19) is simplified to the single specie case and rewritten as:

$$\left(\frac{\partial f_\alpha}{\partial t}\right)_{coll} \sim \nabla \cdot \int \frac{g^2 \underline{\underline{I}} - \vec{g}\vec{g}}{g^3} \cdot f f' \left(\nabla \log f - \nabla' \log f'\right) \mathrm{d}\vec{v}', \tag{22}$$

where $f' = f(\vec{x}, \vec{v}', t)$ and ∇' is the velocity derivative with respect to $\vec{v}'$ analogously.

The Fokker–Planck–Landau operator in this form is multiplied by $-(1+\log f)$ and integrated to obtain:

$$\frac{\partial S}{\partial t} \sim \int\int f f' \frac{g^2 \underline{\underline{I}} - \vec{g}\vec{g}}{g^3} : \left(\nabla \log f - \nabla' \log f'\right) \left(\nabla \log f - \nabla' \log f'\right) \mathrm{d}\vec{v}\, \mathrm{d}\vec{v}', \tag{23}$$

where Green's theorem was applied, assuming that f vanishes when $|\vec{v}| \to \infty$, and symmetry of the inner part of the operator was utilized. Due to symmetry and positivity of the expression for any $f > 0$, it can be concluded that $\partial S/\partial t \geq 0$ and a unique maximum exists. The maximum of entropy is attained when the distribution function reaches the Maxwell–Boltzmann distribution, which takes the following form for electrons:

$$f_M(\vec{x}, \vec{v}, t) = f_M(n_e, \vec{u}, T_e, \vec{v}) = n_e \left(\frac{m_e}{2\pi k_B T_e}\right)^{3/2} \exp\left(\frac{m_e |\vec{v} - \vec{u}|^2}{2 k_B T_e}\right), \tag{24}$$

where $\vec{u}$ is the mean velocity. This provides the sought equilibrium solution, as it also zeros the collision operator itself. This function is then inserted to the Bhatnagar–Gross–Krook (BGK) operator (21) usually [34].

As a final remark, it should be noted that a conserving form of the BGK operator exists, where the parameters of density and temperature are unknown functions [36]. In order to determine them, a system of coupled integral equation must be solved, so the method its convenient tractability.

2.2 Velocity moments

The kinetic description of plasma presented so far used functions defined in the phase space. However, macroscopic measurable quantities like electron density or electric current appear in the configuration space only. The link between the two is provided by the velocity moments of the distribution function.

Proceeding further, elastic binary collisions are considered following chapter 2.1. Under these conditions, mass, momentum and energy are conserved during the scattering event. In particular, they present special cases of summation invariants. In other words, the sum of the quantities before and after (denoted by prime) the collision is equal:

$$\phi_\alpha + \phi_\beta = \phi'_\alpha + \phi'_\beta, \tag{25}$$

where $\phi_\alpha \in \{m_\alpha, m_\alpha \vec{v}_\alpha, \frac{1}{2} m_\alpha |\vec{v}_\alpha|^2\}$.

The conservation properties for a continuous collision operator can be proved as well. Restricting ourself to the single specie case again, the Fokker–Planck–Landau operator in the form (22) is taken and multiplied by one of the summation invariants ϕ, which we consider as functions of velocity now. Integration over the velocity space is performed and the expression is rearranged in a similar manner to (23) to obtain:

$$\int \phi \left(\frac{\partial f_\alpha}{\partial t}\right)_{coll} \mathrm{d}\vec{v} \sim \int\int \left(\nabla\phi - \nabla'\phi'\right) \cdot \frac{g^2 \underline{\underline{I}} - \vec{g}\vec{g}}{g^3} . f f' \left(\nabla \log f - \nabla' \log f'\right) \mathrm{d}\vec{v}\, \mathrm{d}\vec{v}'. \tag{26}$$

This formulation shows that mass, momentum and energy are collisional invariants of the Fokker–Planck operator or any linear combination of 1, $\vec{v}$ and $|\vec{v}|^2$ is conserved more generally. Note that the property of the central tensor was used here, that its product with a vector collinear with $\vec{g}$ is zero.

The governing equations for the velocity moments of the distribution function are obtained using the mean value operator defined as follows for functions $X = X(\vec{v})$:

$$\langle X \rangle_\alpha = \frac{\int X(\vec{v}_\alpha) f_\alpha(\vec{v}_\alpha) \, \mathrm{d}\vec{v}_\alpha}{\int f_\alpha(\vec{v}_\alpha) \, \mathrm{d}\vec{v}_\alpha}. \tag{27}$$

Multiplication of the kinetic equation (1) by ϕ_α and integration over the velocity space yields the moment equation:

$$\frac{\partial}{\partial t} \langle n_\alpha \phi_\alpha \rangle_\alpha + \nabla_{\vec{x}} \cdot \langle n_\alpha \vec{v}_\alpha \phi_\alpha \rangle_\alpha - \frac{q_\alpha}{m_\alpha} \langle n_\alpha (\vec{E} + \vec{v}_\alpha \times \vec{B}) \cdot \nabla_{\vec{v}} \phi_\alpha \rangle_\alpha = \int \phi_\alpha \sum_{\beta \neq \alpha} \left(\tfrac{\partial f_\alpha}{\partial t} \right)_{coll}^{\beta} \mathrm{d}\vec{v}_\alpha, \tag{28}$$

where the Lorenz force was inserted. The collision operator on the right-hand-side is expanded to the contributions from different species, where the contribution from the identical species α vanishes, since ϕ_α are collisional invariants. Due to the symmetry of the Fokker–Planck operator (19), it can be recognized that the sum of the kinetic equations gives on the right-hand-side:

$$\int \sum_\alpha \sum_\beta \phi_\alpha \left(\frac{\partial f_\alpha}{\partial t} \right)_{coll}^{\beta} \mathrm{d}\vec{v}_\alpha = 0, \tag{29}$$

so the total mass, momentum and energy are conserved by collisions.

2.2.1 Mass equation

The first invariant $\phi_\alpha = m_\alpha$ represents the zeroth velocity moment of the kinetic equation. Insertion of ϕ_α to the moment equation (28) yields:

$$\frac{\partial}{\partial t} (m_\alpha n_\alpha) + \nabla \cdot (m_\alpha n_\alpha \vec{u}_\alpha) = 0, \tag{30}$$

where we restricted ourselves only to the single specie case, so the collisional contributions to the equation are zero due to the collisional invariance and this simplification is applied even for other velocity moments for brevity.

In the previous, the definitions of the integral and mean quantities of the particle density and mean velocity were used respectively:

$$n_\alpha = \int f_\alpha \, \mathrm{d}\vec{v}, \qquad \vec{u}_\alpha = \langle \vec{v}_\alpha \rangle_\alpha = \frac{1}{n_e} \int \vec{v} f_\alpha \, \mathrm{d}\vec{v}. \tag{31}$$

It can be recognized from the form of (30) that it represents the law of mass conservation, since integration over the whole volume Ω of the configuration space

yields:

$$\frac{\mathrm{d}M_\alpha}{\mathrm{d}t} = -\oint_\Gamma \rho_\alpha \vec{u}_\alpha \cdot \vec{n}\,\mathrm{d}\Gamma, \tag{32}$$

where $\rho_\alpha = m_\alpha n_\alpha$ is the mass density, $M_\alpha = \int_\Omega \rho_\alpha \,\mathrm{d}\vec{x}$ the total mass and $\vec{n}$ the outer unit normal defined on the boundary $\Gamma = \partial\Omega$. Provided that the system is closed, i.e. there is no exchange of particles over the boundaries, the total mass is conserved.

A closely related phenomenon to the mass conservation is the law of charge conservation. Taking divergence of the Ampère's law (3) and Faraday's law (4) yields:

$$\frac{\partial}{\partial t}\nabla \cdot \vec{E} = -\frac{1}{\varepsilon_0}\nabla \cdot \vec{j}_\alpha, \tag{33}$$

$$\frac{\partial}{\partial t}\nabla \cdot \vec{B} = 0, \tag{34}$$

where $\vec{j}_\alpha = q_\alpha n_\alpha u_\alpha$ is the electric current. Assume that Gauss's law for the electric field and magnetic field holds at the beginning of the reference time in the form:

$$\nabla \cdot \vec{E} = \frac{\rho_\alpha^q}{\varepsilon_0}, \qquad \nabla \cdot \vec{B} = 0, \tag{35}$$

where the charge density is defined as $\rho_\alpha^q = q_\alpha n_\alpha$. Substitution back to (33) and (34) yields the law of non-existence of magnetic monopoles and continuity equation for electric charge:

$$\frac{\partial}{\partial t}\rho_\alpha^q + \nabla \cdot \vec{j}_\alpha = 0. \tag{36}$$

Similarly to (32), the total charge $Q_\alpha = \int_\Omega q_\alpha n_e \,\mathrm{d}\vec{x}$ is conserved when the electric currents through boundaries are zero. Therefore, the electrodynamic theory behaves consistently with the kinetic theory for the collisional invariant $\phi_\alpha = q_\alpha$.

2.2.2 Momentum equation

The first velocity moment of the kinetic equation (1) governs the momentum $\rho_\alpha \vec{u}_\alpha$. It is obtained from (28) by choosing the invariant $\phi_\alpha = m_\alpha \vec{v}_\alpha$:

$$\frac{\partial}{\partial t}\left(\rho_\alpha \vec{u}_\alpha\right) + \nabla \cdot \left(\rho_\alpha \vec{u}_\alpha \vec{u}_\alpha + \rho_\alpha \langle \vec{w}\vec{w}\rangle\right) = \rho_\alpha^q \vec{E} + \vec{j}_\alpha \times \vec{B}, \tag{37}$$

where $\vec{w} = \vec{v}_\alpha - \vec{u}_\alpha$ is the chaotic part of the velocity. The two components of the stress tensor appearing in the divergence can be identified as the dynamic pressure and kinetic pressure:

$$\underline{\underline{D}}^\alpha = \rho_\alpha \vec{u}_\alpha \vec{u}_\alpha = m_\alpha \int \vec{u}_\alpha \vec{u}_\alpha f_\alpha \,\mathrm{d}\vec{v}, \tag{38}$$

$$\underline{\underline{P}}^\alpha = \rho_\alpha \langle \vec{w}\vec{w}\rangle_\alpha = m_\alpha \int (\vec{v} - \vec{u}_\alpha)(\vec{v} - \vec{u}_\alpha) f_\alpha \,\mathrm{d}\vec{v}, \tag{39}$$

Similarly to the continuity equation (30), the integral over the domain give rise

to the law of momentum conservation:

$$\frac{\mathrm{d}\vec{P}_\alpha}{\mathrm{d}t} = -\oint_\Gamma (\underline{\underline{D}}^\alpha + \underline{\underline{P}}^\alpha)\cdot\vec{n}\,\mathrm{d}\Gamma + \int_\Omega \rho_\alpha^q\vec{E} + \vec{j}_\alpha\times\vec{B}\,\mathrm{d}\vec{x}, \tag{40}$$

where the total momentum of α species is defined as $\vec{P}_\alpha = \int_\Omega \rho_\alpha\vec{u}_\alpha\,\mathrm{d}\vec{x}$. The contribution to the boundary integral from $\underline{\underline{D}}^\alpha$ is zero, when the system is closed, since $\vec{u}_\alpha\cdot\vec{n} = 0$. The pressure part can be interpreted as the macroscopic normal and tangential forces acting at the boundary and becomes zero for an isolated system. However, the Lorenz force action do not vanish in general, since the momentum is exchanged with the fields as illustrated further.

The field counterpart of the momentum equation is obtained by vector multiplication of (3) and (4) by $\vec{B}$ and $\vec{E}$ respectively:

$$\frac{\partial\vec{E}}{\partial t}\times\vec{B} - c^2(\nabla\times\vec{B})\times\vec{B} = -\frac{1}{\varepsilon_0}\vec{j}\times\vec{B}, \tag{41}$$

$$\vec{E}\times\frac{\partial\vec{B}}{\partial t} + (\nabla\times\vec{E})\times\vec{E} = 0. \tag{42}$$

The antisymmetric products are reduced to a symmetric tensor through the differential identity:

$$(\nabla\times\vec{A})\times\vec{A} = (\vec{A}\nabla)\vec{A} - \frac{1}{2}\nabla|\vec{A}|^2 = \nabla\cdot\left(\vec{A}\vec{A} - \frac{1}{2}|\vec{A}|^2\underline{\underline{I}}\right) - (\nabla\cdot\vec{A})\vec{A}. \tag{43}$$

When applied to the system (41–42) considering the Gauss's law (35), the sum of the equations results in the equation of electromagnetic momentum:

$$\frac{\partial}{\partial t}\vec{\gamma}_{EM} - \nabla\cdot\left(\underline{\underline{T}}^E + \underline{\underline{T}}^B\right) = -\rho_\alpha^q\vec{E} - \vec{j}_\alpha\times\vec{B}, \tag{44}$$

where $\vec{\gamma}_{EM} = \varepsilon_0^{-1}\vec{E}\times\vec{B}$ is the electromagnetic momentum vector and $\underline{\underline{T}}^E$,$\underline{\underline{T}}^B$ are the electric and magnetic parts of the Maxwell's stress tensor:

$$\underline{\underline{T}}^E = \varepsilon_0\left(\vec{E}\vec{E} - \frac{1}{2}|\vec{E}|^2\underline{\underline{I}}\right), \qquad \underline{\underline{T}}^B = \mu_0^{-1}\left(\vec{B}\vec{B} - \frac{1}{2}|\vec{B}|^2\underline{\underline{I}}\right). \tag{45}$$

Integration of (44) over the configuration space yields the law of electrodynamic momentum conservation:

$$\frac{\mathrm{d}\vec{P}_{EM}}{\mathrm{d}t} = \oint_\Gamma (\underline{\underline{T}}^E + \underline{\underline{T}}^B)\cdot\vec{n}\,\mathrm{d}\Gamma - \int_\Omega \rho_\alpha^q\vec{E} + \vec{j}_\alpha\times\vec{B}\,\mathrm{d}\vec{x}. \tag{46}$$

The boundary term is obviously zero for the normal components of the fields and the second term is again the interaction part or the action of Lorentz force in other words, which appeared in (40). Together, they give the sought law of total momentum conservation for $\vec{P}_\alpha + \vec{\gamma}_{EM}$.

2.2.3 Energy equation

The last, but not least, collisional invariant is the kinetic energy $\phi_\alpha = \frac{1}{2} m_e |\vec{v}|^2$ and the corresponding second velocity moment of the kinetic equation (1). Insertion to the moment equation (28) yields:

$$\frac{\partial}{\partial t}\left(\frac{1}{2}\rho_\alpha u_\alpha^2 + \frac{1}{2}\rho_\alpha \langle w_\alpha^2 \rangle_\alpha\right) + \nabla \cdot \rho_\alpha \left(\frac{1}{2} u_\alpha^2 \vec{u}_\alpha + \frac{1}{2}\langle w^2 \rangle_\alpha \vec{u}_\alpha + \right.$$
$$\left. + \langle \vec{w}_\alpha \vec{w}_\alpha \rangle_\alpha + \frac{1}{2}\langle w_\alpha^2 \vec{w}_\alpha \rangle_\alpha\right) = \vec{j}_\alpha \cdot \vec{E}, \quad (47)$$

where identification with the kinetic pressure tensor (39), kinetic energy density $\epsilon_\alpha^k = 1/2 \rho_\alpha u_\alpha^2$, internal energy density ϵ_α^i and heat flux $\vec{q}_\alpha$ can be made. The latter are defined as:

$$\epsilon_\alpha^i = \frac{1}{2}\rho_\alpha \langle w_\alpha^2 \rangle_\alpha = \frac{1}{2} m_\alpha \int |\vec{v} - \vec{u}_\alpha|^2 f_\alpha \, \mathrm{d}\vec{v}, \quad (48)$$

$$\vec{q}_\alpha = \frac{1}{2}\rho_\alpha \langle w_\alpha^2 \vec{w}_\alpha \rangle_\alpha = \frac{1}{2} m_\alpha \int |\vec{v} - \vec{u}_\alpha|^2 (\vec{v} - \vec{u}_\alpha) f_\alpha \, \mathrm{d}\vec{v}. \quad (49)$$

After the substitution, the equation of energy reads:

$$\frac{\partial}{\partial t}\left(\epsilon_\alpha^k + \epsilon_\alpha^i\right) + \nabla \cdot \left(\epsilon_\alpha^k \vec{u}_\alpha + \epsilon_\alpha^i \vec{u}_\alpha + \underline{\underline{P}}^\alpha \cdot \vec{u}_\alpha + \vec{q}_\alpha\right) = \vec{j}_\alpha \cdot \vec{E}. \quad (50)$$

Integration of (50) over space provides the law of energy conservation for the total energy of α species $E_\alpha = \int_\Omega \epsilon_\alpha^k + \epsilon_\alpha^i \, \mathrm{d}\vec{x}$, which takes the form:

$$\frac{\mathrm{d}E_\alpha}{\mathrm{d}t} = -\oint_\Gamma \left((\epsilon_\alpha^i + \epsilon_\alpha^k)\vec{u}_\alpha \cdot \vec{n} + \underline{\underline{P}}^\alpha : \vec{u}_\alpha \vec{n} + \vec{q}_\alpha \cdot \vec{n}\right) \mathrm{d}\Gamma + \int_\Omega \vec{j}_\alpha \cdot \vec{E} \, \mathrm{d}\vec{x}. \quad (51)$$

The first boundary term is convective and is zero when there is no mass flow over the boundaries. The pressure part describes the action of the boundary forces and becomes zero together with the normal heat flux for an isolated system. The last part describes the total amount of Joule heating, which presents an interaction term between the α particles and electromagnetic fields.

The field counterpart of the energy equation is obtained from (3) and (4) when multiplied by $\vec{E}$ and $\vec{B}$ respectively. The system then takes the form:

$$\frac{1}{2}\frac{\partial}{\partial t}|\vec{E}|^2 - c^2 \nabla \times \vec{B} \cdot \vec{E} = -\frac{1}{\varepsilon_0}\vec{j}_\alpha \cdot \vec{E}, \quad (52)$$

$$\frac{1}{2}\frac{\partial}{\partial t}|\vec{B}|^2 + \nabla \times \vec{E} \cdot \vec{B} = 0. \quad (53)$$

A linear combination of the equation then gives the energy equation for electromagnetic field after some manipulations:

$$\frac{\partial}{\partial t}\epsilon_{EM} + \nabla \cdot \vec{S} = \vec{j}_\alpha \cdot \vec{E}, \quad (54)$$

where the density of electromagnetic energy and Poynting vector are defined as follows:

$$\epsilon_{EM} = \frac{1}{2}\varepsilon_0|\vec{E}|^2 + \frac{1}{2}\mu_0^{-1}|\vec{B}|^2, \qquad \vec{S} = -\mu_0^{-1}\vec{E}\times\vec{B}. \tag{55}$$

The law of electromagnetic energy conservation can be derived from (54) by integration over space:

$$\frac{\mathrm{d}E_{EM}}{\mathrm{d}t} = -\oint_\Gamma \vec{S}\cdot\vec{n}\,\mathrm{d}\Gamma - \int_\Omega \vec{j_\alpha}\cdot\vec{E}\,\mathrm{d}\vec{x}. \tag{56}$$

Provided that the Poynting vector $\vec{S}$ is zero at the boundary, the electromagnetic energy is conserved except the action on particles through the Joule heating term $\vec{j_\alpha}\cdot\vec{E}$. However, comparison of (56) with (51) reveals that the total energy $E_\alpha + E_{EM}$ is conserved.

2.3 Cartesian tensor expansion

The kinetic theory described the distribution function $f = f(\vec{x},\vec{v},t)$ in 7 dimensions of the phase space essentially. Consequently, solution of the kinetic equation (1) is cumbersome, when a non-linear collision operator like the one presented in chapter 2.1.1 is applied especially. For this reason, it is desirable to expand the distribution function and solve only a finite set of equations in a lower number of dimensions. Expansions in spherical harmonics or Cartesian tensors belong to the most frequently used. The rationale of this choice can be seen in the fact that spherical harmonics present eigenvectors of the diffusion operator, greatly simplifying the structure of the Fokker–Planck collision operator. Moreover, the Maxwell–Boltzmann distribution (24) is modelled by the zeroth mode already and higher modes present only anisotropic corrections to it. Alternatively, an expansion in Cartesian tensors can be made, which is also pursued here, but the two approaches are formally equivalent [37].

In the following, the distribution function f is expanded in Cartesian tensors as:

$$f(\vec{x},\vec{v},t) = f(\vec{x},\vec{n},v,t) = f_0(\vec{x},v,t) + \vec{f_1}(\vec{x},v,t)\cdot\vec{n} + \underline{\underline{f_2}}(\vec{x},v,t) : \vec{n}\vec{n} + \ldots, \tag{57}$$

where $v = |\vec{v}|$ and $\vec{n} = \vec{v}/v$. The term f_0 is the isotropic part of the distribution function, $\vec{f_1}$ the first order tensor (i.e. vector) anisotropic correction and $\underline{\underline{f}}_2$ is the second order tensor anisotropic correction, etc. Note that the series is infinite, but it is truncated after several terms typically, as mainly electron–ion collisions isotropize the electron distribution function due to the high mass ratio of the species, which leads to a high momentum exchange during an encounter. However, the energy exchange is significantly slower due to this ratio, so rather the direction of momentum is affected. In a typical collisional plasma, the ordering $f_0 \gg |\vec{f_1}| \gg |\vec{f_2}|$ holds consequently.

The velocity moments of the distribution function, which were defined in chapter

2.2, then take the form:

$$n_e = 4\pi \int_0^{+\infty} f_0 v^2 \,\mathrm{d}v, \qquad \vec{u}_e = \frac{1}{n_e}\frac{4\pi}{3}\int_0^{+\infty} \vec{f}_1 v^3 \,\mathrm{d}v, \tag{58}$$

$$\epsilon_e^T = \frac{1}{2} m_e 4\pi \int_0^{+\infty} f_0 v^4 \,\mathrm{d}v, \qquad \vec{q}_e^T = \frac{1}{2} m_e \frac{4\pi}{3}\int_0^{+\infty} \vec{f}_1 v^5 \,\mathrm{d}v, \tag{59}$$

while the pressure tensors are obtained in the form:

$$\underline{\underline{D}}^e + \underline{\underline{P}}^e = \frac{4\pi}{3} m_e \left(\int_0^{+\infty} f_0 v^4 \,\mathrm{d}v \right) \underline{\underline{I}} + \frac{8\pi}{15} m_e \int_0^{+\infty} \underline{\underline{f_2}} v^4 \,\mathrm{d}v. \tag{60}$$

I must be noted that ϵ_e^T and $\vec{q}_e^T$ are rather the total quantities related to (48), (49) by the following relations:

$$\epsilon_e^T = \epsilon_e^k + \epsilon_e^i, \qquad \vec{q}_e^T = \vec{q}_e + \epsilon_e^T \vec{u}_e + \underline{\underline{P}}^e \cdot \vec{u}_e. \tag{61}$$

It is enlightening and also serves for the purposes of later reference to derive the splitting of the pressure tensor $\underline{\underline{P}}^e = p_e \underline{\underline{I}} + \Pi$ to the scalar pressure p_e and the anisotropic part Π:

$$p_e = \frac{4\pi}{3} m_e \left(\int_0^{+\infty} f_0 v^4 \,\mathrm{d}v \right) - \frac{1}{3}\rho_e u_e^2, \qquad \underline{\underline{\Pi}}^e = \frac{8\pi}{15} m_e \int_0^{+\infty} \underline{\underline{f_2}} v^4 \,\mathrm{d}v + \frac{1}{3}\rho_e u_e^2 - \rho_e \vec{u}_e \vec{u}_e. \tag{62}$$

From the given expression, it is clear that f_0 contributes to the scalar pressure and $\underline{\underline{f_2}}$ to the anisotropic part only.

To proceed further, the expansion (57) is inserted to the kinetic equation (2), where the equations for the first two contributions parts of the distribution function give:

$$\frac{\partial f_0}{\partial t} + \frac{v}{3}\nabla \cdot \vec{f}_1 - \frac{e}{m_e}\frac{1}{3v^2}\frac{\partial}{\partial v}\left(v^2 \vec{E} \cdot \vec{f}_1 \right) = C_0, \tag{63}$$

$$\frac{\partial \vec{f}_1}{\partial t} + v\nabla f_0 - \frac{e}{m_e}\frac{\partial f_0}{\partial v}\vec{E} - \frac{e}{m_e}\vec{B} \times \vec{f}_1 + \\ + \frac{2}{5} v \nabla \cdot \underline{\underline{f_2}} - \frac{2e}{5 m_e v^3}\frac{\partial}{\partial v}\left(v^3 \vec{E} \cdot \underline{\underline{f_2}} \right) = C_1. \tag{64}$$

The equations for higher anisotropic corrections can be found in the literature and are not detailed here [37].

The symbols C_0 and C_1 represent the tensor expansion of the collision operator on the right-hand-side. Their complete prescription for the Fokker–Planck operator can be found in the literature [28]. However, we are particularly interested in a simplified

form of the collision operator for a two-specie plasma:

$$\left(\frac{\partial f}{\partial t}\right)_{coll} = C_{ee} + C_{ei} = C_{ee} + \frac{\nu_{ei}}{2}\frac{\partial^2}{\partial \vec{n}^2} f = \\ = C_{ee} + \frac{\nu_{ei}}{2}\left(\frac{1}{\sin\varphi}\frac{\partial}{\partial\varphi}\left(\sin\varphi\frac{\partial}{\partial\varphi} f\right) + \frac{1}{\sin^2\varphi}\frac{\partial^2}{\partial\theta^2} f\right), \quad (65)$$

where ϕ is the polar angle and θ the azimuthal angle of the velocity vector in spherical coordinates. The symbol C_{ee} represents the Fokker–Planck operator for electron–electron collisions following the definition (6) and C_{ei} is the electron–ion collision operator in the approximation (20). The simplification made here is that electron–ion collisions lead to pure scattering of the electrons on a static background of ions. This procedure assumes that the thermal velocities of ions are significantly lower than that of electrons, i.e. $v_{Ti} \ll v_{Te}$ ($v_{T\alpha}^2 = k_B T_\alpha / m_\alpha$). Moreover, the system is observed for notably shorter times than the thermal relaxation time $1/\nu_{ei}^{\epsilon} \sim m_i/m_e\nu_{ei}$. Due to the high mass ratio between the ions and electrons typically, the approximation is justified. The collisional terms C_0 and C_1 then take the form:

$$C_0 = \frac{\bar{\nu}_{ee}}{v^2}\frac{\partial}{\partial v}\left(C(f_0)f_0 + D(f_0)\frac{\partial f_0}{\partial v}\right) + C_{11}(\vec{f_1}, \vec{f_1}), \quad (66)$$

$$C_1 = -\nu_{ei}\vec{f_1} + C_{01}(f_0, \vec{f_1}), \quad (67)$$

where the Rosenbluth potentials of friction C and diffusion D are defined as:

$$C(f_0) = 4\pi\int_0^v f_0(v')v'^2 dv', \quad (68)$$

$$D(f_0) = \frac{4\pi}{v}\int_0^v v'^2\int_{v'}^{+\infty} f_0(v'')v''dv''dv'. \quad (69)$$

It is evident from the form of (66–67) that the tensor expansion separates the maxwellization process mediated by C_0 and isotropization process mediated by C_1. The angular diffusion operator (also known as Laplace–Beltrami) from (65) simplifies substantially, manifesting the convenient construction of the expansion basis, where spherical harmonics are eigenvectors of this operator. It can be immediately recognized that the basis function $\cos\varphi$ coincides with the scalar product of $\vec{n}$. The collision term C_{01} is responsible for the electron–electron scattering and holds main importance for low-Z plasmas, otherwise electron–ion collisions dominate due to favourable charge and mass ratio. In the Lorentz approximation (for $Z \to \infty$), this term is neglected completely. Finally, the term C_{11} describes growth of f_0 due to electron–electron scattering, but it presents a second order effect $\sim |\vec{f_1}|^2$ and can be neglected usually (assuming $|\vec{f_1}| \ll f_0$). Definitions of both can be found in the literature and it is not detailed due to their complex formulation [28].

For completeness, the formulae for the collision frequencies read:

$$\nu_{ee}(v) = \bar{\nu}_{ee} n_e v^{-3} = \frac{4\pi e^4}{m_e^2} n_e v^{-3} \log \Lambda_{ee}, \tag{70}$$

$$\nu_{ei}(v) = \frac{4\pi e^4}{m_e^2} Z^2 n_i v^{-3} \log \Lambda_{ei}, \tag{71}$$

where Z is the mean ionization. The expressions can be derived from the Fokker–Planck operator (6) after substitution of the Maxwell–Boltzmann distribution (24) as the target distribution f_β, which linearises the operator effectively. It can be shown that a solution exists in the form of Chandrasekhar function [38], which behaves as $\sim v^{-3}$ in the high velocity limit and yields the sought formulae when the approximation $m_e/m_i \approx 0$ is made.

3 Hydrodynamics

The fluid model describes plasma as a continuum governed by the equations for macroscopic quantities. The single-specie model was derived in chapter 2.2 from the kinetic theory through velocity moments of the kinetic equation (1). In particular, it is comprised of the mass equation (30), momentum equation (37) and energy equation (50). These macroscopic quantities then parametrize the shifted Maxwell–Boltzmann distribution (24), which presents the assumed solution of the kinetic problem within the fluid description. Only infinitesimal perturbation are considered classically, in order to model the transport processes as described in chapter 4. This procedure is valid only for well thermalized plasma ($t \gg \nu_{\alpha\alpha}^{-1}$), isotropized ($t \gg \nu_{\alpha}^{-1}$), where ν_α is the total scattering frequency) and dominated by kinetic phenomena ($\epsilon_\alpha^i \gg \epsilon_{EM}$). Under these conditions, the solution attains the near (collisional) equilibrium limit.

3.1 Multi-specie fluid model

The single-specie model derived in chapter 2.2 can be then extended to the multi-specie case by adding the inter-specie interaction according to (28):

$$\frac{\partial \rho_\alpha}{\partial t} + \nabla \cdot (\rho_\alpha \vec{u}_\alpha) = 0, \tag{72}$$

$$\frac{\partial \rho_\alpha \vec{u}_\alpha}{\partial t} + \nabla \cdot (\rho_\alpha \vec{u}_\alpha \vec{u}_\alpha) = -\nabla \cdot \underline{\underline{P}}^\alpha + \rho_\alpha^q \vec{E} + \vec{j}_\alpha \times \vec{B} + \vec{g}_{\alpha\beta}, \tag{73}$$

$$\frac{\partial \rho_\alpha \varepsilon_\alpha^T}{\partial t} + \nabla \cdot \left(\rho_\alpha \varepsilon_\alpha^T \vec{u}_\alpha\right) = -\nabla \cdot (\underline{\underline{P}}^\alpha \cdot \vec{u}_\alpha) - \nabla \cdot \vec{q}_\alpha + \vec{j}_\alpha \cdot \vec{E} + g_{\alpha\beta}, \tag{74}$$

where $\varepsilon_\alpha^T = \epsilon_\alpha^T / \rho_\alpha$ is the total specific energy of α species. The collisional coupling between the species is mediated by the exchange terms:

$$\vec{g}_{\alpha\beta} = \int m_\alpha \vec{v}_\alpha \sum_{\beta \neq \alpha} \left(\frac{\partial f_\alpha}{\partial t}\right)_{coll}^{\beta} \mathrm{d}\vec{v}_\alpha, \tag{75}$$

$$g_{\alpha\beta} = \int \frac{1}{2} m_\alpha |\vec{v}_\alpha|^2 \sum_{\beta \neq \alpha} \left(\frac{\partial f_\alpha}{\partial t}\right)_{coll}^{\beta} \mathrm{d}\vec{v}_\alpha. \tag{76}$$

The multi-specie model (72–74) considers only momentum and energy transfers between the species based on the form of the collision operator (19), where contribution to the zeroth velocity moment is always zero. In other words, the processes resulting in exchange of particles like ionization or recombination are not modelled dynamically, but left for the stationary closure model described later in chapter 3.4.

3.2 One-fluid hydrodynamic model

The multi-specie model of chapter 3.1 offers a complete fluid description of the plasma when the self-consistent fields are obtained from the electromagnetic closure, i.e. the Maxwell's equations (3–4). However, the model represents a non-linear problem, ex-

pensive to solve on long time scales. Therefore, the model is reduced to the one-fluid description, provided that a quasi-static electric field develops between the species and couples them together effectively ($t \gg \omega_{p\alpha}^{-1}$). Hence, the electrically charged particles of different species are separated only on distances of the Debye length $\lambda_{D\alpha}$ and the plasma can be considered quasi-neutral ($\sum_\alpha \rho_\alpha^q \approx 0$). The flows of the particles do not need to be modelled separately as their profiles are inter-dependent. Consequently, the plasma is described with the one-fluid quantities like the mass density ρ, center of mass velocity $\vec{u}$ and specific internal energy ε:

$$\rho = \sum_\alpha \int m_\alpha f_\alpha \,\mathrm{d}\vec{v}_\alpha, \tag{77}$$

$$\vec{u} = \frac{\sum_\alpha \int m_\alpha \vec{v}_\alpha f_\alpha \,\mathrm{d}\vec{v}_\alpha}{\sum_\alpha \int m_\alpha f_\alpha \,\mathrm{d}\vec{v}_\alpha}, \tag{78}$$

$$\varepsilon = \frac{\sum_\alpha \int \frac{1}{2} m_\alpha |\vec{v}_\alpha - \vec{u}_\alpha|^2 f_\alpha \,\mathrm{d}\vec{v}_\alpha}{\sum_\alpha \int m_\alpha f_\alpha \,\mathrm{d}\vec{v}_\alpha}. \tag{79}$$

In particular, the velocities are $\vec{u} \approx \vec{u}_e \approx \vec{u}_i$ and densities are $n_e = Z n_i$ for electron–ion plasma, where Z is the mean ionization. Finally, the one-fluid model is obtained by summing over the α index the system (72–74):

$$\frac{\partial}{\partial t}\,\rho + \nabla \cdot (\rho \vec{u}) = 0, \tag{80}$$

$$\frac{\partial}{\partial t}\,(\rho \vec{u}) + \nabla \cdot (\rho \vec{u}\vec{u}) = -\nabla \cdot \underline{\underline{P}} - \nabla \cdot \underline{\underline{P}}^B, \tag{81}$$

$$\frac{\partial}{\partial t}\,(\rho(\tfrac{1}{2}u^2 + \varepsilon)) + \nabla \cdot (\rho(\tfrac{1}{2}u^2 + \varepsilon)\vec{u}) = -\nabla \cdot (\underline{\underline{P}} \cdot \vec{u}) - \nabla \cdot \vec{q} + \vec{j} \cdot \vec{E}, \tag{82}$$

where $\vec{j} = \sum_\alpha \vec{j}_\alpha$ is the electric current, $\vec{q} = \sum_\alpha \vec{q}_\alpha$ heat flux, $\underline{\underline{P}} = \sum_\alpha \underline{\underline{P}}_\alpha$ and $\underline{\underline{P}}^B = -\underline{\underline{T}}^B$ is the magnetic pressure tensor. The contributions from the collisional momentum and energy exchange terms cancel out according to (29) and the Lorenz force densities vanish due to the quasineutrality condition. However, solenoidal currents can exist even under the quasi-neutrality requirement, because the continuity equation (36) only restricts the potential (or divergent) part. In magneto-hydrodynamics, where the interplay with a magnetic field is modelled, the solenoidal currents are given by the electrostatic Ampère's law $\vec{j} = \mu_0^{-1} \nabla \times \vec{B}$. Their substitution to the Hall term $\vec{j} \times \vec{B}$ yields the magnetic pressure term $-\nabla \cdot \underline{\underline{P}}^B$. Although, the term is proportional to the magnetic energy $1/(2\mu_0)|\vec{B}|^2$ according to the definition (45) and the kinetic pressure tensor $\underline{\underline{P}}$ to the internal energy $\rho\varepsilon$, so it can be neglected in ideal hydrodynamics, where the assumption $\epsilon_{EM} \ll \rho\varepsilon$ is enforced strictly.

The expression for the electric field can be obtained from the momentum equations (73) when multiplied by ρ/ρ_α and summed over the α index, while the velocities are considered equal already. This procedure can be seen as relative temporal variations of the contributions to the total momentum and the electric field is constructed

in such way to zero them all. Finally, the expression for the electric field is obtained:

$$\vec{E} = -\vec{u} \times \vec{B} + \sigma^{-1}\vec{j} + \left(\sum_\alpha \frac{q_\alpha}{m_\alpha}\right)^{-1} \sum_\alpha \frac{1}{\rho_\alpha} \nabla \cdot \underline{\underline{P}}^\alpha, \tag{83}$$

where σ is the total electric conductivity originating from the collisional terms $\vec{g}_{\alpha\beta}$, where a collisional friction between the species exists. In the case of electron–ion plasma, the situation simplifies notably, because the mass and charge ratio favours the electron pressure contribution $-\nabla \cdot \underline{\underline{P}}^e/(en_e)$.

The procedure leading to the one-fluid model (80–82) assumed that there exists a single equilibrium distribution for all species. However, the electron–ion energy exchange time is related to the electron–electron thermalization time as $(\nu^\epsilon_{ei})^{-1} \sim m_i/m_e Z^{-2}\nu^{-1}_{ee}$, so the condition $t \gg \nu^{-1}_{ee}$ can be satisfied securely, but $t \gg (\nu^\epsilon_{ei})^{-1}$ may not. In other words, the equilibrium is reached significantly earlier for electrons separately than the common equilibrium between the species. It is then possible to retain the separate energy equations for electrons and ions instead of the common one (82). This approach is known as two-temperature one-fluid model. The energy equations then read:

$$\begin{aligned} \frac{\partial}{\partial t}\left(\rho_e(\tfrac{1}{2}u^2 + \varepsilon_e)\right) + \nabla \cdot \left(\rho_e(\tfrac{1}{2}u^2 + \varepsilon_e)\vec{u}\right) = &-\nabla \cdot (\underline{\underline{P}}^e \cdot \vec{u}) - \nabla \cdot \vec{q}_e + \vec{j}_e \cdot \vec{E} + \\ &+ G_{ei}(T_i - T_e), \end{aligned} \tag{84}$$

$$\begin{aligned} \frac{\partial}{\partial t}\left(\rho_i(\tfrac{1}{2}u^2 + \varepsilon_i)\right) + \nabla \cdot \left(\rho_i(\tfrac{1}{2}u^2 + \varepsilon_i)\vec{u}\right) = &-\nabla \cdot (\underline{\underline{P}}^i \cdot \vec{u}) - \nabla \cdot \vec{q}_i + \vec{j}_i \cdot \vec{E} + \\ &+ G_{ie}(T_e - T_i), \end{aligned} \tag{85}$$

where most of the terms cancel out as in (82), because the quasi-neutrality still holds, but G_{ei}, G_{ie} are the heat exchange coefficients for the linearized heat transfer approximating g_{ei}, g_{ie} terms respectively. It is applicable only for gentle deviations from the common equilibrium, i.e. $G_{ei}|T_e - T_i|\Delta t \ll 1$ holds ideally (Δt is a typical resolved time scale). Moreover, the symmetry $G_{ei} = G_{ie}$ is required to satisfy energy conservation.

3.3 Lagrangian hydrodynamics

The fluid model presented in chapter 3.2 used the Eulerian description, where the reference frame is fixed (the laboratory frame normally). However, ablative processes during laser–target interaction lead to enormous expansion of the matter, where the Lagrangian description is preferable.

The hydrodynamics is modelled within the reference frame co-moving with the fluid. Only the Galilean transformations of the coordinate system are used, respecting the assumption of non-relativistic motion of the fluid. It is convenient to define the differential operator of substantial (or material) derivative:

$$\frac{\mathrm{D}\vec{h}}{\mathrm{D}t} = \frac{\partial \vec{h}}{\partial t} + (\vec{u}\nabla)\vec{h}, \tag{86}$$

for a vector function $\vec{h}$ (or for a scalar function analogously).

Equipped with the substantial derivative, the one-fluid model (80–82) can be rewritten as:

$$\frac{\mathrm{D}}{\mathrm{D}t}\rho = -\rho\nabla\cdot\vec{u}, \tag{87}$$

$$\rho\frac{\mathrm{D}}{\mathrm{D}t}\vec{u} = -\nabla\cdot\underline{\underline{P}} - \nabla\cdot\underline{\underline{P}}^B, \tag{88}$$

$$\rho\frac{\mathrm{D}}{\mathrm{D}t}\varepsilon = -\underline{\underline{P}} : \nabla\vec{u} - \nabla\cdot\vec{q} + \vec{j}\cdot\vec{E}, \tag{89}$$

where the lower velocity moment equations were substituted to simplify the formulation.

The next step is transformation of the coordinate system itself. The hydrodynamic equations (80–82) are primarily hyperbolic, so the quantities $\rho, \rho\vec{u}, 1/2\rho u^2 + \rho\varepsilon$ are advected along the characteristics. Therefore, the time-dependent flux $\vec{\psi}_t : \vec{X} \to \vec{x}$ of the equations can be defined, which assigns the coordinate of an infinitesimal volume of the solution at time t to its initial (or material) coordinate X, so it ideally holds $\rho(\vec{\psi}_t(X), t) = \rho(X, 0)$, etc. Provided that this assignment is bijective and difeomorphic, so the characteristics do not intersect and no singularities exist, a well-defined invertible transformation of the coordinates $(\vec{X}, t) \to (\vec{x}, t)$ can be defined. The pair of the space-time coordinates $(\vec{X}, t)$ is called the Lagrangian coordinates. A function $\tilde{h} = \tilde{h}(\vec{X}, t)$, defined in the Lagrangian coordinates and corresponding to the function $h = h(\vec{x}, t)$ in the Eulerian coordinates, is then differentiated as follows:

$$\left.\frac{\partial\tilde{h}}{\partial t}\right|_{\vec{X},t} = \left.\frac{\partial h}{\partial t}\right|_{\vec{\psi}_t(\vec{X}),t} = \left.\frac{\partial h}{\partial t}\right|_{\vec{\psi}_t(\vec{X}),t} + \frac{\partial\vec{\psi}_t}{\partial t}\cdot\left.\frac{\partial h}{\partial\vec{x}}\right|_{\vec{\psi}_t(\vec{X}),t} = \left.\frac{\mathrm{D}h}{\mathrm{D}t}\right|_{\vec{\psi}_t(\vec{X}),t}, \tag{90}$$

where the fact was utilized that the slope of the characteristics $\partial\vec{\psi}_t/\partial t$ is equal to the velocity of the convection $\vec{u}$.

In addition to the time derivative, the divergence operator is needed. It can be transformed as follows:

$$\nabla_{\vec{X}}\cdot\tilde{h}|_{\vec{X},t} = \left|\frac{\mathrm{d}\vec{\psi}_t}{\mathrm{d}\vec{X}}\right|_{\vec{X}} \nabla_{\vec{x}}\cdot h|_{\vec{\psi}_t(\vec{X}),t} = \frac{\rho_0(\vec{X})}{\rho(\vec{\psi}_t, t)}\,\nabla_{\vec{x}}\cdot h|_{\vec{\psi}_t(\vec{X}),t}\,, \tag{91}$$

where $\rho_0(\vec{x}) = \rho(\vec{x}, 0)$ is the initial density. This fact already reflects the fact that $\rho|J|$ is an invariant of the flow, i.e. $\mathrm{D}\rho|J|/\mathrm{D}t = 0$, where $J = \mathrm{d}\vec{\psi}_t/\mathrm{d}\vec{X}$ is the Jacoby matrix. This can be seen as a consequence of the mass conservation law (87), provided the relation $\mathrm{D}|J|/\mathrm{D}t = \nabla\cdot\vec{u}|J|$ holds, as can be verified from the definition [39]. The continuity equation then gives:

$$0 = \frac{\mathrm{D}\rho}{\mathrm{D}t} + \rho\nabla\cdot\vec{u} = \frac{\mathrm{D}\rho}{\mathrm{D}t} + \rho|J|^{-1}\frac{\mathrm{D}|J|}{\mathrm{D}t} = |J|^{-1}\frac{\mathrm{D}\rho|J|}{\mathrm{D}t} \tag{92}$$

Following these considerations, the system (88–89) can be transformed to the

following form:

$$\rho_0 \frac{\partial}{\partial t} \tilde{\vec{u}} = -\nabla_{\vec{X}} \cdot \tilde{\underline{\underline{P}}} - \nabla_{\vec{X}} \cdot \tilde{\underline{\underline{P}}}^B, \tag{93}$$

$$\rho_0 \frac{\partial}{\partial t} \tilde{\varepsilon} = -\tilde{\underline{\underline{P}}} : \nabla_{\vec{X}} \tilde{\vec{u}} - \nabla_{\vec{X}} \cdot \tilde{\vec{q}} + \frac{\rho_0}{\tilde{\rho}} \tilde{\vec{j}} \cdot \tilde{\vec{E}}. \tag{94}$$

where the functions in the Lagrangian coordinates are denoted by the upper tilde.

Finally, it must be explained how the Maxwell's equations (3–4) are transformed. The procedure is not as straightforward as in the case of the hydrodynamic part. The fields must be transferred to the Lagrangian frame by the proper Lorentz transformations in the low velocity limit. In the simplest case of Lagrangian magnetohydrodynamics, the local electric force can be identified with the classical local Lorentz force, giving the expression for the electric field [40]:

$$\tilde{\vec{E}}(\vec{\psi}_t^{-1}(\vec{x}), t) = \vec{E}(\vec{x}, t) + \vec{u}(\vec{x}, t) \times \vec{B}(\vec{x}, t). \tag{95}$$

The Faraday's law (4) maintains its form even in the moving frame and becomes:

$$\frac{\partial}{\partial t} \tilde{\vec{B}} = -\nabla \times \tilde{\vec{E}}, \tag{96}$$

where the differential operator in Eulerian coordinates is retained, because the formula (91) cannot be applied here and the final expression is more complex. It should be noted that (96) together with the definition of the electric field (95) and (83) can be interpreted in such way that the convection of the magnetic field was eliminated by the change of the reference frames similarly to the rest of the quantities.

3.4 Equation of state

The (magneto-)hydrodynamic equations (87–89) together with the equations for the electric field (83) and magnetic field (4) eventually still do not pose a closed system of differential equations. The prescriptions of the pressure tensor and heat flux are missing in the hydrodynamic picture. The reason is that both are given by higher velocity moments than appearing in the hydrodynamic system, as in the case of the heat flux according to the definition (49), or multi-directional correlations rather than the scalar in the case of the pressure (39). Discussion of the former is left for the dedicated chapter about the heat transport processes 4, while the latter is the subject of this chapter.

3.4.1 Ideal gas

Based on the kinetic theory, it was recognized after the Cartesian tensor expansion (62) (and also the definition (39)) that the higher order tensors contribute to the anisotropic part of the tensor only. The scalar part was obtained directly from the isotropic part of the distribution function. Considering the equilibrium distribution (24) used throughout the macroscopic model, the scalar pressure (62) can be related

to the internal energy of the plasma:

$$p = (\gamma - 1)\rho\varepsilon. \tag{97}$$

This can be recognized as the ideal gas equation of state, where γ is the Poisson constant. As the degrees-of-freedom of the species motion were not restrained anyhow, the constant attains the adiabatic value $\gamma = 5/3$ in the kinetic model of chapter 2. Because the reduced hydrodynamic description does not self-consistently provide this value, it can be varied depending on the given physical problem, so the value $\gamma = 7/5$ can be used for simple diatomic molecules for example. The ionization is not provided by the model and is assumed constant for the ideal gas.

3.4.2 Quotidian Equation of State

The Quotidian Equation of State (QEOS) [41] is one of the most popular models in hydrodynamic simulations of plasma. It provides the analytic formulae for a wide range of temperatures and densities in the one-temperature or even two-temperature model. Conceptually, it is based on the formulation in terms of the Helmholtz free energy:

$$F_{tot}(\rho, T_e, T_i) = F_i(\rho, T_i) + F_e(\rho, T_e) + F_b(\rho, T_e), \tag{98}$$

where F_i is the ion contribution, F_e electron contribution and F_b bounding correction. The ion part is approximated by the solid and liquid scaling laws and by the Cowan model [42]. The term F_b supplements the model by semi-empirical bonding corrections, which serve to decrease the total pressure for solid material and give correct bulk modulus [43]. The bulk modulus of solid and solid density are externally entered parameters in this model. Finally, the electron term is based on the Thomas–Fermi theory [44].

The basic assumptions behind the Thomas–Fermi theory are such that electrons move in the electrostatic field of a point-like ion. As the model originates from the statistical description in the continuum limit, there should be statistically representative number of electrons at any distance from the nucleus, so the model is fully valid only for infinitely ionized atoms. In essence, the total energy of electrons is given by:

$$E_{TF} = C_{TF}^{kin} \int n^{5/3}(\vec{x})\,\mathrm{d}\vec{x} - \int n(\vec{x}) \frac{Ze^2}{|\vec{x}|}\,\mathrm{d}\vec{x} + \frac{1}{2}e^2 \int\int \frac{n(\vec{x})n(\vec{x}')}{|\vec{x} - \vec{x}'|}\,\mathrm{d}\vec{x}\,\mathrm{d}\vec{x}', \tag{99}$$

the symbol C_{TF}^{kin} is a positive constant. The first term is the kinetic energy of the electrons distributed to Fermi spheres in the phase space, i.e. the volume of phase space occupied by fermionic matter in ground state. The second term is the potential in the field of the ion, which is calculated from the classical solution of the Poisson equation in an agreement with the assumptions already stated. The last term is the expulsion potential of point-like electrons. This energy is then minimized through variations of the density profile for the given total number of electrons. From the form of the equation, it is clear that the resulting solution is only function of the radius, so no higher spherical modes are present and no notion of electron orbitals exists,

except the spherically symmetric ones, but no quantization exists either. On the other hand, the solution scales with the ionization Z, so it can be precomputed once and applied on all ions. Another drawback of the theory is the absence of a proper electron energy exchange term, which would respect Pauli exclusion principle. An answer to this deficiency is given by the Thomas–Fermi–Dirac theory, but the model shares the other inaccuracies and the solution cannot be scaled directly, which presents a notable practical inconvenience. Therefore, the classical Thomas–Fermi approach is applied usually.

The convenient simplicity and versatility of the QEOS model stemmed development of many equations of state originating from it. The model was later adopted in the library MPQeos [45] and further extended in FEOS package. It provides in addition to the basic QEOS model proper treatment of mixtures, where the properties of the modelled atoms do not need to be averaged a priori. There are also improvements of the cold curve and the region of liquid–vapour coexistence is treated rigorously [46].

3.4.3 Other equations of state

The Thomas–Fermi model used in the plain QEOS disregarded shell structure of the atoms, making the model applicable only for high-Z materials approximately. This crude simplification of the atomic description was addressed by many other authors. One of the more advanced models is the BADGER library [47]. The ion model is essentially the same as in the one used in QEOS. However, the correction for the atomic bounds do not use the empirical parameters, but a model based on scaled binding energies (SBE) instead. The ionization model is then separated from the electron equation of state and can be switched independently. The model based on the Thomas–Fermi model described in the previous chapter is one of the options, but the continuum treatment predetermines it only for high-Z materials as already stated. On the other, the screened hydrogenic model with l-splitting (SHM) can be used instead, where the notion of the atomic structure in the approximation of the principal and azimuthal quantum numbers is present. Another option is the individual electron accounting model (IEM) model, where the electrons in the approximation of discrete particles are part of the quantum system of the ion. Finally, the electron equation of state models not only the free electrons, but also the bound electrons, which were disregarded in the QEOS(-like) models, using the already mentioned SHM model. All species then interact through the Coulombic forces and partial charge screening is also present between them.

In addition to the analytic models presented so far, there is another wide group of empirical models. One of the major members of the family is the SESAME library [48, 49, 50]. The experimentally measured values of quantities like pressure or ionization are tabulated for various temperatures and densities. Interpolation of the data is then necessary between the discrete point of the thermodynamic space.

The interpolation routines are part of HerEOS (Hermite-interpolated Equation of State) [51, 52]. The library provides thermodynamically consistent interpolation of the quantities rather than direct interpolation between the given values of pressure and other. In particular, all thermodynamic potentials are calculated from the Helmholtz

free energy $F = F(\rho, T)$, where the temperature is the common one for one-temperature models, electron or ion, depending on the given equation of state. For example, the specific internal energy and pressure are calculated as follows:

$$\varepsilon(\rho, T) = F - T \left(\frac{\partial f}{\partial T} \right)_\rho , \qquad p(\rho, T) = \rho^2 \left(\frac{\partial F}{\partial \rho} \right)_T , \tag{100}$$

where the thermodynamic notation of derivatives is used, so the lower index denotes the quantity constant during the process. This approach guarantees that the derived quantities are true potentials as in the theory of thermodynamics. The potentiality is not self-provided for interpolated functions as inconsistencies arise between the discretely approximated quantities, which may lead to violation of the thermodynamic laws. In contrast, the calculation from F gives fully consistent results provided that the interpolated function F is smooth enough. This is achieved by high-order Hermite polynomials used for the interpolation. Another merit of the interpolation in general is the acceleration of the computation, where the analytic model does not need to be evaluated at the points of the thermodynamic space repeatedly during the numerical simulation.

4 Heat transport

The term heat refers to the energy confined in the chaotic motion of the plasma species. Collisional processes thermalize the plasma and lead to establishing of the collisional equilibrium as explained in chapter 2. However, the physical system rarely attains the full global thermal equilibrium (TE). Due to the presence of strong energy sources like an impinging laser beam (see chapter 6), the physical system is deviated from the global equilibrium and only local thermal equilibrium (LTE) is attained. The heat transport process then emerge, equalizing the thermodynamic conditions.

The kinetic theory provided a description of the heat transfer implicitly together with the rest of the velocity moments of the distribution function (see chapter 2.2). However, the reduction of the kinetic model to the fluid description of chapter 3 truncated the velocity moments expansion yet after the energy moment. Principally, the expansion can be extended further, but higher velocity moments are not invariants of the collision operator according to chapter 2.2. Consequently, they are not governed by conservation laws resembling those of the lower ones. Therefore, heat flux corresponding to the third velocity moment is not provided by the classical fluid model and must be supplied externally. This is circumvented by construction of a closure model for the heat flux, relying on the lower moments only. Various approaches to this problem are subjects of this chapter.

4.1 Diffusion transport

The diffusion treatment of the heat transport is the most frequently adopted one due to its simplicity. Moreover, it is also positivity of the diffusion operator, which guarantees monotonous increase of the entropy in an agreement with the Onsager relations of irreversible processes. Fundamentally, it is based on the linear perturbation theory, so its predictions are valid only for small deviations from the equilibrium. In particular, it will be shown that the perturbation of the Maxwell–Boltzmann distribution (24) scales with mean free path of the electrons λ_e. Therefore, the assumption $\lambda_e \ll L$ is made, where L is the characteristic length scale of the plasma profile (it is $L_T = T_e/|\nabla T_e|$ for the temperature and $L_n = n_e/|\nabla n_e|$ for the density approximately).

Under the conditions stated above, the distribution function f can be formally expanded using the Hilbert expansion in a small parameter λ combined with the expansion in Legendre polynomials in the directional cosine $\mu = \cos\varphi$ of the polar angle φ [53]:

$$f = \sum_{i=0}^{\infty} \lambda^i \sum_{j=0}^{\infty} f_{ij} P_j(\mu) = f_{00} + f_{01}\mu + f_{10}\lambda + f_{11}\lambda\mu + O(\lambda^2, \mu^2). \tag{101}$$

The Chapman–Enskog approach then defines the methodology how to successively solve such a parametric expansion, where the procedure should start with the unperturbed coefficients neglecting the corrections [2, 54, 55]. However, it is clear from chapter 2.1 that the solution is the Maxwell–Boltzmann distribution (24) for collisionally dominant plasma so it can be identified that $f_{00} = f_M$ and $f_{10} = 0$, as it is isotropic. Then, the first order correction are sought, but f_{01} correction can be neglected compared to f_M for the linear theory, so only f_{11} remains to be solved. When the higher order terms

are neglected, this truncated expansion exactly coincides with the Cartesian tensor expansion in chapter 2.3. For convenience and brevity, the equations are not derived again for the expansion (106), but the discussion continues with the the equivalent tensor formulation (57).

The solution of the kinetic problem has an analytic formulation only for the Lorentz approximation [1]. In this limit, the electron–electron collisions are neglected compared to the electron–ion ones. Moreover, the sought solution should be stationary to depend only on the thermodynamic potentials, so the transient term is $\partial \vec{f_1}/\partial t \approx 0$. Finally, we restrict ourselves to the case without a magnetic field. The equation for $\vec{f_1}$ (64) gives the solution:

$$\vec{f_1} = -\lambda_{ei} \left(\nabla f_M - \frac{e}{m_e v} \frac{\partial f_0}{\partial v} \vec{E} \right), \tag{102}$$

where $\lambda_{ei} = v/\nu_{ei}$ is the electron–ion scattering mean free path. Using only the definition of the equilibrium distribution (24), the gradient term can be evaluated as:

$$\nabla f_M = \left(\frac{\nabla n_e}{n_e} + \left(\frac{m_e v^2}{2 k_B T_e} - \frac{3}{2} \right) \frac{\nabla T_e}{T_e} \right) f_M. \tag{103}$$

The expression for the stationary self-consistent electric field can be directly derived under the condition of quasi-neutrality. Essentially, it implies, based on the continuity equation (36), that the electric current must be zero for a single-directional perturbation of the distribution function, so the definition (58) gives the condition:

$$\int_0^{+\infty} \vec{f_1} v^3 \, \mathrm{d}v = 0. \tag{104}$$

Inserting the solution of $\vec{f_1}$ (102) to it, the diffusion electric fields is obtained:

$$\vec{E} = \frac{k_B T_e}{e} \left(\frac{\nabla T_e}{T_e} + \xi^1 \frac{\nabla T_e}{T_e} \right), \tag{105}$$

where the factor $\xi^1 = 5/2$ for the Lorentz gas.

Finally, the electric field (105) is inserted to the $\vec{f_1}$ formula (102) and the full distribution function is constructed from the expanded form (57) to obtain:

$$f = n_e \left(\frac{m_e}{2\pi k_B T_e} \right)^{3/2} \exp\left(-\frac{m_e v^2}{2 k_B T_e} \right) \left(1 - D\left(\frac{m_e v^2}{2 k_B T_e}, \vec{n} \right) \right), \tag{106}$$

where D is the transport function taking the form:

$$D(\zeta, \vec{n}) = \xi^0 \lambda_{ei} (\zeta - 4) \vec{n} \cdot \frac{\nabla T_e}{T_e}, \tag{107}$$

The notation with the transport function D follows the work of Spitzer and Härm [6, 7]

and agrees with the classical results for the Lorentz gas [1]. Considering also electron–electron collisions throughout the derivation is non-trivial and the system must be solved numerically. The results obtained with an expansion in Legendre polynomials were tabulated in the influential paper [7]. The findings were later fitted by analytic formulae giving the correction factors [56]:

$$\xi^0(Z) = \frac{Z + 0.24}{Z + 4.2}, \qquad \xi^1(Z) = 1 + \frac{3}{2}\frac{Z + 0.477}{Z + 2.15}. \tag{108}$$

Finally, the diffusion heat flux reads according to the definition (59):

$$\vec{q}_{SH} = \frac{4\pi}{3}\int_0^{+\infty} \frac{1}{2} m_e v^5 \vec{f}_1 \,\mathrm{d}v = -\frac{128}{3\pi}\xi^0 \lambda_{SH} v_{Te} n_e k_B \nabla T_e, \tag{109}$$

where the Spitzer–Härm mean free path is defined as:

$$\lambda_{SH} = \frac{3 v_{Te}^4 m_e}{4\sqrt{2\pi} Z e^4 \ln \Lambda_{ei}}. \tag{110}$$

To conclude, the diffusion approximation for a small perturbation of the equilibrium distribution resulted in the Fourier's law for heat diffusion $\vec{q}_{SH} = -\kappa_{SH}\nabla T_e$. The electric field had a significant role in eliminating the dependency on the density gradient, which is only true if both gradients are aligned as was tactfully assumed. In the opposite case the solution is more complex and kinetic simulations are needed [57]. The electric field also reduced the heat flux significantly as the electrons cannot free stream in a single direction, but a return current balancing the flow is formed when the quasi-neutrality condition is enforced. Actually, the main contribution to the heat flux is not provided by the electrons with the thermal velocity v_{Te}, but super-thermal species with velocities about $v \approx 3.7 v_{Te}$ [58]. The dependency on the electron–electron collisions manifests that the electron–electron collisions make the transport less efficient, but the densities are lower for low-Z plasmas typically, outweighing the effect by the value of the mean free path.

4.1.1 Diffusion transport in a magnetic field

The diffusion model presented in this chapter did not assume presence of a magnetic field. The theory considering also this effect was summarized by Braginskii [8]. Instead of the simple Fourier's law, the following expressions are given:

$$\vec{E} = -\frac{\nabla p_e}{n_e e} + \frac{\vec{j} \times \vec{B}}{n_e e} + \underline{\underline{\alpha}} \cdot \vec{j} - \underline{\underline{\beta}} \cdot \nabla T_e, \tag{111}$$

$$\vec{q} = -\underline{\underline{\kappa}} \cdot \nabla T_e - T_e \underline{\underline{\beta}} \cdot \vec{j}, \tag{112}$$

where $\underline{\underline{\alpha}}$ is the resistivity coefficient, $\underline{\underline{\beta}}$ thermoelectric coefficient, $\underline{\underline{\kappa}}$ heat conductivity coefficient. All coefficients are tensors depending on the magnetization of the plasma.

In essence, their structure is following when applied on a vector $\vec{r}$:

$$\underline{\underline{A}} \cdot \vec{r} = A_{\parallel}(\vec{b} \cdot \vec{r})\vec{b} + A_{\perp}\vec{b} \times (\vec{r} \times \vec{b}) + A_{\wedge}\vec{b} \times \vec{r}, \tag{113}$$

where $\vec{b} = \vec{B}/|\vec{B}|$ is the unit vector in the direction of the magnetic field and $A_{\parallel}, A_{\perp}, A_{\wedge}$ are transport coefficients parallel, perpendicular and cross-component contributions respectively. The parallel terms are not affected by the magnetic field classically and the values are identical with the findings of Spitzer and Härm [7]. However, the perpendicular coefficients are strongly dependent on the magnetization and the heat flow is limited across the field lines, while the resistivity grows. The most interesting term is the one proportional to the temperature gradient, which is responsible for the Nernst effect in the case of the thermoelectric term $\underline{\beta} \cdot \nabla T_e$ and Righi–Leduc effect in the case of the anisotropic heat conduction term $\underline{\underline{\kappa}} \cdot \nabla T_e$. It means that an electric field and heat flux perpendicular to the both gradients, of the temperature and magnetic field, is generated. These terms then become non-local when the Knudsen number of electrons $Kn_e = \lambda_e/L$ grows [59].

4.1.2 Heat flux limiting

The heat diffusion model is widely used for plasma simulations for the reasons already mentioned in the introduction of this chapter about the diffusion transport. However, it was recognized based on experimental data that the predictions of the diffusion theory significantly overestimate the heat flux in the upstream of a steep front and underestimate in the downstream [11]. It was proposed to use the heat flux limiting techniques to cure this problem crudely. The heat flux is limited to a fraction of the free streaming value $q_{fs} = n_e m_e v_{Te}^3$, which is the absolutely highest value the heat flux can attain when all electrons propagate in a single direction. The heat flux is then limited by one of the formulae typically [60]:

$$\vec{q} = \min(1, f^{lim} q_{fs}/|\vec{q}_{SH}|)\vec{q}_{SH}, \qquad \text{or} \qquad \vec{q} = \frac{\vec{q}_{SH}}{1 + |\vec{q}_{SH}|/(f^{lim} q_{fs})}, \tag{114}$$

where f^{lim} is a factor between 0.02 and 0.15 based on experimental data and Fokker–Planck simulations [61, 62]. However, the redefinition of the flux using the local values of the temperature changes the structure of the diffusion equation, which becomes hyperbolic instead of parabolic locally. This can have unforeseen consequences as the entropy may not increase and non-physical artifacts may appear in the simulations [60]. Therefore, limitation of the conductivity is preferred, which does not guarantee that the flux is lower than the given value, but maintains the parabolic structure of the equation, so the behaviour remains purely diffusive. They are defined as follows:

$$\kappa = \min(1, f^{lim} q_{fs}/|\vec{q}_{SH}|)\kappa_{SH}, \qquad \text{or} \qquad \kappa = \frac{\kappa_{SH}}{1 + |\vec{q}_{SH}|/(f^{lim} q_{fs})}. \tag{115}$$

The problem associated with the flux limiting techniques is given by the fact that the value q_{fs} depends on the local temperature and density without any notion of

the actually transported species. Consequently, the limiter fraction f^{lim} is temporally, spatially and physical problem dependent factor, which can be accurately estimated only on the basis of fully kinetic simulations [63, 64, 65]. This problem led to the development of semi-empirical methods, designed to feasibly cure this loss of predictive capabilities of the hydrodynamic simulations.

4.1.3 Convolution extension

One of the major representatives of the semi-empirical methods is the method of Lucciani, Mora and Virmont (LMV) [15]. The idea was to propose a convolution of the classical diffusion results to take into account the emerging non-locality. The heat flux is then calculated as:

$$\vec{q} = \int_{\Omega} K(\vec{x}, \vec{x}') \vec{q}_{SH} \, \mathrm{d}\vec{x}', \tag{116}$$

where K is the convolution kernel defined in 1D as follows:

$$K(x, x') = \frac{1}{2\lambda_{LMV}(x')} \exp\left(- \left| \frac{\int_x^{x'} n_e(x'') \, \mathrm{d}x''}{\lambda_{LMV}(x') n_e(x')} \right| \right), \tag{117}$$

where λ_{LMV} is a function defined in the reference [15]. The convolution introduces the notion of non-locality, where the flux is dislocated on the length scale comparable with λ_{LMV}. However, a shortcoming of the theory is the asymmetric convolution kernel, where only an ad hoc density correction is present in the form of a path integral. As revealed later in the influential paper, negative entropy is generated and non-physical instabilities may arise [16, 66].

A multi-dimensional extension of the method based on less empirical foundation was proposed by Schurtz, Nicolaï and Busquet (SNB) [17], which remains the most widely used non-local transport model probably and has been implemented in large ICF codes [67, 20]. The generalization is made by reformulation of the problem in multiple dimension in terms of the equivalent linear stationary transport equation:

$$\vec{n} \cdot \nabla \vec{q} = \frac{1}{\lambda_{SNB}} \left(\frac{3}{4\pi} \vec{n} \cdot \vec{q}_{SH} - \vec{q} \right). \tag{118}$$

It can be recognized that the integral solution of the linear transport equation (118) in 1D is the Fredholm equation of the second kind, which nearly coincides with (116), but the kernel is symmetric. The transport equation can be solved by the discrete ordinates method or by angular moments as in the case of radiation transport described in chapter 5. The authors also propose a multi-group extension of the method, so non-locality of the species varying with their velocity can be taken into account approximately. However, one of the most cumbersome simplifications of the model is the non-existence of a non-local electric field. Instead, the mean free path is merely limited by the local value of the Spitzer-Härm electric field (105) based on the work of Bendib, Luciani and Matte (BLM) [68]:

$$\frac{1}{\lambda_{SNB}} = \frac{1}{a\lambda_{SH}} + \frac{|e\vec{E}_{SH}|}{k_B T_e}, \tag{119}$$

where a is a problem dependent positive constant. It is apparent that the configuration of the electric field and non-local fluxes can significantly more complicated in multiple dimensions unlike the 1D case considered by BLM and the local diffusion field is not representative of the actual non-local transport conditions. An effort was then made to reformulate the method with self-consistent electric and magnetic fields [69]. Also the electron–electron collision operator used for theoretical foundation of the model, which was originally approximated by the BGK operator of chapter 2.1.2, was replaced by the more accurate model of Albritton, Williams, Bernstein and Schawrtz (AWBS) [70, 18].

4.2 P1/M1 model of non-local transport

The chapter about the diffusion transport 4.1 revealed that the problem of heat transport becomes non-trivial when steep gradients of the length scale L comparable or smaller than the mean free path of the species λ are present in the plasma. In particular, the condition was specified to $\lambda_{ei}/L \ll 0.06/\sqrt{Z}$ for electrons [71]. This shows that the non-locality emerge very early and a discrepancy between the diffusion predictions and more accurate kinetic simulations arise [63]. The extensions of the diffusion model in chapter 4.1.3 approached the problem empirically or semi-empirically, but did not possess a solid theoretical foundation and empirical factors had to be adjusted for the given physical scenario, decreasing the predictive capabilities of the models. However, solution of the full kinetic problem was and still is prohibitively computationally expensive on the hydrodynamic scales. Therefore, simplified non-local transport models were proposed.

A simplified model directly originating from the kinetic theory is the P1 and M1 method using the terminology of radiation transport (see chapter 5.2). They are based on the angular moments technique, formally equivalent to the Cartesian tensor expansion of chapter 2.3, which is truncated after the first term. The collision operators on the right-hand-side of the system (63–64) do not involve the full non-linear collision operator, but they are simplified in the work of Del Sorbo et al. as follows [18, 72]:

$$C_0 = \nu_{ee} v \frac{\partial}{\partial v} (f_0 - f_M), \tag{120}$$

$$C_1 = \nu_{ee} v \frac{\partial}{\partial v} \vec{f_1} - (\nu_{ee} + \nu_{ei}) \vec{f_1}. \tag{121}$$

The Fokker–Planck operator for electron–electron collisions uses the linear AWBS approximation [70], which is valid for high-velocity species near the equilibrium. However, it has an apparent advantage over the BGK operator described in chapter 2.1.2 in the aspect of conserving mass, but it is still rather an empirical operator as the equilibrium distribution function must be entered explicitly.

The P1 and M1 models then differ in the definition of the closure relation replacing the $\underline{\underline{f_2}}$ contributions to the system of equations (63–64). Setting $\underline{\underline{f_2}} = 0$ yields the P1 model, which is applicable only for very small anisotropy $|\vec{f_1}| \ll f_0$. It must be noted that form of the closure appearing in the reference is different. The reason is

that formally equivalent technique of angular moments is followed there instead of the tensor expansion (57).

In contrast to the P1 model, M1 method is designed to approximately treat strongly anisotropic media. The idea is that $\underline{\underline{f_2}}$ should maximize the entropy as random scatterings do in long term. The procedure is not detailed here as it is essentially identical with the one performed in the case of radiative transport in chapter 5.2. The system is solved in the stationary limit, i.e. $\partial f_0/\partial t = 0, \partial \vec{f_1}/\partial t = 0$. The electric field is also calculated as stationary, where the solution can be derived immediately from (64) in the Lorenz limit for the zero current condition (104) in the form:

$$\vec{E} = -\frac{m_e}{6e}\frac{\int_0^{+\infty} \nabla f_0 v^7 \,\mathrm{d}v}{\int_0^{+\infty} f_0 v^5 \,\mathrm{d}v}. \tag{122}$$

This formula gives the Spitzer–Härm electric field (105) for the Maxwell–Boltzmann distribution (24). The electron–electron collisions in (121) are taken into account through a correction factor. The whole procedure of solution is performed iteratively until quasi-neutrality is achieved [18].

4.3 BGK model of non-local transport

A problem of the P1/M1 methods is given by their originally kinetic nature, which requires to solve the global system of equations for tens or hundreds of velocity bins as in the case of VFP codes, making it expensive to compute. The reason can be seen in the fact that the equilibrium distribution function is described as any other distribution function without any distinction. Secondly, the anisotropy of the distribution function is strongly limited by the truncated Cartesian expansion. It was assumed that $|\vec{f_1}| \ll f_0$ and when this condition is not fulfilled, a strong flux of electrons causes negativity of the distribution function in the opposite direction as both directions are artificially connected though a single component of $\vec{f_1}$ vector. The entropy maximizing closure then leads to an excessively diffusive system even for nearly coherent electron fluxes [73].

These drawback led us to the construction of a model based on the first-principles similar by its nature to the discrete ordinates method used in radiative transport of chapter 5.3. The primary quantity in the description is the electron specific heat flux intensity $I_e^v = I_e^v(\vec{x}, \vec{n}, v, t)$ [19, 74, 60]. Essentially, it determines the differential amount of energy $\mathrm{d}E_e$ transported by the electrons with velocities in the interval $(v, v + \mathrm{d}v)$ along the unit vector $\vec{n}$ in time $\mathrm{d}t$ across an infinitesimal oriented surface $\mathrm{d}\vec{S}$ into the solid angle $\mathrm{d}\vec{n}$:

$$\mathrm{d}E_e = I_e^v(\vec{x}, \vec{n}, v, t)\vec{n} \cdot \mathrm{d}\vec{S}\,\mathrm{d}\vec{n}\,\mathrm{d}v\,\mathrm{d}t. \tag{123}$$

Taking the phase space volume expressed in the spherical coordinates similarly to chapter 2.3, the intensity is defined as follows:

$$I_e^v(\vec{x}, \vec{n}, v, t)\,\mathrm{d}\vec{x}\,\mathrm{d}\vec{n}\,\mathrm{d}v = \frac{1}{2}m_e|\vec{v}|^3 f_e(\vec{x}, \vec{x}, t)\,\mathrm{d}\vec{x}\,\mathrm{d}\vec{v} = \frac{1}{2}m_e v^5 f_e(\vec{x}, \vec{n}, v, t)\,\mathrm{d}\vec{x}\,\mathrm{d}\vec{n}\,\mathrm{d}v. \tag{124}$$

The connection to the definition of the heat flux (59) is obvious and the heat flux becomes then:

$$\vec{q}_e^T = \int_0^{+\infty} \int_{4\pi} I_e^v \vec{n} \, \mathrm{d}\vec{n} \, \mathrm{d}v = \int_{4\pi} I_e \vec{n} \, \mathrm{d}\vec{n}. \tag{125}$$

This expression also defines the total electron intensity I_e, which is the velocity integral of I_e^v.

The BGK non-local electron heat transport model is based on the kinetic equation (2) in the stationary limit (considering long times compared to the collision time ν_e^{-1}) equipped with the BGK operator (21):

$$\vec{n} \cdot \nabla f - \frac{e}{m_e v} \frac{\partial f}{\partial v} \vec{n} \cdot \vec{E} = -\frac{\nu_e}{v}(f - f_M), \tag{126}$$

where presence of a magnetic field is not considered. Next, the averaging operator is defined for a function of velocity h as follows:

$$\langle h \rangle^I = \int_0^{+\infty} \frac{1}{2} m_e v^5 h \, \mathrm{d}v. \tag{127}$$

Application of this operator on the kinetic equation (126) yields:

$$\vec{n} \cdot \nabla I_e + \frac{4e}{m_e} \left\langle \frac{f}{v^2} \right\rangle^I \vec{n} \cdot \vec{E} = \left\langle \frac{f_M}{\lambda_e} \right\rangle^I - \left\langle \frac{f}{\lambda_e} \right\rangle^I, \tag{128}$$

where $\lambda_e = v/\nu_e$ is the electron mean free path. Approximating the unknown distribution function by a Maxwellian, the averaging can be performed to obtain:

$$\vec{n} \cdot \nabla I_e = -\frac{e}{k_B T_e} I_e \vec{n} \cdot \vec{E} + \frac{1}{\alpha \lambda_{SH}} \left(\frac{\sqrt{2}}{\pi^{3/2}} \rho_e v_{Te}^3 - I_e \right). \tag{129}$$

Following this approach, a problem arises in the case of the electric field term, where the zero current condition (104) is related to a different velocity moment of the distribution function. Approximation of the third velocity moment of the angular distribution function by the fifth, i.e. by the intensity, would only non-physically shift the equilibrium intensity and the mean free path. Therefore, the electric field is approximated only by the corrective factor α of the mean free path, which is adjusted to give an agreement of the method with the diffusion heat flux (109) in the limit. The calculation shows that it has the value [19]:

$$\alpha(Z) = \frac{64}{3\sqrt{2\pi}} \xi^0(Z) \doteq 8.51 \xi^0(Z). \tag{130}$$

The main benefits of the method can be seen in an arbitrary anisotropy of the transport, which depends only on the numerical quadrature used for the solution of the steady state transport (129). It is also the tractable formulation making the calculation inexpensive and solvable by various numerical methods, while the intensity-based formulation guarantees that the method is always conservative. It can be also extended

to an arbitrary number of velocity groups by performing only partial integration in the averaging operator (127). However, the main drawback of the method is the absence of a self-consistent non-local electric field. It is this field that limits the heat transport in the non-local limit and couples the energy groups together. Still, the method provides good results when the mean free path is known experimentally for example [25].

5 Radiation transport

The description of the transport processes in plasma in chapters 3, 4 was limited to only convection, i.e. transport by means of an ordered motion, or conduction, i.e. by a chaotic motion, of massive particles. However, strong changes of momenta of the charged particles lead to emission of the thermal radiation, which presents the third mean of energy transport. There exist two fundamental approaches to derivation of the equation of radiative transport similarly to the light itself possessing the wave and particle descriptions.

Considering its wave nature, it can be modelled as an electromagnetic wave propagating through space following the Maxwell's equations (3–4). This methodology is applied in chapter 6 for description of the coherent radiation of a laser, but it is not feasible for the thermal radiation having a broad frequency spectrum. However, the short wavelengths allow to treat the radiation as an energy continuum described by the radiometric quantities, where the final model coincides with the particle approach followed here.

The particle description is chosen to support the analogy between the radiative and heat transport of chapter 4, which is most pronounced in the case of the non-local transport and led us to formulation of the model of chapter 4.3. Within the framework of the particle theory, the radiation can be seen as an ensemble of photons, quanta of electromagnetic force. Similarly to chapter 2, they can be described by the photon distribution function $f_R = f_R(\vec{x}, \vec{n}, \nu, t)$ [75]. It determines the number of photons with frequencies in the interval $(\nu, \nu+\mathrm{d}\nu)$ in the volume $\mathrm{d}\vec{x}$ propagating along the unit vector $\vec{n}$ at position $\vec{x}$ and time t. The distinction of the formalism is given by the presence of the frequency ν instead of the velocity, which was related to the non-relativistic kinetic energy of the species, but becomes meaningless for the massless particles. The correspondence can be recovered through the relation $\vec{p}^{\,\nu} = (h\nu/c)\vec{n}$ for the momentum of a photon.

Considerations about the fundamental processes in the medium like absorption and scattering lead to reformulation of the Boltzmann equation (1) for the photons distribution [76]:

$$\frac{\partial f_R}{\partial t} + c\vec{n}\cdot\nabla f_R = q^\nu - ck^\nu f_R + c\int_0^{+\infty}\int_{4\pi} \sigma_s^\nu(\nu', \nu, \vec{n}'\cdot\vec{n}) f_R(\nu', \vec{n}') - \\ - \sigma_s^\nu(\nu, \nu', \vec{n}\cdot\vec{n}') f_R(\nu, \vec{n})\,\mathrm{d}\vec{n}'\,\mathrm{d}\nu'. \quad (131)$$

The isotropic emission is modelled through the emission function $q^\nu = q^\nu(\nu, \vec{x}, t)$ and absorption by the absorption coefficient $k^\nu = k^\nu(\nu, \vec{x}, t)$. The scattering processes are treated by the Bolzmann collision operator with the isotropic differential scattering coefficient $\sigma_s^\nu(\nu, \nu', \vec{n}\cdot\vec{n}') = \sigma_s^\nu(\nu, \nu', \vec{n}\cdot\vec{n}', \vec{x}, t)$, such that the the probability of scattering from ν to ν' and from $\vec{n}$ to $\vec{n}'$ in time $\mathrm{d}t$ and spectral interval $(\nu, \nu + \mathrm{d}\nu)$ is given by $c\sigma_s^\nu(\nu, \nu', \vec{n}\cdot\vec{n}')\,\mathrm{d}\nu\,\mathrm{d}\vec{n}\,\mathrm{d}t$.

Similarly to chapter 4.3, the specific radiation intensity $I_R^\nu = I_R^\nu(\vec{x}, \vec{n}, \nu, t)$ can be defined, which describes the infinitesimal amount of energy $\mathrm{d}E_R$ transported by radiation with the frequency in the interval $(\nu, \nu + \mathrm{d}\nu)$ along the unit vector $\vec{n}$ at

position $\vec{x}$ and time t across an infinitesimal oriented surface $\mathrm{d}\vec{S}$ in time $\mathrm{d}t$ and solid angle $\mathrm{d}\vec{n}$:

$$\mathrm{d}E_R = I_R^\nu(\vec{x},\vec{n},\nu,t)\vec{n}\cdot\mathrm{d}\vec{S}\,\mathrm{d}\vec{n}\,\mathrm{d}\nu\,\mathrm{d}t. \tag{132}$$

The relation between the distribution function and the specific intensity can be found by transforming the phase space volume to the spherical coordinates. Realizing also that the energy of a photon is $h\nu$, the formula reads:

$$I_R^\nu(\vec{x},\vec{n},\nu,t)\,\mathrm{d}\vec{x}\,\mathrm{d}\vec{n}\,\mathrm{d}\nu = h\nu c f_R(\vec{x},\vec{p}^{\,\nu},t)\,\mathrm{d}\vec{x}\,\mathrm{d}\vec{p}^{\,\nu} = \frac{h^4\nu^3}{c^2} f_R(\vec{x},\vec{n},\nu,t)\,\mathrm{d}\vec{x}\,\mathrm{d}\vec{n}\,\mathrm{d}\nu. \tag{133}$$

Equipped with these relations, the Boltzmann equation of radiation (131) can be rewritten for the intensity. The Boltzmann integral is further simplified for nearly isotropic media by approximation of the BGK operator of chapter 2.1.2, but the relaxation is made towards the implicitly defined angular mean of the intensity $\bar{I}_R^\nu = 1/(4\pi)\int_{4\pi} I_R^\nu\,\mathrm{d}\vec{n}$. This choice guarantees that the radiation energy is conserved as shown later. The equation of radiation transfer then reads in the form most commonly found in the literature [75]:

$$\frac{1}{c}\frac{\partial I_R^\nu}{\partial t} + \vec{n}\cdot\nabla I_R^\nu = j^\nu - k^\nu I_R^\nu + \sigma^\nu(\bar{I}_R^\nu - I_R^\nu) = -\chi^\nu I_R^\nu + j^\nu + \sigma^\nu \bar{I}_R^\nu, \tag{134}$$

where $j^\nu = h^4\nu^3/c^3 q^\nu$ is the (spectral) emissivity, σ^ν the scattering coefficient and $\chi^\nu = k^\nu + \sigma^\nu$ the total extinction coefficient.

Following this notation, the spectral radiation energy density ϵ_R^ν, radiation flux $\vec{q}_R^{\,\nu}$ and radiation pressure $\underline{\underline{P}}^{R,\nu}$ present angular moments of the intensity:

$$\epsilon_R^\nu = \frac{1}{c}\int_{4\pi} I_R^\nu\,\mathrm{d}\vec{n}, \qquad \vec{q}_R^{\,\nu} = \int_{4\pi} I_R^\nu \vec{n}\,\mathrm{d}\vec{n}, \qquad \underline{\underline{P}}^{R,\nu} = \frac{1}{c}\int_{4\pi} I_R^\nu \vec{n}\vec{n}\,\mathrm{d}\vec{n}. \tag{135}$$

An analogy can be seen here with the velocity moments of the distribution function elaborated in chapter 2.2. The difference is given by the fact that the velocity of propagation is assumed to be constant. Practically, it can be reasoned that way the refractive index in the X-ray range, which is mostly spectrally covered by the high-temperature laser plasma [77], are close to the vacuum values in the coronal region. In contrast, the transport is dominated by many subsequent absorptions and reemissions in the dense regions rather than the behaviour of a single photon [78]. Therefore, the velocity of photons and the related transient term in the radiation transfer equation (134) are of an lesser importance here. Furthermore, the transition to the fluid reference frame is not performed as the mean velocities in the hydrodynamics were assumed non-relativistic, i.e. $|\vec{u}| \ll c$.

Integration of (134) over all solid angles yields the zeroth angular moment equation for the radiation energy:

$$\frac{\partial \epsilon_R^\nu}{\partial t} + \nabla\cdot\vec{q}_R^{\,\nu} = 4\pi j^\nu - c k^\nu \epsilon_R^\nu = -g_R^\nu. \tag{136}$$

Similarly to the energy conservation equation for massive particles (74), it has form

of a conservation law, where an interaction term appears on the right-hand-side of the equation. Consistently with other species, this term provides coupling with the electron distribution function, where the emission and absorption processes symmetrically exchange the energy, so the total energy is conserved. Analogously, the first angular moment of (134) provides the equation for the radiation flux in the form:

$$\frac{1}{c^2}\frac{\partial \vec{q}_R^{\,\nu}}{\partial t} + \nabla \cdot \underline{\underline{P}}^{R,\nu} = -\frac{\chi}{c}\vec{q}_R^{\,\nu} = -\vec{g}_R^{\,\nu}, \tag{137}$$

where the momentum exchange term appears on the right-hand-side for coupling with the equation of electron momentum (73).

In order to simplify the equation of radiative transfer (134) even further, the source spectrum is approximated by the gray body emission, i.e. the black body emission reduced by the opacity of the medium. This is a great simplification, because the matter is not in an equilibrium with the radiation in general and the source function $S^\nu = j^\nu/k^\nu$ is not known a priori [75]. However, following this approximation under the assumption that the physical system is not far from the LTE regime, the gray body radiative transfer equation for the total quantities becomes:

$$\frac{1}{c}\frac{\partial I_R}{\partial t} + \vec{n}\cdot\nabla I_R = \rho\kappa_P\left(\frac{\sigma_{SB}}{\pi}T_e^4 - I_R\right) + \sigma_P\left(\bar{I}_R - I_R\right), \tag{138}$$

where σ_{SB} is the Stefan–Boltzmann constant, $I_R = \int_0^{+\infty} I_R^\nu \,\mathrm{d}\nu$ is the (total) radiation intensity, κ_P the Planck specific opacity and σ_P the (total) scattering coefficient. Here, the mean opacities were used, which are defined as follows:

$$\rho\kappa_P = S_B^{-1}\int_0^{+\infty} k^\nu S_B^\nu \,\mathrm{d}\nu, \qquad \sigma_P = S_B^{-1}\int_0^{+\infty} \sigma^\nu S_B^\nu \,\mathrm{d}\nu, \tag{139}$$

where $S_B^\nu = S_B^\nu(\nu)$ represents the Planck's law of radiation and $S_B = \sigma_{SB}/\pi T_e^4$ the Stefan–Boltzmann law for the total emission.

As shown in the chapter dedicated to the radiation diffusion 5.1, the averaging procedure (139) is not the only one. Essentially, it depends on the regime of transport how the averaging should be performed. In the optically thin limit, $k^\nu L \ll 1$ holds as it takes a photon a long distance to get absorbed. The gradient term on the left-hand-side of (134) dominates over the right-hand-side and the intensity is only weakly attenuated like $\sim \exp(-k^\nu s)$, where s is the path integral. The Planck averaging is then justified. However, the diffusion limit $k^\nu L \gg 1$ leads to a strong coupling between the emission and absorption and the Rosseland averaging of chapter 5.1 will be more appropriate. This problem is tackled by splitting the transport to more energy groups, which is known as the multi-group transport, or definition of an transport conditions dependent averaging process [79].

5.1 Radiation diffusion

Similarly to the velocity moments of the electron distribution function, the system (136–137) is not closed. There are still three unknowns ϵ_R^ν, $\vec{q}_R^{\,\nu}$ and $\underline{\underline{P}}^{R,\nu}$ for all spectral

frequencies. It remains also here to define an appropriate closure relation. In the diffusion limit $k^\nu L \gg 1$, the photons perform only close random walks in the medium and the radiation can be considered nearly isotropic. In an analogy to chapter 4.1, the intensity is expanded in the Legendre polynomials and the small parameter $(k^\nu)^{-1}$ to the first term:

$$I_R^\nu = I_0^\nu + \mu(k^\nu)^{-1} I_1^\nu, \tag{140}$$

where $\mu = \cos(\varphi)$ is the directional cosine for the polar angle φ from the z axis. The solution for I_0^ν is found from the transport equation (134) immediately, since all terms multiplied by the small parameter can be neglected and only the source function remains [80]. Having the zeroth approximation, the first one is obtained when I_0^ν is inserted instead of the unknown intensity, so the solution reads:

$$I_0^\nu = S^\nu, \qquad I_1^\nu = -\frac{\partial}{\partial z} S^\nu. \tag{141}$$

Substitution of the solution to the definitions of the angular moments (135) gives:

$$\epsilon_R^\nu = \frac{4\pi}{c} S^\nu, \qquad \vec{q}_R^\nu = -\frac{4\pi}{3\chi^\nu} \nabla S^\nu, \qquad \underline{\underline{P}}^{R,\nu} = \frac{4\pi}{3c} S^\nu \underline{\underline{I}} = \frac{1}{3} \epsilon_R^\nu \underline{\underline{I}}. \tag{142}$$

The procedure led to the Eddington's approximation of the transport, where the radiation pressure tensor is isotropic and given by the value of the energy density.

The equation of diffusion is obtained by insertion of the flux (142) to the energy equation (136), which yields:

$$\frac{\partial \epsilon_R^\nu}{\partial t} - \nabla \cdot \left(f_R^{lim} \frac{c}{3\chi^\nu} \nabla \epsilon_R \right) = 4\pi j^\nu - c k^\nu \epsilon_R^\nu. \tag{143}$$

The factor $f_R^{lim} = f_R^{lim}(Kn_R)$ is the flux limiter depending on the radiation Knudsen number $Kn_R = |\nabla \epsilon_R|/(k^\nu \epsilon_R)$ [81]. In the diffusion limit $Kn_R \to 0$, it must converge to the unity. However, it should attain values of $3/Kn_R$ in the free streaming limit, i.e. $Kn_R \to +\infty$. The reason is that this value eliminates the gradient term in the diffusion operator of (143) and changes the whole equation to a hyperbolic wave equation for ϵ_R^ν. Conceptually, this is a similar approach to the flux limiting performed in chapter 4.1.2. There exist numerous formulae in the literature for the definition of the limiter. As the most common can be considered the "sum" flux limiter, the limiter of Larsen [82], Levermore and Pomraning [83] or Minerbo [84], which are defined as follows respectively:

$$f_R^{\text{sum}} = 1/(1 + Kn_R/3), \qquad f_R^{\text{Larsen}} = (1 + (Kn_R/3)^n)^{-1/n} \qquad n \in \mathbb{R}^+, \tag{144}$$

$$f_R^{\text{LP}} = \frac{2 + Kn_R}{2 + Kn_R + Kn_R^2/3}, \qquad f_R^{\text{Minerbo}} = \begin{cases} \frac{2}{1+\sqrt{1+\frac{4}{3}Kn_R^2}} & Kn_R \leq 3/2 \\ \frac{3}{1+Kn_R+\sqrt{1+2Kn_R}} & Kn_R > 3/2 \end{cases}, \tag{145}$$

All of them are based on different assumptions and their description is beyond the

scope of this text. A better insight is provided in chapter 5.2 by relating to a different method, the variable Eddington factor. However, the variety of the formulations shows already the inconsistency of the diffusion model, which cannot model the non-local optically thin regime correctly.

Finally, the diffusion equation (143) can be simplified to the gray body approximation by integration over the frequencies:

$$\frac{\partial \epsilon_R}{\partial t} - \nabla \cdot \left(f_R^{lim} \frac{c}{3\rho\kappa_R} \nabla \epsilon_R \right) = c\rho\kappa_P (a_R T_e^4 - \epsilon_R), \tag{146}$$

where $a_R = 4\sigma_{SB}/c$ presents the radiation constant. The scattering opacity can be included in principle, but laser plasmas are typically dominated by the absorption processes [85, 78]. The Rosseland opacity κ_R is calculated as:

$$(\rho\kappa_R)^{-1} = \left(\frac{\partial S_B}{\partial T_e} \right)^{-1} \int_0^{+\infty} (k^\nu)^{-1} \frac{\partial S_B^\nu}{\partial T_e} \, \mathrm{d}\nu. \tag{147}$$

This kind of averaging procedure originates from the equilibrium diffusion approximation, where the temperatures of the radiation and matter are approximately the same, i.e. $T_R \approx T_e$, where the radiation temperature is defined as $\epsilon_R = a_R T_R^4$. The diffusion flux (142) is then given only by the gradient of the source, so the intensity reads [76]:

$$I_R^\nu = S^\nu - \frac{1}{\chi^\nu} \frac{\partial S^\nu}{\partial T_e} \vec{n} \cdot \nabla T_e. \tag{148}$$

The gray body approximation crudely simplifies the transport, but provides the first quantitative estimate for many radiation-hydrodynamic codes [86] and solution of the coupled non-linear radiation–diffusion problem (146),(74) is non-trivial numerically [87, 81]. Radiative shocks may propagate in the medium and exactly the intermediate regime of transport is attained [85].

5.2 Angular moments method

A problem of the diffusion treatment of the radiate transfer was inability to described optically thin regime self-consistently, which led many authors to proposition of various flux limiters to at least crudely approximate the non-locality of the transport. However, the diffusion equations still possesses the infinite signal velocity of the radiation and parabolic nature of the differential operators.

The basic improvement of the model is generalization of the derivation of the diffusion theory performed in the previous chapter. The Legendre expansion method is followed until the closure relation for the pressure tensor is obtained in (142). Rather than taking the definition of the radiation flux directly, only the closure relation is

inserted to the system (136–135), which yields:

$$\frac{\partial \epsilon_R^\nu}{\partial t} + \nabla \cdot \vec{q}_R^\nu = ck^\nu \left(\frac{4\pi}{c} S^\nu - \epsilon_R^\nu \right), \tag{149}$$

$$\frac{1}{c} \frac{\partial \vec{q}_R^\nu}{\partial t} + c\nabla(f_E \epsilon^\nu) = -\chi \vec{q}_R^\nu, \tag{150}$$

where $f_E = |\underline{\underline{P}}^{R,\nu}|/\epsilon^\nu$ is the variable Eddington factor, which reflects anisotropy of the transport. The formulation of the closure is identical with the formula (142) for the value $f_E = 1/3$ defining the method known as P1 approximation [82]. This provides already the simplest non-local model of radiative transfer, as the system is hyperbolic and combination of the equations gives a single wave equation for one of the quantities, ignoring the right-hand-side for the moment. However, it is apparent that the velocity of propagation is $c/\sqrt{3} \doteq 0.58c$, which is far from the correct speed of light. A simple improvement is scaling the velocity in the first term of (150) by one third as well, which gives the correct velocity of the transport, but leads to excessive attenuation in the optically thin limit [88]. In principle, the value of f_E should be within the interval $(1/3, 1)$ and numerous interpolating formulas were proposed [82]. For example, a simple yet popular expression is $f_E = 1/3 + 2/3(|\vec{q}_R|/(c\epsilon_R))^2$ [89].

It cannot remain unnoticed that there exists a relation between the flux-limiters and the variable Eddigton factor [90]. Based on fundamental properties of the pressure tensor and existence of symmetries due to numerical construction of the schemes for example, an improved prescription of the pressure tensor is given (for the total radiation for simplicity):

$$\underline{\underline{P}}^R = \left(\frac{1}{2}(1 - f_E)\underline{\underline{I}} + \frac{1}{2}(3f_E - 1)\frac{\nabla\epsilon_R \nabla\epsilon_R}{|\nabla\epsilon_R|^2} \right) \epsilon_R. \tag{151}$$

The flux limiter and the Eddington factor are related based on implicit constraints between $\vec{q}_R$ and $\underline{\underline{P}}^R$ by:

$$f_E = \frac{f_R^{lim}}{3} + \frac{(f_R^{lim})^2}{9} Kn_R^2. \tag{152}$$

A method of particular interest is the one proposed by Minerbo [84]. The idea was that the ensemble is close to the Maxwell–Boltzmann distribution and entropy is maximized. It must be noted that this concept is applicable on both, fermionic and bosonic, species, which attain Maxwell–Boltzmann statistics in the high velocity limit, so this method was also applied in the electron heat transport in chapter 4.2. The Eddington factor then reads:

$$f_E^{\text{Minerbo}} = \begin{cases} \frac{1}{3} & 0 \leq \frac{|\vec{q}_R|}{c\epsilon_R} \leq \frac{1}{3} \\ \frac{1}{2}\left(1 - \left(\frac{|\vec{q}_R|}{c\epsilon_R}\right)\right)^2 + \left(\frac{|\vec{q}_R|}{c\epsilon_R}\right)^2 & \frac{1}{3} < \frac{|\vec{q}_R|}{c\epsilon_R} \leq 1 \end{cases}, \tag{153}$$

where a cut-off for low anisotropies is made, since it was believed that the value should not be lower than 1/3, but other authors suggest that this is not a true physical

requirement [82].

As a final remark, it should be noted that the angular moments method can be extended to an arbitrary order, which is known as the P_N method. However, there exist multiple variants depending on the closure relation for the last angular moment [76].

5.3 Discrete ordinates method

In addition to the angular moments method presented in chapter 5.2, there exists another large family of methods known as the discrete ordinates method or S_N method. Unlike the P_N methods, where a series of coupled equations for the Cartesian tensors of an increasing order, the S_N methods give freedom in the choice of the angular discretization and the structure of the solved equations remains identical. They are based on the work of Chadrasekhar [91], but became widely used later due to Pomraning [76].

In essence, the method is based on the approximation of the angular integral over the unit sphere as follows:

$$\frac{1}{4\pi}\int_{4\pi} I_R^\nu(\vec{n}) \approx \sum_i \Psi_i I_R^\nu(\vec{n}_i) = \sum_i \Psi_i (\mathbf{I}_R^\nu)_i, \tag{154}$$

where Ψ_i are weights of the quadrature, $\vec{n}_i$ are its abscissae and $(\mathbf{I}_R^\nu)_i$ are values of the intensity along the discrete directions (ordinates). The weights must satisfy at least the conditions of partitioning of the unity and symmetry, i.e. $\sum_i \Psi_i = 1$ and $\sum_i \Psi_i \vec{n}_i = 0$. The equation of radiative transfer (134) after the substitution splits to the series of equations:

$$\frac{1}{c}\frac{\partial}{\partial t}(\mathbf{I}_R^\nu)_i + \vec{n}_i \cdot \nabla(\mathbf{I}_R^\nu)_i = j^\nu + \sigma_s^\nu \bar{\mathbf{I}}_R^\nu - \chi^\nu(\mathbf{I}_R^\nu)_i. \tag{155}$$

The function $\bar{\mathbf{I}}_R^\nu = \sum_i \Psi_i (\mathbf{I}_R^\nu)_i$ is the discrete angular mean of the intensity.

The linear system of equations is solved numerically in an explicit manner classically, where the domain is swept by the discrete rays, i.e. the characteristics of the hyperbolic equation (155). However, a problem arise for the laser plasma, where the spatial scales are minuscule and the radiation crosses the domain quickly. Rather than the transient transport, the steady state transfer is modelled, but strong coupling with the matter may exist. Therefore, it was proposed in [92] to solve an implicit set of equations for the radiation and matter, where the source function is expanded to the Taylor series in temperature $S^\nu = S_A^\nu T_e + S_b^\nu$, which enables the implicit coupling.

Another problem of the classical models was the locking phenomenon, where the methods were unable to treat the diffusive regime correctly and infeasible number of cells was needed to resolve the mean free path of photons $\lambda_R = (\rho\kappa_P)^{-1}$ [93]. This remedy was solved with the advent of the high-order discontinuous Galerkin (DG) methods effectively [94, 92, 74].

Finally, the method traditionally suffered from the ray effects, i.e. artificial effects originating from the fact that preferred directions of the quadrature exist in space [95, 96]. An answer to this issue can be application of the angular finite element method, which enables the local refinement techniques to be employed straightforwardly [97].

6 Laser absorption

Laser absorption has a major role in the laser plasma modelling as it presents the main driving force. Similarly to the kinetic theory of chapter 2, the interaction of the laser radiation with plasma can be divided to collisional and collective effects [32]. The former originates from an interaction of a single particle of the medium with the incoming radiation, while the latter is given by a resonant excitation of the collective fields. For dense plasmas and moderate intensities of the laser and/or rather short wavelength of the laser, the dominant mechanism of the laser–plasma interaction is the collisional absorption. More specifically, the limit is about the value $I_L\lambda_L^2 < 1 \cdot 10^{15}\,\mathrm{W/cm^2}\mu\mathrm{m}^2$, where I_L is the intensity of the laser and λ_L its wavelength [98]. For higher intensities or longer wavelengths than the given value, the resonance absorption is dominant and other collective effects may contribute significantly like parametric instabilities or Landau damping.

In order to understand the collisional absorption for moderate intensities of the laser, the linear model of the plasma response is sufficient as the distribution function is not distorted significantly. Essentially, the description of motion of a single particle provides the full picture of interaction as already stated. For this purpose, the equation of motion for a single electron in the electric field of the laser $\vec{E}$ is considered in the form:

$$m_e \frac{\mathrm{d}\vec{v}_e}{\mathrm{d}t} = -e\vec{E} - m_e \bar{\nu}_{ei} \vec{v}_e. \tag{156}$$

The linear dumping of the oscillations, through the BGK operator with the mean electron–ion collision frequency $\bar{\lambda}_{ei}$, is applied. The ions are considered relatively cold, so their thermal velocity v_{Ti} is negligible compared to the velocity of the oscillating electrons $\vec{v}_e$. Also non-relativistic intensities of the laser are considered, so the effect of the magnetic field can be neglected in the first approximation.

The electromagnetic field of the laser is governed by the Maxwell's equations (3–4). For the purposes of the derivation, the laser radiation is approximated as a monochromatic planar wave with the angular frequency ω_L and wave vector $\vec{k}$, which has the harmonic amplitude $\sim \exp(i\vec{k} \cdot \vec{x} - i\omega_L t)$. It is also assumed that the electron is only weakly dumped and its quiver velocity is synchronous with the driving field. Insertion of the harmonic profile to (3–4) and (156) then yields:

$$i\omega_L \vec{v}_e = \frac{e}{m_e}\vec{E} + \bar{\nu}_{ei}\vec{v}_e, \tag{157}$$

$$i\vec{k} \times \vec{E} = i\omega_L \vec{B}, \tag{158}$$

$$i\vec{k} \times \vec{B} = -\frac{1}{c^2} i\omega_L \vec{E} - \mu_0 n_e e \vec{v}_e, \tag{159}$$

where the current $\vec{j} = -en_e\vec{v}_e$ is inserted simply averaging the process over an ensemble of particles provided that the interaction is linear as already stated. Multiplication of (158) by $\times\vec{k}$ and subsequent substitution of (157) and (159) gives the stationary wave

equation for the electric field:

$$(\vec{k}\cdot\vec{E})\vec{k} - \left(\vec{k}\cdot\vec{k} - \frac{\omega_L^2}{c^2} + \frac{\omega_{pe}^2}{c^2(1+i\bar{\nu}_{ei}/\omega_L)}\right)\vec{E} = 0. \tag{160}$$

The electron plasma frequency is defined classically as $\omega_{pe}^2 = e^2 n_e/(\epsilon_0 m_e)$. The wave equation gives the dispersion relation of the transverse electromagnetic waves ($\vec{k}\cdot\vec{E} = 0$) and the definition of the complex relative refractive index $\hat{n}$ as well as the dielectric constant $\hat{\varepsilon}$:

$$\hat{\varepsilon} = \hat{n}^2 = 1 - \frac{\omega_{pe}^2}{\omega_L(\omega_L + i\bar{\nu}_{ei})}, \tag{161}$$

where the relation $|\vec{k}| = \hat{n}\omega_L/c = \hat{n}k_0$ holds. It is evident from the expression that a resonance occurs when $\omega_L = \omega_{pe}$ (despite the fact that this phenomenon is not modelled correctly by the formula due to the assumptions made). In other words, the density must be smaller than the critical density:

$$n_c = \frac{m_e\varepsilon_0}{e^2}\omega_L^2 = 4\pi^2 c^2 \frac{m_e\varepsilon_0}{e^2\lambda_L^2}, \tag{162}$$

where $\lambda_L = 2\pi c/\omega_L$ is the vacuum wavelength. Beyond the critical surface where $n_e = n_c$, only evanescent field exists there, exponentially decaying on distances comparable with the penetration depth $\delta_{pen} = \lambda_L/(2\pi \mathrm{Im}\ \hat{n})$.

The resonance absorption mechanism is caused by a p-polarized laser, which has a longitudinal component of the electric field. This causes stimulation of the plasma waves near the caustic of the beam, which reach the resonance conditions at the critical plane. To see this, the dielectric approximation can be applied using the dielectric function (161). The macroscopic Gauss's law then gives the equation for the longitudinal waves:

$$0 = \nabla\cdot(\hat{\varepsilon}\vec{E}) = \hat{\varepsilon}\nabla\cdot\vec{E} + \nabla\hat{\varepsilon}\cdot\vec{E}. \tag{163}$$

It was observed that $\hat{\varepsilon}$ has a resonance at the critical point, so once the plasma waves and the corresponding longitudinal oscillations with $\nabla\cdot\vec{E} \neq 0$ are generated, the dielectric function having the values $\mathrm{Re}\ \hat{\varepsilon} \to 0$ close to the critical plane causes their resonant excitation and absorption due to the collisions (correlating with the non-zero imaginary part).

When the main absorption mechanisms are understood, the modelling within the framework of the kinetic and hydrodynamic models must be explained. As already mentioned in the chapter about the radiative transfer 5, the small dimensions of the plasma justify stationary treatment also of the laser radiation on the hydrodynamic time scales. The equation of energy conservation for the electromagnetic field (54) then misses the inertial term and only the convective and interaction parts are present. Substitution of the latter in the energy equation of the particles (50) results in the usual form of the equation, where $\partial\epsilon_\alpha^T/\partial t \sim -\nabla\cdot\vec{S}$. The contribution to the momentum equation (37) is neglected normally, since the assumption $\epsilon_{EM} \ll \epsilon_\alpha^i$ was made to guarantee dominance of the collisional effects. However, mild effects of the ponderomotive

force can be included even within the hydrodynamic description [32]. The content of the following chapters is then to present the basic methods giving the closure model for the Poynting vector $\vec{S}$.

6.1 Ray-tracing models

Modelling of laser absorption in the context of the hydrodynamic models like the one-fluid model of chapter 3.2 limits the response frequencies of the medium strongly. Unlike electrons, ions cannot swiftly react on the field local field due to their higher inertia and the center of mass system of the one-fluid model is tightly coupled with them due to their the $m_i/m_e \gg 1$ mass ratio. Moreover, the laser is typically modelled within the hydrodynamic description as only a source of energy as already reasoned, so its dynamic effects are limited. Therefore, the frequency splitting between the slowly evolving envelope and high frequency carrying wave can be made, i.e. $L \gg \lambda_L$. The electric field is then described as:

$$\vec{E} = \hat{E}(\vec{x}, t) \exp(i\Phi(\vec{x}, t)), \tag{164}$$

where $\hat{E} = \hat{E}(\vec{x}, t)$ is the aforementioned amplitude and $\Phi = \Phi(\vec{x}, t)$ is the phase. Further, the analysis of the of propagation of transverse electromagnetic waves in the plasma made in the introduction this chapter is used. Following the derivation of the system (157–159), the stationary wave equation for the transverse waves reads:

$$\nabla \times \nabla \times \vec{E} - k_0^2 \hat{n}^2 \vec{E} = 0. \tag{165}$$

Inserting the expression (164) to (165) yields:

$$(\nabla\Phi)^2 \vec{E} - (\vec{E} \cdot \nabla\Phi)\nabla\Phi - k_0^2 \hat{n}^2 \vec{E}. \tag{166}$$

Considering that $\vec{k} = \nabla\Phi$ essentially, the central term is zero for the transverse waves and the eikonal equation is obtained:

$$(\nabla\Phi)^2 = k_0^2 \hat{n}^2. \tag{167}$$

This procedure separated the phase from the amplitude and the rays in the geometric approximation follow the gradient of the phase. The phase can be also seen as a potential, where the Fermat's principle minimizes the (optical) path integral and defines the unique metric of the space [99]. The widely used ray equation can be obtained by differentiation along the path element $\mathrm{d}s$:

$$\frac{\mathrm{d}\vec{k}}{\mathrm{d}s} = \frac{1}{|\vec{k}|}(\vec{k}\nabla)\vec{k} = \frac{1}{2|\vec{k}|}\nabla|\vec{k}|^2 - \frac{\vec{k}}{|\vec{k}|} \times \nabla \times \vec{k} = \frac{1}{2|\vec{k}|}\nabla|\vec{k}|^2 - \frac{\vec{k}}{|\vec{k}|} \times \nabla \times \nabla\Phi. \tag{168}$$

The second term is evidently zero and the ray equation reads:

$$\frac{\mathrm{d}\vec{k}}{\mathrm{d}s} = k_0 \nabla\hat{n}. \tag{169}$$

Another common formulation is known as the equation of motion of the rays and can be readily obtained from the definition of the group velocity $v_g = \partial\omega/\partial|\vec{k}| = c|\nabla\Phi|/k_0$, which gives [100]:

$$\frac{\mathrm{d}^2\vec{x}_{RT}}{\mathrm{d}t^2} = \frac{\mathrm{d}\vec{v}_{RT}}{\mathrm{d}t} = \frac{c}{k_0}\frac{\mathrm{d}\nabla\Phi}{\mathrm{d}t} = \frac{c}{k_0}(\vec{v}_{RT}\cdot\nabla)\nabla\Phi = \\ = \frac{c^2}{k_0^2}(\nabla\Phi\cdot\nabla)(\nabla\Phi) = \frac{c^2}{2k_0^2}\nabla|\nabla\Phi|^2 = \frac{c^2}{2}\nabla\hat{n}^2, \quad (170)$$

where $\vec{x}_{RT}$ is the trajectory of the ray and $\vec{x}_{RT}$ its (group) velocity vector. This can be also seen as the Hamilton's equations [101]:

$$\frac{\mathrm{d}\vec{x}_{RT}}{\mathrm{d}t} = \vec{v}_{RT}, \qquad \frac{\mathrm{d}\vec{v}_{RT}}{\mathrm{d}t} = \frac{c^2}{2}\nabla\hat{n}^2, \qquad H = \frac{1}{2}((\vec{v}_{RT})^2 - c^2\hat{n}^2), \quad (171)$$

where $H = H(\vec{x}_{RT}, \vec{v}_{RT}, t)$ is the Hamiltonian of the system.

Either way, the incoming radiation is modelled as a bundle of independent rays following the density gradients, since Re $\hat{n}^2 \sim 1 - n_e/n_c$ as can be recognized from the definition (161). The common approach is then to simply replace the dielectric function by the normalized density n_e/n_c [102]. The geometric optics is then limited to the cases where Im $\hat{\varepsilon} \ll$ Re $\hat{\varepsilon}$. However, it is also possible to solve the equation (169) or (170) in the complex domain, which is known as the complex geometrical optics (CGO) [103]. It has the advantage of being able to solve the (165) behind the caustics. A fundamental problem of the methods is the missing diffraction, where a high number of the rays must be used, but artificial effects can be still noticed as the ray models the behaviour of the wave only on its axis. This led to formulation of numerous paraxial methods [104] (and the references therein). A recent method method of this kind is the paraxial complex geometrical optics (PCGO), which expands the eikonal equation (167) around the central ray in a Taylor series to describe the curvature of the wave front [101]. This results in an additional Riccati type ordinary differential equation, which must be solved along the ray, but reduces the number of rays greatly. Rather then a simple average, the energy deposition is calculated from a mesh-less interpolation of the Gaussian beamlets [73].

Finally, the absorption rate must be specified. The phase Φ is integrated along the characteristics $\vec{x}_{RT} = \int \vec{v}_{RT}\,\mathrm{d}t$ provided they are known already:

$$\Phi(\vec{x}, t) = \pm\int_{\vec{x}_0}^{\vec{x}} \vec{k}\,\mathrm{d}\vec{x}' - \omega t = \pm k_0\int_{s_0}^{s}\hat{n}\,\mathrm{d}s - \omega t. \quad (172)$$

The Wentzel–Kramers–Brillouin (WKB) solution for the Helmholtz equation (165) is obtained in the form [32]:

$$\vec{E} = \left(\frac{Q(s_0)}{\hat{n}(s)Q(s)}\right)^{1/2}\left(\hat{E}_+\exp\left(ik_0\int_{s_0}^{s}\hat{n}\,\mathrm{d}s\right) + \hat{E}_+\exp\left(ik_0\int_{s_0}^{s}\hat{n}\,\mathrm{d}s\right)\right)\exp\left(-i\omega t\right), \quad (173)$$

where $Q = Q(s)$ is the "cross-section" of the beam (a function of the path). Substitution

to (165) reveals that $\mathrm{d}Q/\,\mathrm{d}s = 0$, i.e. the beam is not attenuated by gradual reflections, when the second derivatives are neglected compared to the first. The conditions are precisely:

$$\frac{\mathrm{d}^2\hat{E}}{\mathrm{d}s^2} \ll k_0\hat{E}\,\frac{\mathrm{d}\hat{n}}{\mathrm{d}s}\,, \qquad \frac{\mathrm{d}^2\hat{E}}{\mathrm{d}s^2} \ll k_0\hat{n}\,\frac{\mathrm{d}\hat{E}}{\mathrm{d}s}\,, \quad \Rightarrow \quad \frac{\mathrm{d}\hat{E}}{\mathrm{d}s} \ll \hat{n}\hat{E}, \tag{174}$$

where $\hat{E}(s) = (Q(s_0)/(\hat{n}(s)Q(s)))^{1/2}$. This relation can be translated to the refractive indices as $|\,\mathrm{d}\hat{n}/\,\mathrm{d}s| \ll |\hat{n}|^2$. However, this criterion cannot be satisfied near the critical plane, where rather the opposite is true. Hence, WKB approximation can never self-consistently describe the interaction in the vicinity of the critical density [98].

The intensity of the ray is taken as the average magnitude of the Poynting vector, which gives after substitution of (173) the relation:

$$I_L(s) = \frac{1}{\mu_0}\overline{|\vec{E}\times\vec{B}|} = \frac{1}{2}\varepsilon_0 c\hat{n}_r\hat{E}\hat{E}^*\exp(-2k_0\int_{s_0}^{s}\hat{n}_i\,\mathrm{d}s') = I(s_0)\exp(-\int_{s_0}^{s}\alpha_L\,\mathrm{d}s'), \tag{175}$$

where $\hat{n}_r = \mathrm{Re}\ \hat{n}$, $\hat{n}_i = \mathrm{Im}\ \hat{n}$ and the upper line means averaging over a period and the asterisk denotes the complex conjugate. Finally, the absorption coefficient is $\alpha_L = -2k_0\mathrm{Im}\ \hat{n}$. In other words, the intensity of the ray follows the differential Beer–Lambert law in the form:

$$\frac{\mathrm{d}I_L}{\mathrm{d}s} = \nabla\cdot\overline{\vec{S}} = -\alpha_L I_L. \tag{176}$$

This means that the intensity carried by a ray is linearly attenuated along its path.

6.2 Stationary Maxwell's equations

It was recognized in chapter 6.1 that the optical approximation is mostly valid in the coronal region, where the densities of the plasma are low and vary slowly compared to the wavelength of the laser. However, it is unable to self-consistenly model the vicinity of the critical plane, where $|\nabla\hat{\varepsilon}|/|\hat{\varepsilon}| \gg k_0\hat{n}_r$ always holds. The problem is circumvented by formulation of an empirical factor for reflection and absorption at the critical density typically [105]. An alternative approach presents the wave optics, which relies on the fundamental principles of electrodynamics without retreating to strongly simplifying assumptions of optics. On the other hand, the differential treatment of the stationary wave equation (165) is prohibited by the requirement on the spatial step, where a single wavelength $\lambda_L/\hat{n}_r$ must be resolved classically. Moreover, the microscopic conditions for the electromagnetic fields are not known as the hydrodynamic model requires only the period averaged value of the Poynting vector. Therefore, the phase of the field is not involved in the model and can be considered as an independent unknown.

These considerations led to development of the approach based on the stationary Maxwell's equations (SME) [106, 107]. Rather than solving the Helmholtz equation (165) directly, the method relies on the Maxwell's equations (3–4) rewritten for the

harmonic waves (following the introduction of chapter 6) in 1D:

$$H' + ik_0\hat{n}^2 E = 0 \ , \tag{177}$$

$$E' + ik_0 H = 0 \ , \tag{178}$$

where the prime denotes the spatial derivative. It must be noted that the Gaussian system of units is used here in accordance with the references [106, 107]. The key idea of the method is then decomposition of the field to the incoming wave $P = P(x)$ (from the left hand side without the loss of generality) and outgoing (reflected) wave $R = R(x)$:

$$E = P + R, \qquad H = \hat{n}(R - P). \tag{179}$$

Substitution to the system (177–178) yields the governing equations for both waves:

$$P' = +ik_0\hat{n}P - \frac{\hat{n}'}{2\hat{n}}(P - R) \ , \tag{180}$$

$$R' = -ik_0\hat{n}R + \frac{\hat{n}'}{2\hat{n}}(P - R). \tag{181}$$

The next step is definition of the (complex) reflection coefficient $V(x) = R(x)/P(x)$. This procedure implicitly assumes that the incoming wave P does not vanish, but we are interested only in such solutions. Reformulation of the coupled system (180–181) to the new primary variables P and V yields:

$$V' = -2ik_0\hat{n}V + \frac{\hat{n}'}{2\hat{n}}(1 - V^2) \ , \tag{182}$$

$$P' = +ik_0\hat{n}P - \frac{\hat{n}'}{2\hat{n}}P(1 - V). \tag{183}$$

The solution of the given system is equivalent with the wave solution in terms of E and B as back substitution can be made. However, the complex amplitude of the incoming wave P can be reduced to the real function A proportional to the magnitude of the incoming wave $\sim |\tilde{P}|^2 = PP^*$. The governing equation then reads:

$$A' = -2k_0\hat{n}_i A - \mathrm{Re}\left(\frac{\hat{n}'}{\hat{n}}(1 - V)\right)A. \tag{184}$$

The new formulation in terms of A and V is no longer equivalent to the original system as the piece of information about the phase is lost in the case of A. However, the solution fully suffices for the purposes of the hydrodynamic simulations, where only the Poynting vector $|\vec{S}| \sim A$ is needed. In particular, the expression for the Poynting vector reads [107]:

$$|\vec{S}| = A(k_0\hat{n}(|\tilde{V}|^2 - 1) - 2k_0\hat{n}_i \mathrm{Im}\ V). \tag{185}$$

It can be recognized that the Beer–Lambert law (175) is obtained in the limit $|\hat{n}'/\hat{n}| \ll k_0|\hat{n}|$. Therefore, the theory is fully consistent with the WKB approximation, but the additional terms represent the exact gradual reflections of the wave and the theory then holds even in the vicinity of the critical plane. As the derivative of the

refractive index goes to infinity, the reflection coefficient V closes to the unity, i.e. the wave is completely reflected at the critical point.

The cornerstone of the method is the observation that the equation for the reflection coefficient (182) is decoupled from P or A and can be solved independently. After the solution for V is known, the complementary equation for A or P can be solved. Unlike the classical methods for the Maxwell's equations, the boundary conditions are known even in the macroscopic description, since the reflection coefficient can be set $V \approx 0$ several penetration depths δ_{pen} behind the critical plane. The other boundary condition is given by the known magnitude of the intensity of the laser outside the domain, i.e. $|\vec{S}| = I_L$ at the outer boundary.

Another important advantage of the method is the fact that it can be directly reformulated for an oblique incidence of the of the laser. The structure of the equations remains nearly the same and the refractive index is replaced by the effective value [108]. As the approach is fully wave-based, the resonance absorption in the dielectric approximation is naturally included in the solution, but it is not modelled directly as only the perpendicular components are simulated.

The equation for the reflection coefficient (182) presents a non-linear ordinary differential equation of the Riccati type. We proposed two possible approaches to its solution in [107]. The first one is semi-analytic, where the equation is integrated over a computational cell, where the density profile is approximated by a piecewise constant profile [109, 110, 60] or later extended to arbitrary profile as we proposed in [107]. The advantage of the semi-analytic treatment is the fact it is not principally limited by the constrained on the resolution of the wavelength $\lambda_L/\hat{n}_r$, so it can be readily applied even in the coronal plasma. However, the solution itself is still oscillatory, so aliasing effects may be encountered, but strongly rarefied coronal plasma can be considered nearly transparent and a cut-off can be applied [60]. Another fundamental approach is the differential solution of the equation or an equivalent set of linear first order equations not asimilar to the system (182–183). We proposed to use the high-order finite element method for this purpose, where an arbitrary order of convergence can be attained depending on the choice of the basis only [107]. This is in a contrast with the semi-analytic method, where only the second order convergence is attained.

Concluding the chapter of laser absorption, the methods of geometrical optics and wave optics can be seen as mutually complementary. The former is ideally suited for modelling of the absorption in the far coronal plasma, where the dynamics of the plasma involves remarkably longer length scales that the wavelength of the laser, i.e. $L \gg \lambda_L/\hat{n}_r$. On the other hand, it fails to describe the vicinity of the critical plane, where abrupt heating of the plasma occurs and highly non-local electrons are produced [111, 112]. The coupling of the laser and non-local transport of these is crucial for the fusion research for example [113]. The wave optics provides an answer to this problem by modelling the processes self-consistently, but its inherent complexity makes full simulations of the wave propagation for multi-dimensional hydrodynamic codes infeasible. The method based on the stationary Maxwell's equations then presents an attractive option for solution near the critical point. A combination of the geometrical and wave approach was then proposed in the literature [114], but remains a topic of the future work to accommodate for the SME method, where its benefits could be utilized.

7 Contributions of the author

The theoretical background and the current status of the research of the non-local transport in many aspects was presented the previous chapters. However, the topics cannot be considered exhausted even by far. There remain unsolved problems and unexplored frontiers of the non-local transport research. This motivated us to continue in this endeavour and contribute to the theoretical understanding of the non-local effect.

Our work was already referred where appropriate, but no compact summary was given. This is the subject of this chapter to map the scientific efforts made in the past years. As the non-local transport is rich on the physical mechanisms involved, also our research can be divided to more than one category. Therefore, there are presented four chapters schematically sorting the scientific publications. Chapter 7.1 is dedicated to the hydrodynamic description and simulation of the plasma, chapter 7.2 follows with the non-local electron heat transport model extending the discussion of chapter 4. The chapter about the non-local radiation transport 7.3 follows the lines of chapter 5 and the laser absorption modelling of chapter 7.4 extends the methods of chapter 6.

7.1 Lagrangian hydrodynamics

Despite the fact that hydrodynamics in general and Lagrangian hydrodynamics with no exception is a well-established discipline, the classical numerical schemes rather rely on the low order discretizations typically. This correlates with the macroscopic physical phenomena typically studied, but makes them inappropriate for modelling of the small scale effect important for the description of the non-local transport. Moreover, the rigid structure of the classical simulation codes makes integration and testing of new physical models difficult.

For this reasons, the development of our new multi-dimensional hydrodynamic code started as reviewed in the proceedings [115]. This new simulation code named Plasma Euler and Transport Equations version 2 (PETE2) was preceded by PETE, which is an older 1D code originally developed by M. Holec as part of [74] and partially described in [92]. Further extensions of PETE were implemented to investigate the radiation transport effects and are detailed in chapter 7.3. Returning to PETE2, it essentially relies on curvilinear high-order finite elements. This modern numerical approach provides the code flexibility in the choice of the polynomial order of the elements and connected spatial order of convergence of the method. Moreover, it is easily extensible and scalable due to use of the MFEM library [116].

Fundamentally, the numerical code is based on the two-temperature Lagrangian one-fluid model of chapters 3.2 and 3.3, but extended by additional models of other

chapters. The solved system of equations reads:

$$\frac{\mathrm{D}\rho}{\mathrm{D}t} = -\rho\nabla\cdot\vec{u}, \tag{186}$$

$$\rho\frac{\mathrm{D}\vec{u}}{\mathrm{D}t} = -\nabla\cdot(\underline{\underline{P}}^e + \underline{\underline{P}}^i), \tag{187}$$

$$\rho c_{Ve}\frac{\mathrm{D}T_e}{\mathrm{D}t} = -\underline{\underline{P}}^e : \nabla\vec{u} + G_{ei}(T_i - T_e) - \nabla\cdot(\vec{q}_e + \vec{S}), \tag{188}$$

$$\rho c_{Vi}\frac{\mathrm{D}T_i}{\mathrm{D}t} = -\underline{\underline{P}}^i : \nabla\vec{u} + G_{ie}(T_e - T_i), \tag{189}$$

where c_{Ve}, c_{Vi} are the specific heats. They are introduced to the model in order to tackle the classical problem of the hydrodynamic codes that the functions of internal energies $\varepsilon_e(\rho, T_e), \varepsilon_i(\rho, T_i)$ must be inverted to obtain the temperature. i.e. the inverse equation of state is evaluated. This is a time consuming iterative procedure in classical codes. Therefore, PETE2 differentiates (similarly to PETE) the term to use the temperatures as the primary variables. However, the problem of this approach is the consequent violation of energy conservation. This is circumvented by use of corrections similar to the Symmetrical Semi-Implicit (SSI) method [117], which guarantee the asymptotic conservation of energy. The equation of state is taken from the HerEOS library detailed in chapter 3.4.3.

The hydrodynamic scheme implements the high-order curvilinear finite element method [118], which has many appealing features. It conserves mass, momentum and energy numerically for arbitrary orders of the finite elements. Moreover, the thermodynamic quantities are conserved locally as their basis functions are discontinuous, which provides robustness of the scheme in treatment of propagating shocks in the medium. This discretization is also compatible in the lowest order of the elements with the compatible staggered hydrodynamics [119] used in the numerical code PALE2 that is being developed at our faculty [120, 121], which enables their interoperability. Finally, the method relies on the isoparametric elements, meaning that their spatial mapping uses the identical basis as the interpolation of the values. In other words, the elements are curvilinear, which prevents entangling of the mesh.

The electron heat flux $\vec{q}_e$ closure is provided by a diffusive model, which was covered in chapter 4.1 from the physical point of view. However, the coupled system of equations for the heat flux (109) and temperature (188) must be solved together. Instead of solving the equation for temperature, it is reformulated to the dual form for the heat fluxes, which guarantees numerical conservativity. For the purposes of numerical solution, we have developed a diffusion solver based on the mixed hybrid FEM (MHFEM) method [122]. It matches the hydrodynamic discretization perfectly and the use of the hybridization technique reduces the size of the resulting sparse matrix greatly, so the solution of the linear system is computationally inexpensive even for the high-order finite elements.

Finally, the laser absorption is modelled by the simple Beer–Lambert law (175) in the normal direction to the target. Numerically, the discontinuous Galerkin FEM (DGFEM) elements are employed with a simple upwinding [123]. However, this point constrains the applicability of the whole code to only the physical scenarios where the

spot size of the laser is significantly wider than the ablation depth as no notion of beam convergence exists. An additional model of absorption is present in the code as described in chapter 7.4, but it is also a one-dimensional model in principle. Therefore, an extension of the code by a multi-dimensional ray-tracing method, explained in chapter 6.1, is highly desirable.

The first results were obtained in 3D for ablation of an Aluminum target at the room temperature irradiated by a laser with the intensity $I_L = 1 \cdot 10^{14}\,\mathrm{W/cm^2}$ and spot size $r_L = 5\,\mu\mathrm{m}$. The simulation details can then found in the reference [115]. The situation is illustrated for the time $t = 30\,\mathrm{ps}$ in Figure 1. The deformation of the curvilinear elements is clearly visible as well as the high-order interpolation.

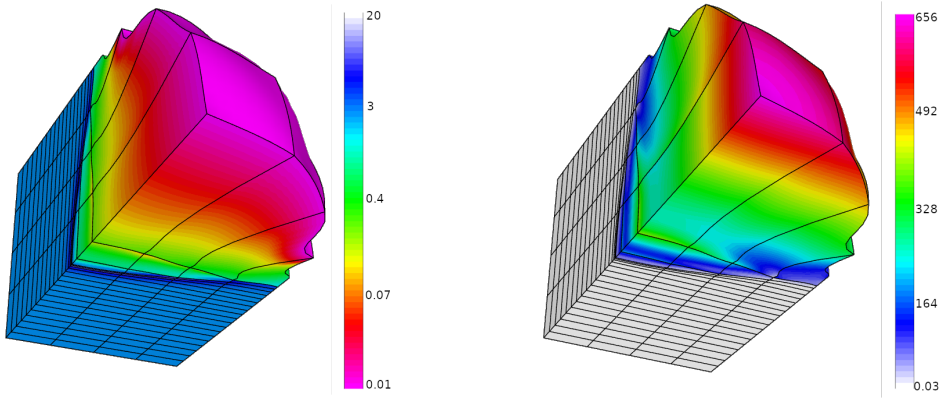

(a) Density [g/cm^3] (b) Temperature [eV]

(c) Heat flux [erg/s/cm^2] (d) Laser intensity [erg/s/cm^2]

Figure 1: The plasma profiles in the simulation of Aluminum ablation in the 3D Cartesian geometry at 30 ps. Quadratic thermodynamic and cubic kinematic finite elements were used.

Another direction of the current research is promotion of the PETE2 code to the magneto-hydrodynamic model and extension of the PALE2 code by the mechanisms of the magnetic field generation as we outlined in [124]. The mechanism of particular interest is the Biermann battery effect [125], which originates from the electron pressure term appearing in the equation of the quasi-static electric field (83). The effect on generation of the magnetic field can be seen when inserting the term to the Farraday's

law (4), which yields:

$$\frac{\partial \vec{B}}{\partial t} \sim \nabla \times \frac{\nabla p_e}{e n_e} = \frac{k_B}{e n_e} \nabla n_e \times \nabla T_e. \tag{190}$$

This implies that gigantically strong magnetic fields can be generated in laser plasma at the places where the gradients are not collinear as can happen due to (non-local) heat transport processes (see section 4) acting on top of the pure convection of the hydrodynamic model [126].

7.2 Electron non-local transport

7.2.1 Hydrodynamic closure models

The state-of-the-art hydrodynamic codes PETE and PETE2 are unique due to the fact that they are equipped with the BGK S_N non-local transport model detailed in chapter 4.3. The topic of this chapter is a short review of the closure model for the non-local electron heat transport.

We proposed the method of the BGK transport model in [19]. The identical derivation of the model as done in chapter 4.3 was presented there, but in a slightly more detailed manner. My contribution was on the side of implementation and explanation of the laser absorption code, which was already based on the stationary Maxwell's equations of chapter 6.2, but without the high-order extension, which is subject of chapter 7.4. Furthermore, it was implementation of the reference diffusion solver to PETE. Another part of my work are the numerical tests and some of the realistic simulations. Finally, it was also a critical assessment of certain parts of the model, which led to its correction.

Understanding the foundations of the model, attention can be turned to the numerical tests and comparison with other methods. One of the basic tests of the non-local transport is known as the Short–Epperlein test [56, 127]. It is an asymptotic kind of problem, which investigates the behaviour only for infinitesimal perturbations of the quantities. In particular, the temperature is perturbed as $T_e = T_e^0 + \delta T_e \cos(kx)$, where the $T_0 = 1000\,\mathrm{eV}$ and $\delta T_e = 10^{-4} T_e^0$. Other profiles are kept uniform. The average heat flux magnitude is evaluated for different values of the wave number k, which changes the regime of the transport from strongly diffusive for $k\lambda^e \ll 1$ to moderately non-local for $k\lambda^e \sim 1$. The symbol λ^e represents the thermal mean free path, but the models of transport are independent of its specific value in this test. Instead of the heat fluxes themselves, the effective heat conductivities $\kappa = |\vec{q}_e|/(kT_e)$ are assessed. The results are plotted in Figure 2. The reference profiles for the LMV model [15], AWBS [70] and the Fokker–Planck (FP) are taken from [56]. It is clear from the analysis that the BGK S_N model behaves similarly to the other simplified models, having the non-local limit $(k\lambda^e)^{-2}$. As was recognized based on a Fourier analyses, this is the case for all models based on a linear transport equation [16]. The kinetic simulations exhibit rather the dependency $\sim (k\lambda^e)^{-1}$. While being closer to the FP curve for the stronger non-local regime, the results are relatively far from it for the weak regime, where the model tends to overestimate the values of the heat flux.

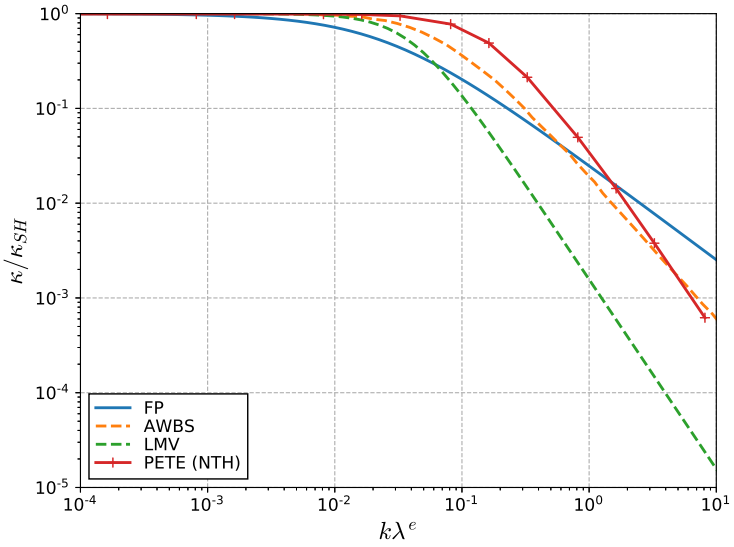

Figure 2: Effective heat conductivities normalized to the results of the diffusion theory as a function of the Knudsen number $k\lambda^e$. The curves correspond to different non-local electron transport models.

Another problem of interest, which is non-asymptotic unlike the previous one, is the hotspot relaxation problem [128]. The initially Gaussian profile of the temperature with the base value 1 keV and the maximum 5 keV is let to relax by means of the heat transport methods. As the profile non-linearly relaxes, also the regime of transport changes from highly non-local at the beginning to nearly diffusive at the end. This problem has a better relevance to real simulations and clearly shows the importance of the non-local transport modelling. The results are plotted in Figure 3 for different models of the transport closure along with the reference kinetic solution taken from [128]. At the very early stage of the simulation, the unlimited heat diffusion greatly overestimates the heat fluxes, while the flux-limited diffusion and our non-local model relatively well agree with the reference solution in temperatures. However, the fluxes show that they are departing from the reference dynamically, while the unlimited diffusion closes. The later stage shows that the heat flux limiting excessively inhibit the transport and its non-linear nature causes the "heat flux starvation", where a non-physical profile of the temperature appears. In contrast, the BGK S_N model gives smooth profiles of the temperature and very closely copies the profile of the reference. The unlimited diffusion slows down and becomes more accurate as the system transits to the diffusion regime.

Another approach to the non-local transport we proposed in [129], where the P_1 model is used as described in chapter 4.2, but the BGK operator is applied for the electron–electron collisions. An implicit numerical scheme for f_0 and $\vec{f}_1$ based on high-order finite elements is formulated and an implicit coupling with temperatures of the temperatures of the bulk electrons is made through the expansion of the equilibrium distribution as $f_M(T^{n+1}) = \partial f_M/\partial T(T^{n+1} - T^n) + f_M(T^n)$, where the upper index de-

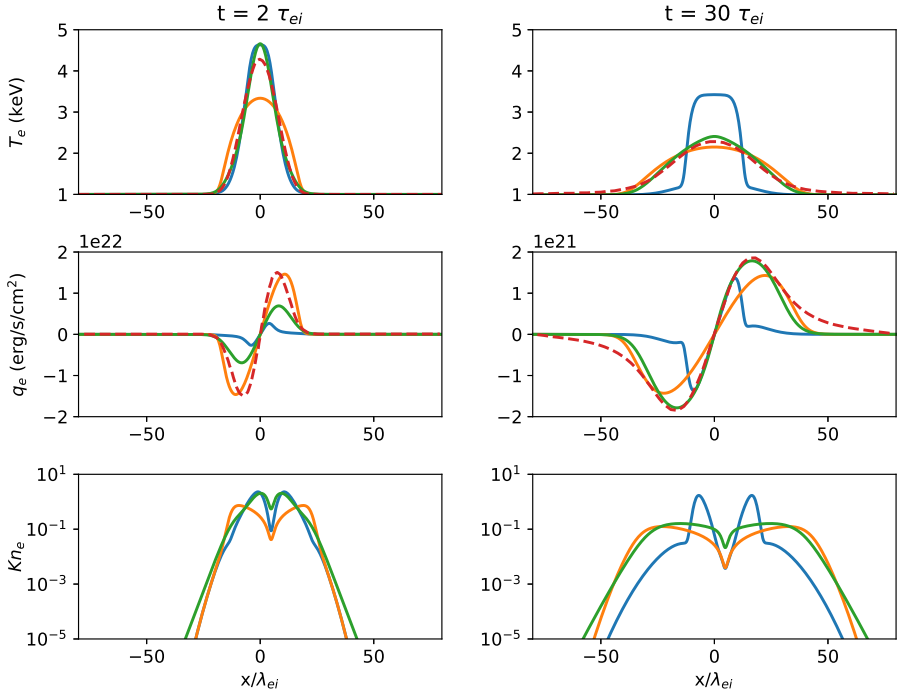

Figure 3: The hotspot relaxation problem for different models of electron heat transport at two different times. The profile of the electron temperature T_e, heat flux q_e and Knudsen number Nn_e are plotted. The curves corresponds to the following: blue – diffusion solution with $f^{lim} = 0.05$, orange – unlimited heat diffusion, green – BGK S_N non-local transport, dashed red – reference Fokker–Planck.

notes the time level. This procedure is similar to the one used for the radiative transfer in chapter 5.3. An advantage of the P_1 approach over the S_N is the existence of the stationary electric field formula (122), so the effects of the electric field on the transport can be evaluated correctly. However, a basic numerical analysis of the resulting linear system reveals that the electric field destabilizes the transport numerically even for relatively small magnitudes when treated explicitly.

7.2.2 Vlasov–Fokker–Planck–Maxwell

Our latest effort to simulate the non-local transport was made in [130], where a reduced Vlasov–Fokker–Planck–Maxwell (VFPM) code was developed, which principally solves the problem of non-local transport in the greatest detail of the methods mentioned in this chapter. In spite of the fact that the computational costs are higher than in the case of the hydrodynamic closure models, its implicit nature enables to choose the temporal step relatively long compared to the collision times $\tau_{ee} = \nu_{ee}^{-1}$.

In essence, the code solves the equations of the Cartesian expansion to the first order (63–64) with the collision operators (66–67), where the contributions C_{01} and C_{11} are neglected. The system is closed by the coupled and fully implicit Maxwell's

equations (3–4). A similarly composed method appeared in the literature for studies of non-local magnetic fields generation and inertial fusion [131, 132], but the novelty is given by the fact that the method conserves not only mass, but also energy. Moreover, its multi-dimensional construction enables 2D as well as 3D simulation. Finally, high-order finite elements are employed, implying that the method has an arbitrary order of convergence in space (depending only on their polynomial order virtually).

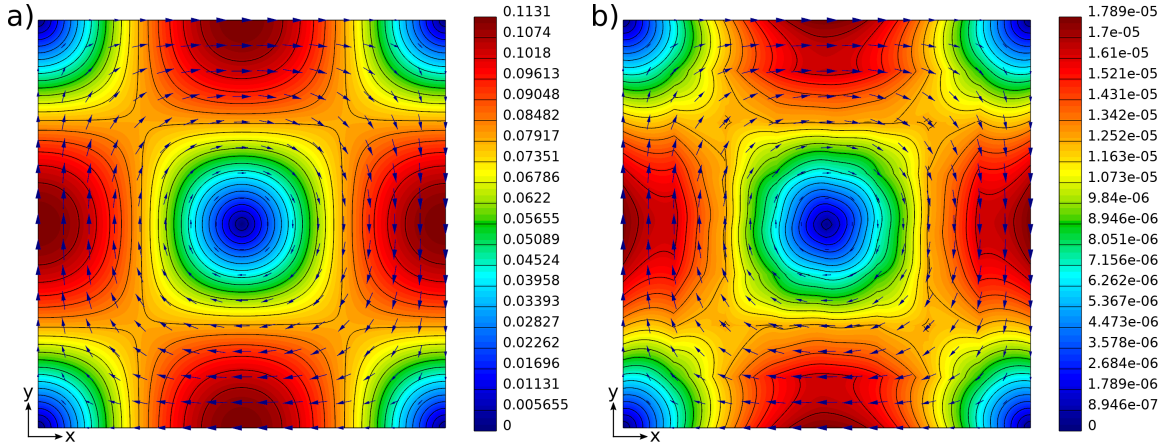

Figure 4: The total heat flux of the solution (a) and its error (b) in the problem of diffusion transport in the presence of a magnetic field. The computational mesh has 8×8 cells with the cubic finite elements and 160 velocity levels. (The values are in the normalized units).

Following the lines of chapter 2.3, the velocity moments can be elaborated and the full magneto-hydrodynamic system (72–74) is obtained with the only exception that the dynamic and kinetic pressure tensors (60) are rather scalars than tensors. It is also evident that the diffusion analysis of chapter 4.1 is fully applicable as only the first order Legendre expansion was applied (actually the tensor expansion was used for convenience). Therefore, the full Braginskii transport solution (111–112) is obtained in the diffusion limit. However, the transport coefficients are given self-consistently and there is no need of a closure model in contrast to the hydrodynamic simulations. This is also one of the numerical tests in the paper. An rectangular domain is considered with the initial conditions:

$$\tilde{n}_e(\tilde{x},\tilde{y}) = 1 + \delta\tilde{n}_e(\cos(\pi\tilde{x}/\Delta\tilde{x}) + \cos(\pi\tilde{y}/\Delta\tilde{y})), \tag{191}$$

$$\tilde{T}_e(\tilde{x},\tilde{y}) = 1 + \delta\tilde{T}_e(\cos(\pi\tilde{x}/\delta\tilde{x}) - \cos(\pi\tilde{y}/\Delta\tilde{y})), \tag{192}$$

$$\tilde{B}(\tilde{x},\tilde{y}) = \delta\tilde{B}\sin(\pi\tilde{x}/\Delta\tilde{x})\sin(\pi\tilde{y}/\Delta\tilde{y}), \tag{193}$$

where $\delta\tilde{n}_e = \delta\tilde{T}_e = \delta\tilde{B} = 10^{-3}$. Note that the values and the whole system are normalized to the initial values of temperature and density. The normalized magnetic field value represents the magnetization, i.e. the product of the electron–ion collision time and cyclotron frequency $\tilde{B} = eB/(m_e\nu_{ei})$. The size of the domain is $\Delta\tilde{x} = \Delta\tilde{y} = 10^4$, where the spatial unit is the electron–ion mean free path. The system is solved in the diffusion approximation, i.e. for stationary $\vec{f}_1$, $\vec{E}, \vec{B}$ and $f_0 = f_M$. Other

simulation details can be found in the article [130]. The solution along its error at the final time $t = 10^{-4}\tau_{ei}$ is drawn in Figure 4. The results manifest that the symmetry of the solution is maintained to a great extend and even a low number of elements with a higher polynomial order is able to capture its features precisely. Physically, the transport is dominated by the conductive term $\underline{\underline{\alpha}} \cdot \vec{j}$ and the corresponding convective heat flux $\sim 5/2 v_{Te}^2 \vec{j}$. Therefore, the flux follows the electric field lines mostly and circulates around the domain.

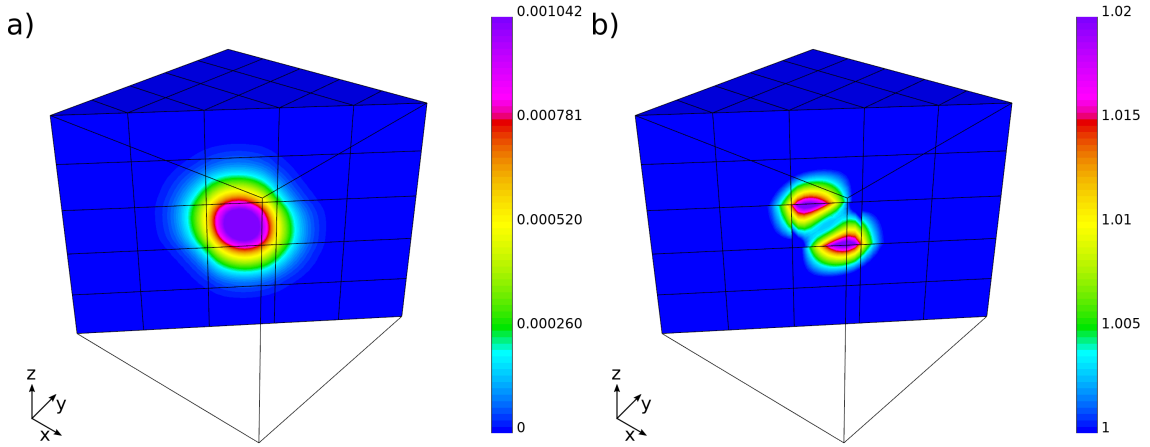

Figure 5: Magnetic field magnitude (a) and electron temperature (b) in the magnetic diffusion problem. The computational domain has $5 \times 5 \times 5$ cells with the cubic finite elements and 40 velocity levels. (The values are in the normalized units).

A similar kind of problem, but with a non-stationary magnetic field and evolving f_0, is the magnetic diffusion problem. An initially Gaussian profile of the magnetic field $\tilde{\vec{B}}(\tilde{\vec{x}}) = \delta\tilde{\vec{B}} \exp(-|\tilde{\vec{x}}|^2/\tilde{\sigma_B})$ diffuses due to the eddy currents. The solution for the magnetic field then can be obtained readily:

$$\vec{E} = \alpha\vec{j} = \frac{1}{\mu_0}\alpha\nabla \times \vec{B}, \tag{194}$$

$$\frac{\partial \vec{B}}{\partial t} = -\nabla \times \vec{E} \simeq \frac{1}{\mu_0}\alpha\Delta\vec{B} = \eta_B\Delta\vec{B}, \tag{195}$$

where α is the scalar resistivity and $\tilde{\eta}_B = \tilde{\sigma}_B$ is the normalized diffusivity of the magnetic field. The size of the domain 10^4 in the normalized units in each dimension and $\tilde{\sigma}_B = 0.15 \cdot 10^4$. The magnetic field strength is chosen $\delta\tilde{B} = 10^{-3}$ in each Cartesian component of the $\tilde{\vec{B}}$ vector. The 3D solution at the time $t = 10\tau_{ei}$ is illustrated in Figure 5. The diffusion of the magnetic field notably progressed and the Joule heating process heats the electrons. Numerically, a reasonable detail of the solution is provided despite the low number of cells and also the discontinuity of the finite elements used for the temperature is apparent.

The last, but not least, problem regards the non-local transport. As already stated, the non-locality is inherently modelled with the VFPM method. The physical scenario is similar to the hotspot problem of chapter 7.2.1, but the temperature profile

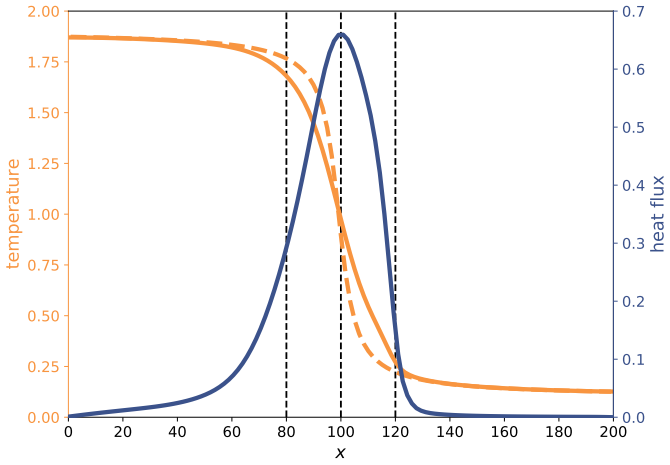

Figure 6: The electron temperature (orange) and heat flux (blue) for the heat bath problem at the final time $t = 10\tau_{ei}$. The initial profile is drawn by the dashed line. (The values are in the normalized units).

is asymmetric here. In particular, it has the transition profile:

$$\tilde{T}_e(\tilde{x}) = 1 + \delta\tilde{T}_e \frac{2}{\pi} \arctan(\tilde{x}/\tilde{\sigma}_T). \tag{196}$$

The parameters are set $\delta\tilde{T}_e = 0.9$, $\tilde{\sigma}_T = \delta\tilde{T}_e/(2Kn_e)$. The Knudsen number is chosen $Kn_e = 10^{-1}$, which corresponds to moderately strong non-local transport. The simulation is performed in 1D on the domain $\Delta\tilde{x} = 200$. The rest of the details can be found in the article [130]. The initial condition and the final solution are plotted in Figure 6. The temperature profile is smeared, but the heat flux is strongly asymmetric pointing to the non-linear regime of the transport.

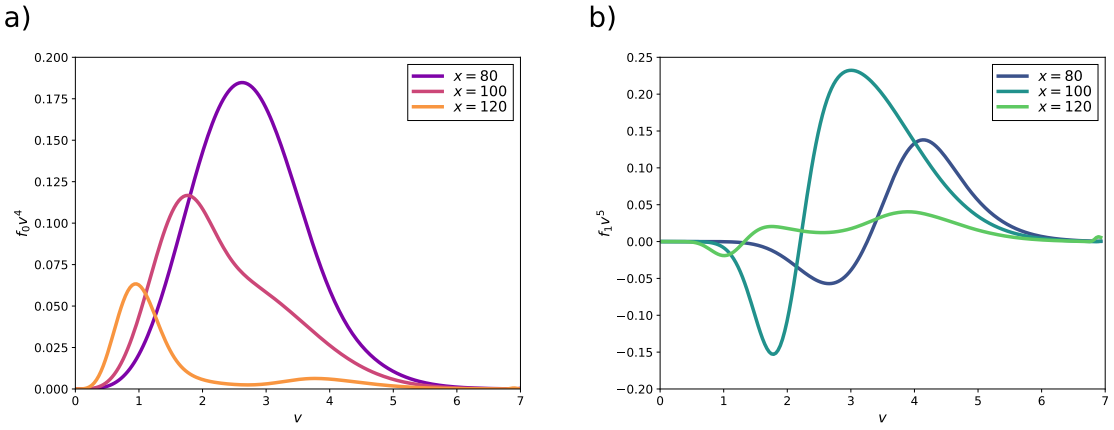

Figure 7: Energy weighted isotropic part (a) and heat flux weighted anisotropic part (b) of the distribution function in the heat bath problem at the final time $t = 10\tau_{ei}$. (The values are in the normalized units).

A better insight is provided by the kinetics of the transport. The energy weighted f_0 and heat flux weighted $\vec{f_1}$ are evaluated at the points designated by the vertical lines in Figure 6. These distributions are then plotted in Figure 7. It is visible on the isotropic part that the initially equilibrium distribution in the upstream splits to a two-temperature distribution down the stream due to the non-local species. It is clear that such significant deviation is far beyond the perturbative regime of the classical diffusion theory. The heat fluxes confirm this trend and the classical heat flux structure is completely destroyed in the downstream.

7.3 Radiation non-local transport

The non-local transport of energy on the hydrodynamic scale is not only an effect of the drifting high-velocity electrons, but also of the photons as explained in chapter 5. The numerical codes PETE and PETE2 include both approaches presented there, the radiation diffusion and discrete ordinates method for non-local radiation transport. Their effects and the interplay with the non-local electron transport are then of a great interest not only from the theoretical point of view, but also for various applications.

We presented a comparison of the impact of the diffusion and non-local radiation model on the numerical simulations under realistic conditions in [81]. In addition, the article overviews the numerical code PETE, which was already briefly described in chapter 7.2.1. Physically, it also solves the system (186–189), but the additional radiation coupling term is present following the energy equation of radiative transfer (136). However, the conservative form is preferred, where the equation of electron energy (188) is modified as follows:

$$\rho c_{Ve}\frac{\mathrm{D}T_e}{\mathrm{D}t}+\frac{\mathrm{D}\epsilon_R}{\mathrm{D}t}=-\underline{\underline{P}}^e:\nabla\vec{u}+G_{ei}(T_i-T_e)-\nabla\cdot(\vec{q}_e+\vec{q}_R+\vec{S}). \tag{197}$$

The newly appearing terms $\vec{q}_R$ and ϵ_R are obtained from the radiative transfer closure. The non-local radiation transport method is based on the discrete ordinates method described in chapter 5.3. Numerically, it relies on the high-order discontinuous Galerkin finite elements (DGFEM), which was presented in [92] and its implementation was developed as part of [74].

The radiation diffusion model follows chapter 5.1 and solves the coupled system (146) and (197), where the operator splitting technique is employed, so only the electron temperature and the terms related to the radiation transport are evolved in the latter. As part of my work, I developed an implicit numerical scheme for its solution. It extends the method of mimetic operators from [133] for the purposes of the radiation diffusion, where the physical system is reformulated in terms of the energies:

$$\frac{\epsilon_R^{n+1}-\epsilon_R^n}{\Delta t}-\nabla\cdot f\frac{c}{3\rho\kappa_R}\nabla\epsilon_R^{n+1}=c\rho\kappa_P(\Theta^{n+1}-\epsilon_R^{n+1}), \tag{198}$$

$$\frac{\mathrm{D}\Theta}{\mathrm{D}t}=\frac{1}{\tau}(\epsilon_R^{n+1}-\Theta), \tag{199}$$

where $\Theta = a_R T_e^4$ and the upper index denotes the discrete time levels. This semi-

discrete form can be solved for Θ^{n+1}, where the solution can be written $\Theta^{n+1} = \beta\Theta^n + (1-\beta)\epsilon_R^{n+1}$ as inspired by [134]. Two options for the coefficient β were given, where one is obtained from a fully implicit discretization of (199) and the other one solves the relaxation analytically provided that the diffusion operator does not contribute significantly. While the former maintains symmetry of the problem, but assumes only weak relaxation, the latter has exactly the opposite properties. Both methods operate correctly only on the time scales comparable with the relaxation time, so splitting of the time step is necessary. The details about the method and the final form of the numerical scheme in terms of the mimetic operators can be found in the article [81].

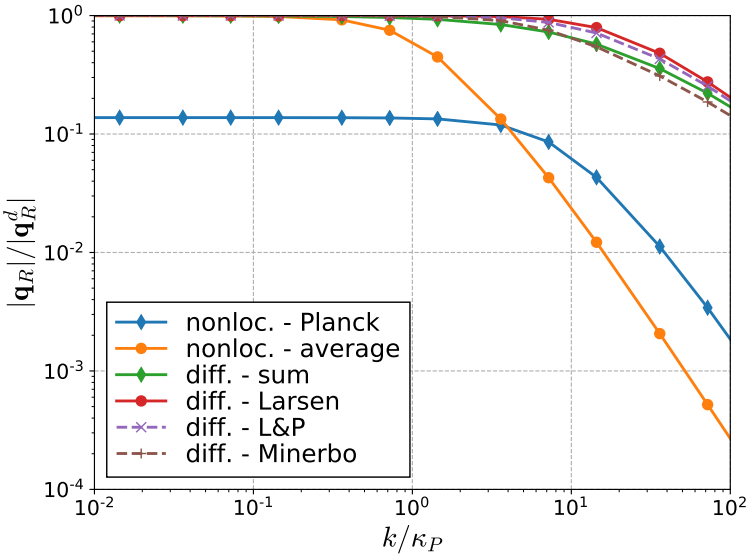

Figure 8: Dependencies of the radiation flux on the function $k/(\rho\kappa_P) \sim Kn_R$. The curves corresponds to the following: blue – S_N non-local model with Planck opacity, orange – S_N non-local model with the average opacity, the rest – the radiation diffusion model with the respective flux limiters ((144)–(145)).

A similar problem to the Short–Epperlein analysis of the non-local transport made in chapter 7.2.1 was also performed here. The equilibrium is assumed initially, i.e. $T_e = T_R$, and the base temperatures are chosen $T^0 = 1\,\mathrm{keV}$ and $\delta T = 5 \cdot 10^{-2} T^0$. The results are plotted in Figure 8. The findings are similar to the ones of chapter 7.2.1, the linear transport equation has the non-local dependency $\sim (Kn_R)^{-2}$ for the single-group transport, but the flux-limited diffusion gives rather the flux saturation, i.e. the dependency $\sim (Kn_R)^{-1}$. However, the value of the limiting flux depends on the base temperature T^0, which should be independent of the perturbations δT, meaning that the value of the limit is arbitrary in this idealized configuration. This manifests the non-viability of the flux-limited methods. Another important observation is that the radiation equation with the Planck opacity does not converge to the diffusion limit, but an average opacity formulation does, following the discussion from the introduction of chapter 5. In particular, the average opacity formula is taken from [79].

A comparative study of the laser–target interaction simulations was made then for

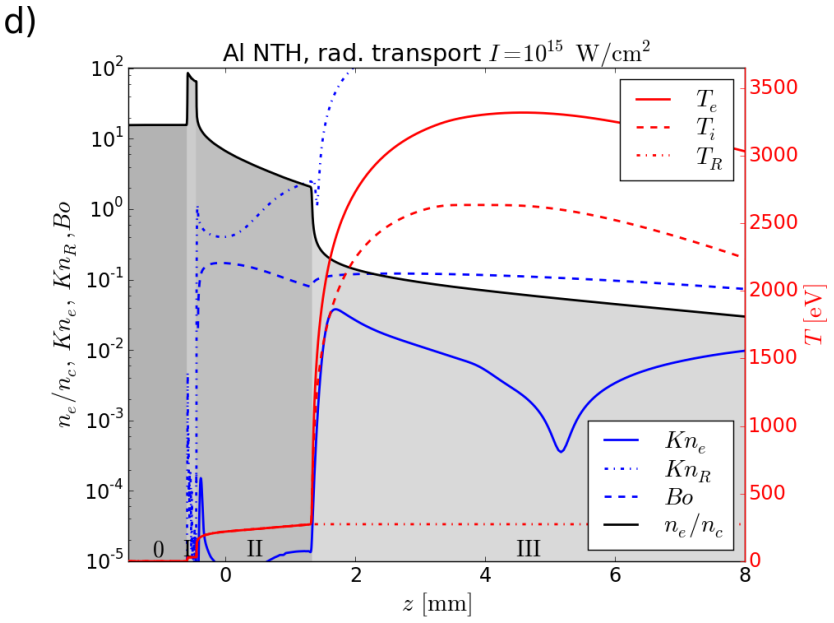

Figure 9: The profiles of the temperature T_e, density n_e, Knudsen numbers Kn_e, Kn_R and Boltzmann number Bo for the laser interaction with a solid Aluminum target.

different intensities of the laser, materials and the diffusion vs. the non-local radiation transport method. It was concluded that the effect of the radiation transport depends on all the mentioned physical parameters, but also on the choice of the numerical method strongly. This implies that an attention must be paid to the conditions in the plasma and the numerical treatment must be chosen adequately. However, a relatively strong non-locality in the radiation transport was observed even for the laser intensities as low as $1 \cdot 10^{13}\,\mathrm{W/cm^2}$ in the given configuration. An example of the simulation results is presented in Figure 9 and Figure 10. The Aluminum target of the room temperature and density $\rho = 2.7\,\mathrm{g/cm^3}$ is irradiated by a flat-top laser (pre-)pulse of the length 10 ns with the intensity $I_L = 1 \cdot 10^{15}\,\mathrm{W/cm^2}$ and wavelength $\lambda_L = 0.35\,\mu\mathrm{m}$ (a small Gaussian ramp of FWHM 1.2 ns is present at the beginning). The resulting profiles have the classical structure [78], where the different zones are designated by the Roman numbers in the figure. They can be classified as follows: 0 – unperturbed target, I – shock wave, II – conduction zone, III – corona. The full discussion of the interaction is beyond the scope of this text. However, the non-local effects are worth of mentioning. The electron heat transport operates only in the close vicinity of the critical plane, i.e. between zones II and III. This is given by the short mean free path of the electrons, which is $\bar{\lambda}_e \lesssim 1\,\mu\mathrm{m}$ in this case. The physical conditions are not favourable for the electrons as the short wavelength of the laser leads to mostly collisional absorption according to the introduction of chapter 6. The absorption profile is relatively smooth and no significant amount of electrons is generated at the critical surface. In contrast, the photon mean free path is remarkably longer and comparable with the length of the conduction zone. The strong conversion to the thermal radiation then causes formation of the double ablation front (DAF) structure known from the inertial fusion research [135], which is manifested by nearly the flat high density profile

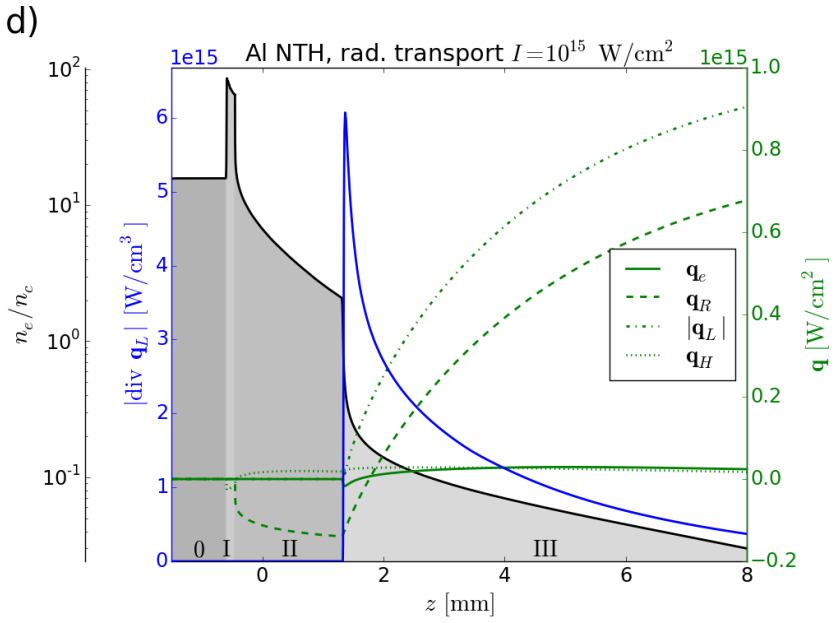

Figure 10: The profiles of the density n_e, laser absorption rate $|\nabla \cdot q_L|$, heat flux q_e, radiation energy flux q_R, Poynting vector q_L and convective flux q_H for the laser interaction with a solid Aluminum target.

of the conduction zone. This can be understood as a dynamic equilibrium between the hydrodynamic convection and the radiation transport, which is the best expressed by the Boltzmann number $Bo = 5/2(p_e + p_i)|\vec{u}|/\sigma_{SB}T_R^4$. As can be noticed, its profile is nearly flat in the conduction zone, so the mechanisms of energy transport are nearly perfectly balanced.

The prepulse effects can be illustrated on the results of a different study we made [23], where I authored most of the text and performed the hydrodynamic simulations. An Aluminum target is considered with the identical parameters as before, but the laser has the intensity in the pre-pulse $1 \cdot 10^{12}\,\mathrm{W/cm^2}$ and the wavelength $\lambda_L = 1.057\,\mu\mathrm{m}$. The length of the pre-pulse was 6 ns in this case. A particle-in-cell (PIC) simulation then followed and simulated the interaction of the main pulse with the created pre-plasma, where the intensity at maximum was $1 \cdot 10^{23}\,\mathrm{W/cm^2}$ and FWHM 150 fs. Two cases were studied, where the radiative transport was modelled in one and was not in the other. The results drawn in Figure 11. In the case with the non-local radiative transport (NLRT), a strong filamentation can be observed as the laser interacts with the DAF structure. This increases the overall absorption from 27 % to 38 %, but the effect of filamentation might be more important for the non-linear interaction with the target.

We also presented the effects of the prepulses with similar parameters in [22], where my contribution was elaboration of the final simulations and formulation of the laser absorption and introductory text. Unlike the previous scenario, a plastic target with density $n_e \doteq 86 n_c$ was considered, which favoured more the electron transport. The length of the pre-pulse was 10 ns again and the intensities of the main pulse $1 \cdot 10^{22}\,\mathrm{W/cm^2}$ and $1 \cdot 10^{23}\,\mathrm{W/cm^2}$, where also radiation–reaction effects were modelled.

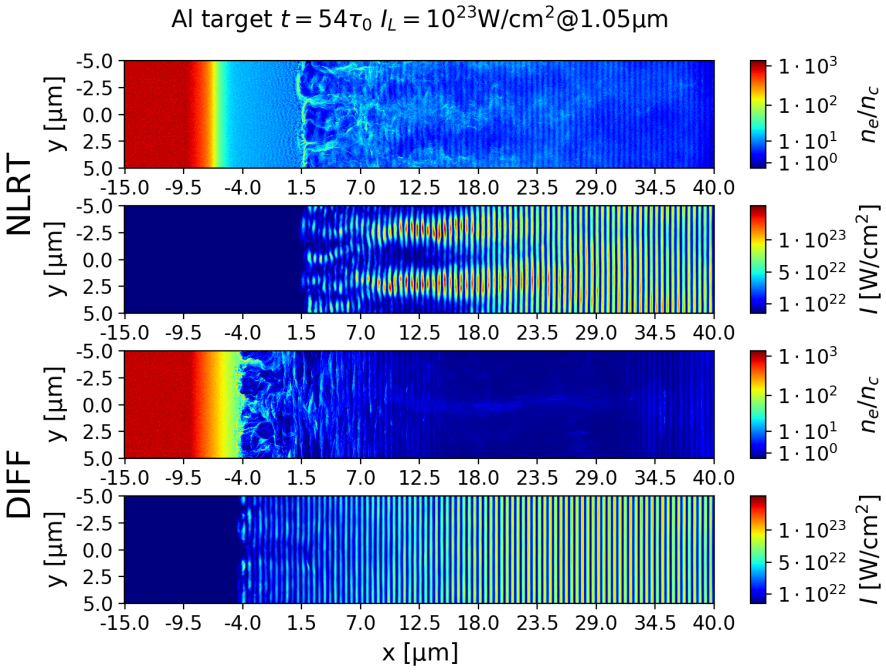

Figure 11: The profiles of the density n_e and laser intensity I in the particle-in-cell simulation of the interaction with a pre-plasma at time 54 optical cycles or 189 fs from the beginning of the main pulse. (The underlying PIC simulation data were provided by M. Jirka).

Without going into details, let us note the final result that the simulations with the DAF structure due to the energy transport increased the absorption of the pulse from 18.5 % to 54.8 % in the first case and 13.7 % to 61.1 %. Moreover, a strong filamentation was observed in the pre-plasma. This shows that the pre-pulse physics has a significant impact on the main pulse and cannot be neglected in the assessments of the experiments for intense lasers [21].

7.4 Laser absorption

The brief introduction to the topic of laser absorption in chapter 6 pointed to the fact that the optical methods are unable to precisely determine the behaviour of the laser beam in the vicinity of the critical plane. This is not an important consideration in the classical hydrodynamic models as the overall energy balance can be recovered by introduction of a semi-empirical factor of laser reflection at the critical density for example [105]. However, the simulations of the non-local transport in chapter 7.3 clearly show that exactly this delicate region near the singularity point is crucial for generation of the non-local electrons. Consequently, more detailed methods of laser absorption are required.

Our effort in this direction is the further development of the stationary Maxwell's equations method in [107] continuing along the lines of chapter 6.2. The original semi-analytic method is extended to an arbitrary order of the polynomial approximation of

the density profile (or complex refractive index $\hat{n}$ more precisely) in the computational cells. This is achieved by the analytic solution of the Riccati equation for the complex reflection index (182). The final form of the expression for V is non-trivial and involves calculation of a matrix exponential over the cell, but the formula for the amplitude of the incoming wave P and its magnitude A simplifies greatly and is proportional to $\sim \exp(i \int k_0 \hat{n} \, \mathrm{d}x)$ (for slowly varying V). This is a predictable result as the linear interaction should lead to dependency only on the average values in the weak reflection limit. However, the expression also conceptually shows why the method is limited to the only second order of convergence. Provided that the space is sufficiently well resolved, the differential approach is not only applicable, but may provide an arbitrary order of convergence to the method. As both approaches are complementary in this sense, a local switching technique is proposed for them, where a local criterion is formulated:

$$\left| \hat{n}_r k_0 - \frac{1}{4} \mathrm{Im} \left(\frac{\hat{n}'}{\hat{n}} \right) \right| \frac{\Delta x_c}{p_c} > C_\lambda, \tag{200}$$

where Δx_c is the size of the cell and p_c the polynomial order of the elements in the cell. This can be seen as a slightly modified version of the classical expression $\Delta x_c \gtrsim \lambda_L / \hat{n}_r$. The constant C_λ is a dimensionless factor and the numerical tests showed that $C_\lambda = 0.025$ seems to be an optimal value. When the criterion is satisfied, the semi-analytic solution should be used and provides more accurate results than the differential treatment. When the opposite is true, the differential solution based on the finite element method gives better results usually. The construction of the numerical scheme is also not detailed here, but it follows more or less standard procedure for the linear system of the first order differential equations obtained from the backward decomposition of (182) to the form similar to the original system (180–181). It is worth noting that the profiles of the refractive index do not need to be continuous in neither of the methods. An analytic solution for the discontinuity can be formulated [109, 110], which increases the overall robustness of the method and enables to correctly treat the plasma–vacuum boundary.

The numerical model was tested on the transition layer profiles also known as the Epstein profiles [136]. They present one of the few problems with an analytic solution for the full Hemholtz equation in a dissipative inhomogeneous medium. The profile of the dielectric function is defined as follows:

$$\hat{n}^2 = \hat{\varepsilon} = \hat{\varepsilon}^l + (\hat{\varepsilon}^r - \hat{\varepsilon}^l) \frac{1}{\exp(-\zeta) + 1} \,, \qquad \zeta = \frac{k_0 x}{\Delta \xi} = \frac{\xi}{\Delta \xi}, \tag{201}$$

where $\hat{\varepsilon}^l$ and $\hat{\varepsilon}^r$ are the limit values of $\hat{\varepsilon}$ in $-\infty$ and $+\infty$ respectively. In the example presented here, they have values $\varepsilon^l = (10^{-2} + 10^{-6} i)^2$ and $\varepsilon^r = (5 \cdot 10^{-4} + 10^{-2} i)^2$. The width of the profile $\Delta \xi = (\xi_r - \xi_l)\sigma$, where $\xi_l = -400\pi$ and $\xi_r = 400\pi$ are positions of the boundaries. The profiles are illustrated in Figure 12.

The analytic solution in terms of the Poynting vector and its divergence, which are of the primary importance for the hydrodynamic simulations, is plotted in Figure 13. It shows the complexity of the exact solution, where its wave nature is manifested as well

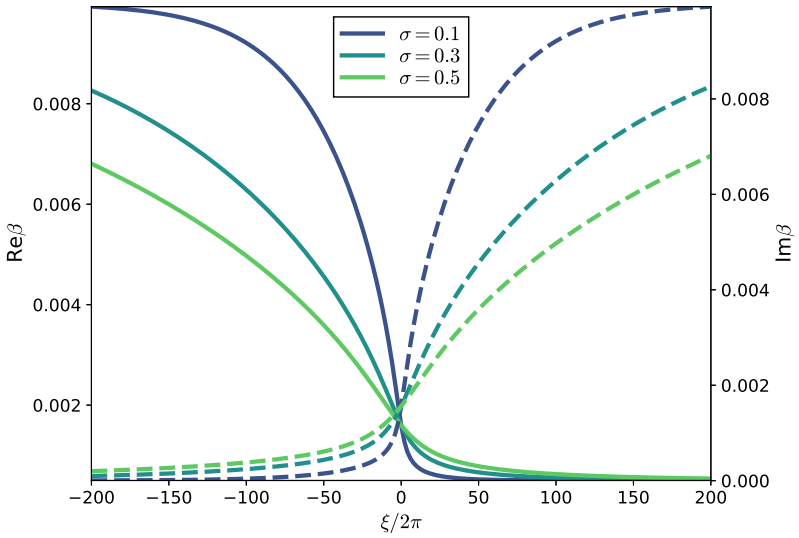

Figure 12: The refractive index β transition profiles as a function of the phase ξ for the different widths of the profile σ.

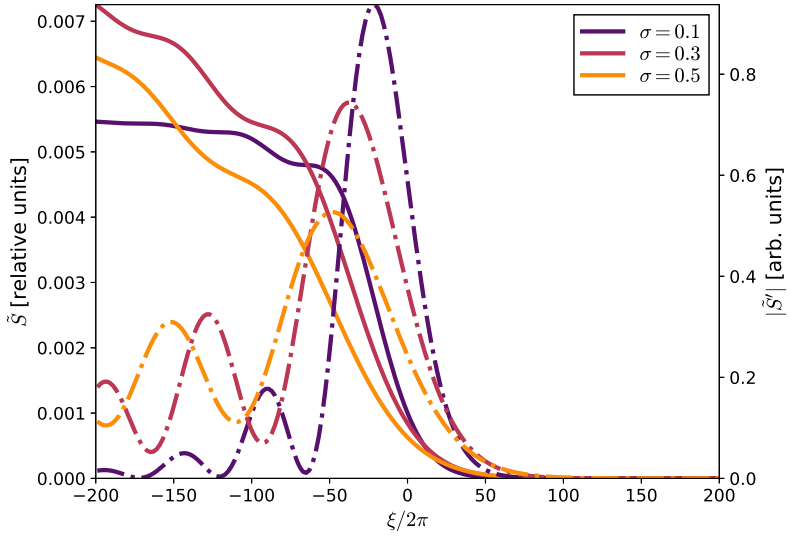

Figure 13: The normalized values of the Poynting vector $\tilde{S}$ (full lines) and magnitude of its divergence $|\tilde{S}'|$ (dash-dot lines) as functions of the phase ξ for the transition profiles of the different widths σ.

as the dependency of the local wavelength on the steepness of the transition profile. It is evident that the classical WKB methods described in chapter 6.1 cannot capture these phenomena even approximately.

The reflection and absorption on a steep profile is not the only interesting effect

for hydrodynamic simulations. It is also the skinning effect, which may play a vital role. In fact, the full wave based method gives a non-propagating solution even behind the critical point. Normally, the penetration depth is minuscule, but the situation changes in strongly rarefied media like low-density foams. We recently performed this kind of experiments and theoretical calculations in [137], where my contribution were the hydrodynamic simulations in the code PALE2. It is also equipped with the SME based solver in the classical semi-analytic formulation, which was made numerically applicable in 2D for normal incidence of a broad laser beam as part of my previous work [60].

8 Conclusions

The theoretical aspects of the non-local transport and the background theory necessary for its understanding were given in chapters 2–6. The fundamental principles of the kinetic theory were covered in chapter 2, describing plasma in an unmatched detail. However, solution in the full phase space is infeasible, as it poses a 7D problem in general. Hence, the model was reduced to the hydrodynamic framework described in chapter 3, where the simplifying assumption of the kinetic equilibrium was made. This procedure eliminated the notion of non-locality from the description completely as only the convective processes are present in the ideal hydrodynamics. The topic of chapter 4 was then to reintroduce the heat transport processes. At first, it was achieved by allowing only infinitesimal deviations from the equilibrium in the classical diffusive paradigm of chapter 4.1. The additional models of non-local electron transport in chapters 4.2–4.3 partially borrowed from the kinetic description again, but only in a limited extent to maintain feasibility of the methods. Along the same lines, also the radiation transport description continued and a good analogy between the descriptions of both species, electrons and photons, was recognized, which underpinned construction of some of the methods actually. The laser absorption modelling described in chapter 6 circumvented the problem of the non-existent high-frequency fields by formulation of the closure models for the electromagnetic energy flux vector (Poynting vector), which reduced the laser model to a mere energy source from the hydrodynamical point of view. The optical approximation in chapter 6.1 separated the envelope from the phase completely. However, the assumptions of the slowly varying envelope break down in the vicinity of the resonant points like the critical density in the context of laser plasma. This was addressed by the wave-based method of chapter 6.2, but only in a single dimension, making the methods complementary in essence.

Chapter 7 then summarized our scientific efforts in understanding and modelling of the non-local transport phenomenon. The variety and plurality of the research directions reflects the complexity of its nature. An overview of the structure of the new multi-dimensional hydrodynamic code was given chapter 7.1, where its possible extension to the magneto-hydrodynamic model was also envisioned. The flexible nature of the code design enables to integrate additional models and a high numerical precision is achieved thanks to the curvilinear high-order finite elements used.

The subject of chapter 7.2.1 was then extension of the hydrodynamical description by an additional closure model of non-local transport. Our model, based on the solution of a linear transport equation for heat flux intensities of the electrons, provides a feasible option for simulations of this effect. However, certain shortcomings of the model were recognized theoretically and also on the numerical tests performed. In contrast, chapter 7.2.2 presented our new fully kinetic code, which can describe the non-local transport in a great detail, but at expense of higher computational costs. This inconvenience was addressed by its implicit formulation, which enabled to choose longer computational time steps and increased overall robustness of the approach. The numerical performance was then illustrated on test problems, showing also consistency with the classical diffusion methods. However, the strength of the method in treatment of the non-local transport in a physically relevant scenario was also presented. This

new numerical tool then might present a nearly perfect reference for the simplified transport models of the hydrodynamic codes.

Non-locality of the radiation transport was topic of chapter 7.3. The previously developed method of non-local radiation transport was compared to the flux-limited radiation diffusion method, where limitations of the latter approach in treating the non-locality were identified. For the purposes of this analysis, a new numerical scheme of the radiation diffusion was proposed. Both methods were then applied in realistic simulations of laser (pre-)pulses, revealing significant impact of the modelling on the results. The effects of the radiation transport were even more pronounced in the interaction of a ultra-intense laser pulse with a solid target, where the particle simulations showed drastic filamentation and notable increase of absorption in the pre-plasma.

The final topic regarded the laser absorption as described in chapter 7.4. As the plasma is formed under an intense laser irradiation in our context, an accurate model of the absorption mechanisms has an essential importance. Moreover, the detailed description of the vicinity of the critical plane is crucial for the non-local electron transport, as it originates from the steep gradients in the plasma. Inability of the geometrical optics to self-consistently model this region led us to an extension of a wave-based method. Its validity and completeness was demonstrated on the physically relevant problem of the transition profiles, where an analytic solution exists.

In conclusion, various physical models and numerical methods were proposed to address the problem of non-local energy transport in plasma. They approached the topic in multiple aspects and contributed to the global research in this field. Our plan is to continue in this effort and further refine the methods of non-local transport and related models in hydrodynamics and laser absorption. The final goal still remains the formulation of a single robust yet computationally feasible method of the non-local transport.

List of publications

Journal papers

[1] J. Nikl, I. Göthel, M. Kuchařík, S. Weber and M. Bussmann. Implicit reduced Vlasov–Fokker–Planck–Maxwell model based on high-order mixed elements. *Journal of Computational Physics*, 2020. Submitted.

[2] J. Nikl, M. Kuchařík, J. Limpouch, R. Liska and S. Weber. Wave-based laser absorption method for high-order transport–hydrodynamic codes. *Advances in Computational Mathematics*, 45(4):1953–1976, 2019. doi:10.1007/s10444-019-09671-3.

[3] J. Nikl, M. Holec, M. Zeman, M. Kuchařík, J. Limpouch and S. Weber. Macroscopic laser-plasma interaction under strong non-local transport conditions for coupled matter and radiation. *Matter and Radiation at Extremes*, 3:110–126, 2018. doi:10.1016/j.mre.2018.03.001.

[4] M. Holec, J. Nikl and S. Weber. Nonlocal transport hydrodynamic model for laser heated plasmas. *Physics of Plasmas*, 25(3):032704, 2018. doi:10.1063/1.5011818.

[5] M. Holec, J. Nikl, M. Vranic and S. Weber. The effect of pre-plasma formation under nonlocal transport conditions for ultra-relativistic laser-plasma interaction. *Plasma Physics and Controlled Fusion*, 60(4):044019, 2018. doi:10.1088/1361-6587/aab05a.

[6] J. Limpouch, V. Tikhonchuk, J. Dostal, R. Dudzak, M. Krupka, N. Borisenko, J. Nikl, A. Akunets, L. Borisenko and V. Pimenov. Characterization of the homogenization time of a plasma created by laser ionization of a low-density foam. *Plasma Physics and Controlled Fusion*, 62(3):035013, 2020. doi:10.1088/1361-6587/ab6b4d.

[7] R. Lokasani, H. Kawasaki, Y. Shimada, M. Shoji, K. Anraku, T. Ejima, T. Hatano, W. Jiang, S. Namba, J. Nikl, M. Zeman, G. O'Soullivan, T. Higashiguchi and J. Limpouch. Soft X-ray spectral analysis of laser produced molybdenum plasmas using fundamental and second harmonics of a Nd:YAG laser. *Optics Express*, 27(23):33351–33358, 2019. doi:10.1364/OE.27.033351.

[8] P. Pokorný, M. Novotný, P. Fitl, J. Zuklín, J. Vlček, J. Nikl, E. Marešová, P. Hruška, J. Bulíř, J. Drahokoupil, M. Čerňanský and J. Lančok. Apparatus for measurements of thermal and optical stimulated exo-electron emission and luminescence. *Measurement Science and Technology*, 29(6):065902, 2018. doi:10.1088/1361-6501/aabc80.

Proceedings

[1] J. Nikl, M. Kuchařík and S. Weber. Modelling of the non-local transport of energy in laser plasmas with high-order numerical methods. In *Europhysics Conference Abstracts – 46th EPS Conference on Plasma Physics*, volume 43C, page P5.2010. European Physical Society, 2019. ISBN 979-10-96389-11-7.

[2] J. Nikl, M. Jirka, M. Kuchařík, M. Holec, M. Vranic and S. Weber. The effect of pre-plasma formed under the non-local transport conditions on the interaction of the ultra-high intensity laser with a solid target. In *Research using Extreme Light: Entering New Frontiers with Petawatt-Class Lasers IV*, volume 11039 of *Proc. of SPIE*, page 110391E. 2019. doi:10.1117/12.2522450.

[3] J. Nikl, M. Kuchařík, M. Holec and S. Weber. Curvilinear high-order Lagrangian hydrodynamic code for the laser-target interaction. In S. Coda, J. Berndt, G. Lapenta, M. Mantsinen, C. Michaut and S. Weber, editors, *Europhysics Conference Abstracts – 45th EPS Conference on Plasma Physics*, volume 42A, page P1.2019. European Physical Society, 2018. ISBN 979-10-96389-08-7.

[4] M. Kuchařík, J. Limpouch, R. Liska and J. Nikl. Hydrodynamic simulations of laser/plasma interactions via ALE methods. In *Europhysics Conference Abstracts – 46th EPS Conference on Plasma Physics*, volume 43C, page P5.2009. European Physical Society, 2019. ISBN 979-10-96389-11-7.

References

[1] H. Lorentz. The motion of electrons in metallic bodies I. *KNAW, Proceedings*, 7:438, 1905.

[2] S. Chapman. VI. On the law of distribution of molecular velocities, and on the theory of viscosity and thermal conduction, in a non-uniform simple monatomic gas. *Philosophical Transactions of the Royal Society of London. Series A, Containing Papers of a Mathematical or Physical Character*, 216(538-548):279–348, 1916. doi:10.1098/rsta.1916.0006.

[3] L. D. Landau. Kinetic equation for the Coulomb effect. *Phys. Z. Soviet Union*, 10:154, 1936.

[4] S. Chandrasekhar. Dynamical Friction I. General Considerations: the Coefficient of Dynamical Friction. *Astrophysical Journal*, 97:255, 1943. doi:10.1086/144517.

[5] T. G. Cowling. The electrical conductivity of an ionized gas in a magnetic field, with applications to the solar atmosphere and the ionosphere. *Proceedings of the Royal Society of London. Series A. Mathematical and Physical Sciences*, 183(995):453–479, 1945. doi:10.1098/rspa.1945.0013.

[6] R. S. Cohen, L. Spitzer and P. M. Routly. The electrical conductivity of an ionized gas. *Physical Review*, 80(2):230–238, 1950. doi:10.1103/PhysRev.80.230.

[7] L. Spitzer and R. Härm. Transport phenomena in a completely ionized gas. *Physical Review*, 89(5):977–981, 1953. doi:10.1103/PhysRev.89.977.

[8] S. I. Braginskii. Transport processes in a plasma. *Reviews of Plasma Physics*, 1:205–311, 1965.

[9] M. N. Rosenbluth, W. M. MacDonald and D. L. Judd. Fokker-planck equation for an inverse-square force. *Physical Review*, 107(1):1–6, 1957. doi:10.1103/PhysRev.107.1.

[10] J. M. Dawson. On the production of plasma by giant pulse lasers. *Physics of Fluids*, 7(7):981, 1964. doi:10.1063/1.1711346.

[11] R. C. Malone, R. L. McCrory and R. L. Morse. Indications of Strongly Flux-Limited Electron Thermal Conduction in Laser-Target Experiments. *Physical Review Letters*, 34(12):721–724, 1975. doi:10.1103/PhysRevLett.34.721.

[12] D. Gray and J. D. Kilkenny. The measurement of ion acoustic turbulence and reduced thermal conductivity caused by a large temperature gradient in a laser heated plasma. *Plasma Physics*, 22:81–111, 1980. doi:10.1088/0032-1028/22/2/001.

[13] T. H. Kho and D. J. Bond. Application of a moment method to calculation of heat flow in a plasma with a Fokker-Planck collision term. *Journal of Physics D: Applied Physics*, 14(8):L117–L119, 1981. doi:10.1088/0022-3727/14/8/001.

[14] J. P. Matte and J. Virmont. Electron Heat Transport down Steep Temperature Gradients. *Physical Review Letters*, 49(26):1936–1939, 1982. doi: 10.1103/PhysRevLett.49.1936.

[15] J. F. Luciani, P. Mora and J. Virmont. Nonlocal heat transport due to steep temperature gradients. *Physical Review Letters*, 51(18):1664–1667, 1983. doi: 10.1103/PhysRevLett.51.1664.

[16] M. K. Prasad and D. S. Kershaw. Nonviability of some nonlocal electron heat transport modeling. *Physics of Fluids B: Plasma Physics (1989-1993)*, 1(12):2430–2436, 1989. doi:http://dx.doi.org/10.1063/1.859178.

[17] G. P. Schurtz, P. D. Nicolaï and M. Busquet. A nonlocal electron conduction model for multidimensional radiation hydrodynamics codes. *Physics of Plasmas*, 7(10):4238, 2000. doi:10.1063/1.1289512.

[18] D. Del Sorbo, J.-L. Feugeas, P. Nicolaï, M. Olazabal-Loumé, B. Dubroca, S. Guisset, M. Touati and V. Tikhonchuk. Reduced entropic model for studies of multidimensional nonlocal transport in high-energy-density plasmas. *Physics of Plasmas*, 22(8):082706, 2015. ISSN 1070-664X. doi:10.1063/1.4926824.

[19] M. Holec, J. Nikl and S. Weber. Nonlocal transport hydrodynamic model for laser heated plasmas. *Physics of Plasmas*, 25(3):032704, 2018. doi:10.1063/1.5011818.

[20] J. P. Brodrick, R. J. Kingham, M. M. Marinak, M. V. Patel, A. V. Chankin, J. T. Omotani, M. V. Umansky, D. Del Sorbo, B. Dudson, J. T. Parker, G. D. Kerbel, M. Sherlock and C. P. Ridgers. Testing nonlocal models of electron thermal conduction for magnetic and inertial confinement fusion applications. *Physics of Plasmas*, 24(9), 2017. doi:10.1063/1.5001079.

[21] T. Z. Esirkepov, J. K. Koga, A. Sunahara, T. Morita, M. Nishikino, K. Kageyama, H. Nagatomo, K. Nishihara, A. Sagisaka, H. Kotaki, T. Nakamura, Y. Fukuda, H. Okada, A. S. Pirozhkov, A. Yogo, M. Nishiuchi, H. Kiriyama, K. Kondo, M. Kando and S. V. Bulanov. Prepulse and amplified spontaneous emission effects on the interaction of a petawatt class laser with thin solid targets. *Nuclear Instruments and Methods in Physics Research, Section A: Accelerators, Spectrometers, Detectors and Associated Equipment*, 745:150–163, 2014. doi: 10.1016/j.nima.2014.01.056.

[22] M. Holec, J. Nikl, M. Vranic and S. Weber. The effect of pre-plasma formation under nonlocal transport conditions for ultra-relativistic laser-plasma interaction. *Plasma Physics and Controlled Fusion*, 60(4):044019, 2018. doi: 10.1088/1361-6587/aab05a.

[23] J. Nikl, M. Jirka, M. Kuchařík, M. Holec, M. Vranic and S. Weber. The effect of pre-plasma formed under the non-local transport conditions on the interaction of the ultra-high intensity laser with a solid target. In *Research using Extreme Light: Entering New Frontiers with Petawatt-Class Lasers IV*, volume 11039 of *Proc. of SPIE*, page 110391E. 2019. doi:10.1117/12.2522450.

[24] M. Zhao, A. Chankin and D. Coster. Kinetic simulations of electron heat flux in the scrape-off layer. *Nuclear Materials and Energy*, 12:819–824, 2017. ISSN 23521791. doi:10.1016/j.nme.2017.01.025.

[25] K. Falk, M. Holec, C. J. Fontes, C. L. Fryer, C. W. Greeff, H. M. Johns, D. S. Montgomery, D. W. Schmidt and M. Šmíd. Measurement of preheat due to nonlocal electron transport in warm dense matter. *Physical Review Letters*, 120(2):1–5, 2018. doi:10.1103/PhysRevLett.120.025002.

[26] R. L. Liboff, R. S. Berry, J. L. Birman and H. E. Stanley. *Kinetic Theory: Classical, Quantum, and Relativistic Descriptions*. Graduate Texts in Contemporary Physics. Springer-Verlag, third edition edition, 2003. ISBN 0-387-95551-8. doi: 10.1007/b97467.

[27] N. N. Bogoliubov. Problems of a Dynamical Theory in a Statistical Physics. In J. DeBoer and G. E. Uhlenbeck, editors, *udies in Statistical Mechanics*. North-Holland, 1962.

[28] I. P. Shkarofsky, T. W. Johnston and M. P. Bachynski. *The particle kinetics of plasmas*. Addison-Wesley, London, 1966.

[29] P. Kulhánek. *Úvod do teorie plazmatu*. AGA, 2011.

[30] P. Degond and B. Lucquin-Desreux. The Fokker-Planck asymptotics of the Boltzmann collision operator in the Coulomb case. *Mathematical Models and Methods in Applied Sciences*, 02(02):167–182, 1992. doi:10.1142/S0218202592000119.

[31] T. J. Boyd, T. J. M. Boyd and J. J. Sanderson. *The physics of plasmas*. Cambridge University Press, 2003. ISBN 0521452902.

[32] P. Mulser and D. Bauer. *High Power Laser-Matter Interaction*, volume 238 of *Springer Tracts in Modern Physics*. Springer Berlin Heidelberg, 2010. ISBN 978-3-540-50669-0. doi:10.1007/978-3-540-46065-7.

[33] Y. T. Lee and R. M. More. An electron conductivity model for dense plasmas. *Physics of Fluids*, 27(5):1273, 1984. doi:10.1063/1.864744.

[34] P. L. Bhatnagar, E. P. Gross and M. Krook. A model for collision processes in gases. I. Small amplitude processes in charged and neutral one-component systems. *Physical Review*, 94(3):511–525, 1954. doi:10.1103/PhysRev.94.511.

[35] W. Manheimer, D. Colombant and A. Schmitt. Analytic insights into nonlocal energy transport. I. Krook models. *Physics of Plasmas*, 25(8):082711, 2018. doi: 10.1063/1.5039530.

[36] W. Manheimer, D. Colombant and V. Goncharov. The development of a Krook model for nonlocal transport in laser produced plasmas. I. Basic theory. *Physics of Plasmas*, 15(8):1–10, 2008. doi:10.1063/1.2963078.

[37] T. W. Johnston. Cartesian tensor scalar product and spherical harmonic expansions in Boltzmann's equation. *Physical Review*, 120(4):1103–1111, 1960. doi:10.1103/PhysRev.120.1103.

[38] S. Chandrasekhar. Brownian motion, dynamical friction, and stellar dynamics. *Reviews of Modern Physics*, 21(3):383–388, 1949. doi:10.1103/RevModPhys.21.383.

[39] S. Childress. *An introduction to theoretical fluid mechanics*, volume 19. American Mathematical Society, 2009.

[40] F. Wu, R. Ramis and Z. Li. A conservative MHD scheme on unstructured Lagrangian grids for Z-pinch hydrodynamic simulations. *Journal of Computational Physics*, 357:206–229, 2018. doi:10.1016/j.jcp.2017.12.014.

[41] R. M. More, K. H. Warren, D. A. Young and G. B. Zimmerman. A new quotidian equation of state (QEOS) for hot dense matter. *Physics of Fluids*, 31(10):3059, 1988. doi:10.1063/1.866963.

[42] C. Cranfill and R. M. More. IONEOS: A Fast, Analytic Ion Equation-of-State Routine. Technical Report LA–7313–MS, Los ALamos Scientific Laboratory, 1978.

[43] J. F. Barnes. Statistical atom theory and the equation of state of solids. *Physical Review*, 153(1):269–275, 1967. doi:10.1103/PhysRev.153.269.

[44] R. Feynman, N. Metropolis and E. Teller. Equations of State of Elements Based on the Generalized Fermi-Thomas Theory. *Physical Review*, 75(10), 1949.

[45] A. J. Kemp and J. Meyer-ter-Vehn. An equation of state code for hot dense matter, based on the QEOS description. *Nuclear Instruments and Methods in Physics Research, Section A: Accelerators, Spectrometers, Detectors and Associated Equipment*, 415(3):674–676, 1998. doi:10.1016/S0168-9002(98)00446-X.

[46] S. Faik, M. M. Basko, A. Tauschwitz, I. Iosilevskiy and J. A. Maruhn. Dynamics of volumetrically heated matter passing through the liquid–vapor metastable states. *High Energy Density Physics*, 8(4):349–359, 2012.

[47] T. A. Heltemes and G. A. Moses. BADGER v1.0: A Fortran equation of state library. *Computer Physics Communications*, 183(12):2629–2646, 2012. doi:10.1016/j.cpc.2012.07.010.

[48] J. Abdallah Jr, G. Kerley, B. Bennett, J. Johnson, R. Albers and W. Huebner. HYDSES: a subroutine package for using Sesame in hydrodynamic codes. Technical Report LA-8209, Los Alamos Scientific Lab., NM (USA), 1980.

[49] G. T. SESAME report on the Los Alamos equation-of-state library. Technical Report LALP-83-4, Los Alamos National Laboratory, Los Alamos, 1983.

[50] S. P. Lyon and J. D. Johnson. Sesame: the Los Alamos National Laboratory equation of state database. Technical Report LA-UR-92-3407, Los Alamos National Laboratory, Los Alamos, NM, 1992.

[51] M. Zeman, M. Holec and P. Váchal. HerEOS: A framework for consistent treatment of the Equation of State in ALE hydrodynamics. *Computers and Mathematics with Applications*, 2018. doi:10.1016/j.camwa.2018.10.014.

[52] M. Zeman. *Thermodynamically Consistent Interpolation of the Equation of State for Hydrodynamic Calculations*. Bachelor's project, FJFI ČVUT v Praze, 2016.

[53] R. Courant and D. Hilbert. *Methods of mathematical physics*. Wiley, 1953.

[54] D. Enskog. The numerical calculation of phenomena in fairly dense gases. *Arkiv Mat. Astr. Fys*, 16(1):1–60, 1921.

[55] S. Chapman, T. G. Cowling and D. Burnett. *The mathematical theory of non-uniform gases*. Cambridge University Press, third edition edition, 1990. ISBN 052140844X.

[56] E. M. Epperlein and R. W. Short. A practical nonlocal model for electron heat transport in laser plasma. *Phys. Fluids B*, 3(1991):3092–3098, 1991. doi:10.1063/1.859789.

[57] J. J. Bissell, C. P. Ridgers and R. J. Kingham. Super-Gaussian transport theory and the field-generating thermal instability in laser–plasmas. *New Journal of Physics*, 15(2):025017, 2013. doi:10.1088/1367-2630/15/2/025017.

[58] A. V. Brantov and V. Y. Bychenkov. Nonlocal transport in hot plasma. Part I. *Plasma Physics Reports*, 39(9):698–744, 2013. doi:Doi10.1134/S1063780x13090018.

[59] C. P. Ridgers, R. J. Kingham and A. G. R. Thomas. Magnetic Cavitation and the Reemergence of Nonlocal Transport in Laser Plasmas. *Physical Review Letters*, 100(7):075003, 2008. doi:10.1103/PhysRevLett.100.075003.

[60] J. Nikl. *Some aspects of numerical methods for laser plasma hydrodynamics*. Master's thesis, FJFI ČVUT v Praze, 2017.

[61] M. D. Rosen, D. W. Phillion, V. C. Rupert, W. C. Mead, W. L. Kruer, J. J. Thomson, H. N. Kornblum, V. W. Slivinsky, G. J. Caporaso, M. J. Boyle and K. G. Tirsell. The interaction of 1.06 μm laser radiation with high Z disk targets. *Physics of Fluids*, 22(10):2020, 1979. doi:10.1063/1.862501.

[62] A. Sunahara, J. A. Delettrez, C. Stoeckl, R. W. Short and S. Skupsky. Time-dependent electron thermal flux inhibition in direct-drive laser implosions. *Physical Review Letters*, 91(9):950031–950034, 2003. doi:10.1103/PhysRevLett.91.095003.

[63] A. R. Bell, R. G. Evans and D. J. Nicholas. Elecron energy transport in steep temperature gradients in laser-produced plasmas. *Physical Review Letters*, 46(4):243–246, 1981. doi:10.1103/PhysRevLett.46.243.

[64] T. H. Kho and M. G. Haines. Nonlinear Kinetic Transport of Electrons and Magnetic Field in Laser-Produced Plasmas. *Physical Review Letters*, 55(8):825–828, 1985. doi:10.1103/PhysRevLett.55.825.

[65] L. Drska, J. Limpouch and R. Liska. Fokker-Planck simulations of ultrashort-pulse laser-plasma interactions. *Laser and Particle Beams*, 10(3):461–471, 1992. doi:10.1017/S0263034600006704.

[66] M. K. Prasad and D. S. Kershaw. Stable solutions of nonlocal electron heat transport equations. *Physics of Fluids B: Plasma Physics (1989-1993)*, 3(11):3087–3091, 1991. doi:http://dx.doi.org/10.1063/1.859995.

[67] G. Schurtz, S. Gary, S. Hulin, C. Chenais-Popovics, J. C. Gauthier, F. Thais, J. Breil, F. Durut, J. L. Feugeas, P. H. Maire, P. Nicola??, O. Peyrusse, C. Reverdin, G. Soulli??, V. Tikhonchuk, B. Villette and C. Fourment. Revisiting nonlocal electron-energy transport in inertial-fusion conditions. *Physical Review Letters*, 98(9):3–6, 2007. doi:10.1103/PhysRevLett.98.095002.

[68] A. Bendib, J. F. Luciani and J. P. Matte. An improvement of the nonlocal heat flux formula. *Physics of Fluids*, 31(4):711, 1988. doi:10.1063/1.866806.

[69] P. D. Nicolaï, J. L. A. Feugeas and G. P. Schurtz. A practical nonlocal model for heat transport in magnetized laser plasmas. *Physics of Plasmas*, 13(3):1–14, 2006. doi:10.1063/1.2179392.

[70] J. R. Albritton, E. A. Williams, I. B. Bernstein and K. P. Swartz. Nonlocal electron heat transport by not quite Maxwell-Boltzmann distributions. *Physical Review Letters*, 57(15):1887–1890, 1986. doi:10.1103/PhysRevLett.57.1887.

[71] V. Y. Bychenkov, W. Rozmus, V. T. Tikhonchuk and A. V. Brantov. Nonlocal electron transport in a plasma. *Physical Review Letters*, 75(24):4405–4408, 1995. doi:10.1103/PhysRevLett.75.4405.

[72] D. Del Sorbo, J.-L. Feugeas, P. Nicolaï, M. Olazabal-Loumé, B. Dubroca and V. Tikhonchuk. Extension of a reduced entropic model of electron transport to magnetized nonlocal regimes of high-energy-density plasmas. *Laser and Particle Beams*, 34(03):412–425, 2016. doi:10.1017/S0263034616000252.

[73] A. Colaïtis. *Multiscale Description of the Laser-Plasma Interaction, Application to the Physics of Shock Ignition in Inertial Confinement Fusion*. Ph.D. thesis, Université de Bordeaux, France, 2015.

[74] M. Holec. *Nonlocal Transport Hydrodynamic Modeling of Laser Heated Plasmas*. Doctoral thesis, FJFI ČVUT v Praze, 2016.

[75] D. Mihalas and B. W. Mihalas. *Foundations of Radiation Hydrodynamics*. Oxford University Press, 1984. ISBN 0195034376.

[76] G. Pomraning. *Equations of Radiation Hydrodynamics*. Pergamon Press, 1973.

[77] R. Lokasani, H. Kawasaki, Y. Shimada, M. Shoji, K. Anraku, T. Ejima, T. Hatano, W. Jiang, S. Namba, J. Nikl, M. Zeman, G. O'Soullivan, T. Higashiguchi and J. Limpouch. Soft X-ray spectral analysis of laser produced molybdenum plasmas using fundamental and second harmonics of a Nd:YAG laser. *Optics Express*, 27(23):33351–33358, 2019. doi:10.1364/OE.27.033351.

[78] R. Sigel, K. Eidmann, F. Lavarenne and R. F. Schmalz. Conversion of laser light into soft x rays. Part I: Dimensional analysis. *Physics of Fluids B: Plasma Physics*, 2(1):199–207, 1990. doi:10.1063/1.859528.

[79] N. Vaytet, M. González, E. Audit and G. Chabrier. The influence of frequency-dependent radiative transfer on the structures of radiative shocks. *Journal of Quantitative Spectroscopy and Radiative Transfer*, 125:105–122, 2013. doi:10.1016/j.jqsrt.2013.03.003.

[80] J. Castor. *Radiation hydrodynamics*. Cambridge University Press, New York, 2004. ISBN 0511231334.

[81] J. Nikl, M. Holec, M. Zeman, M. Kuchařík, J. Limpouch and S. Weber. Macroscopic laser-plasma interaction under strong non-local transport conditions for coupled matter and radiation. *Matter and Radiation at Extremes*, 3:110–126, 2018. doi:10.1016/j.mre.2018.03.001.

[82] G. L. Olson, L. H. Auer and M. L. Hall. Diffusion, P1, and other approximate forms of radiation transport. *Journal of Quantitative Spectroscopy and Radiative Transfer*, 64(6):619–634, 1999. doi:10.1016/S0022-4073(99)00150-8.

[83] C. D. Levermore and G. C. Pomraning. A flux-limited diffusion theory. *Astrophysical Journal*, 248:321, 1981.

[84] G. N. Minerbo. Maximum entropy Eddington factors. *Journal of Quantitative Spectroscopy and Radiative Transfer*, 20(6):541–545, 1978. doi:10.1016/0022-4073(78)90024-9.

[85] Y. Raizer and Y. Zeldovich. *Physics of Shock Waves and High-Temperature Hydrodynamic Phenomena*. Dover Publications, New York, 2002.

[86] N. J. Turner and J. M. Stone. A Module for Radiation Hydrodynamic Calculations With ZEUS-2D Using Flux-Limited Diffusion. *The Astrophysical Journal Supplement Series*, 135(1):30, 2001. doi:10.1086/321779.

[87] C. C. Ober and J. N. Shadid. Studies on the accuracy of time-integration methods for the radiation-diffusion equations. *Journal of Computational Physics*, 195(2):743–772, 2004. doi:10.1016/j.jcp.2003.10.036.

[88] J. Morel. Diffusion-limit asymptotics of the transport equation, the P1/3 equations, and two flux-limited diffusion theories. *Journal of Quantitative Spectroscopy and Radiative Transfer*, 65(5):769–778, 2000. doi:10.1016/S0022-4073(99)00148-X.

[89] D. S. Kershaw. Flux Limiting Nature's Own Way: A New Method for Numerical Solution of the Transport Equation. *Lawrence Livermore National Laboratory, UCRL-78378*, 1976. doi:10.2172/104974.

[90] C. Levermore. Relating Eddington factors to flux limiters. *Journal of Quantitative Spectroscopy and Radiative Transfer*, 31(2):149–160, 1984. doi:10.1016/0022-4073(84)90112-2.

[91] S. Chandrasekhar. *Radiative transfer*. Dover Publications, New York, 1960.

[92] M. Holec, J. Limpouch, R. Liska and S. Weber. High-order discontinuous Galerkin nonlocal transport and energy equations scheme for radiation hydrodynamics. *International Journal for Numerical Methods in Fluids*, 83(10):779–797, 2017. doi:10.1002/fld.4288.

[93] I. Babuška and M. Suri. On Locking and Robustness in the Finite Element Method. *SIAM Journal on Numerical Analysis*, 29(5):1261–1293, 1992. doi:10.1137/0729075.

[94] J. C. Ragusa, J. L. Guermond and G. Kanschat. A robust S N-DG-approximation for radiation transport in optically thick and diffusive regimes. *Journal of Computational Physics*, 231(4):1947–1962, 2012. doi:10.1016/j.jcp.2011.11.017.

[95] J. C. Chai, H. S. Lee and S. V. Patankar. Ray effect and false scattering in the discrete ordinates method. *Numerical Heat Transfer, Part B: Fundamentals*, 24(4):373–389, 1993. doi:10.1080/10407799308955899.

[96] B. Hunter and Z. Guo. Numerical smearing, ray effect, and angular false scattering in radiation transfer computation. *International Journal of Heat and Mass Transfer*, 81:63–74, 2015. doi:10.1016/j.ijheatmasstransfer.2014.10.014.

[97] R. O. Castro and J. P. Trelles. Spatial and angular finite element method for radiative transfer in participating media. *Journal of Quantitative Spectroscopy and Radiative Transfer*, 157:81–105, 2015. doi:10.1016/j.jqsrt.2015.02.008.

[98] S. Eliezer. *The interaction of high-power lasers with plasmas*. IOP Publishing Ltd, 2002. ISBN 0750307471.

[99] M. Born and E. Wolf. *Principles of optics: Electromagnetic Theory of Propagation, Interference and Diffraction of Light*. Cambridge University Press, 7th edition, 1999. ISBN 0521642221. doi:10.1016/S0030-3992(00)00061-X.

[100] T. B. Kaiser. Laser ray tracing and power deposition on an unstructured three-dimensional grid. *Physical Review E*, 61(1):895–905, 2000. doi:10.1103/PhysRevE.61.895.

[101] A. Colaïtis, G. Duchateau, P. Nicolaï and V. Tikhonchuk. Towards modeling of nonlinear laser-plasma interactions with hydrocodes : The thick-ray approach. *Physical Review E*, 89(3):033101, 2014. doi:10.1103/PhysRevE.89.033101.

[102] J. Velechovský. *Numerické metody modelování laserového plazmatu*. Master's thesis, FJFI ČVUT v Praze, 2011.

[103] Y. A. Kravtsov. Complex rays and complex caustics. *Radiophysics and Quantum Electronics*, 10(9-10):719–730, 1971. doi:10.1007/BF01031601.

[104] Y. A. Kravtsov and P. Berczynski. Gaussian beams in inhomogeneous media: A review. *Studia Geophysica et Geodaetica*, 51(1):1–36, 2007. doi:10.1007/s11200-007-0002-y.

[105] R. Ramis, K. Eidmann, J. Meyer-Ter-Vehn and S. Hüller. MULTI-fs - A computer code for laser-plasma interaction in the femtosecond regime. *Computer Physics Communications*, 183(3):637–655, 2012. doi:10.1016/j.cpc.2011.10.016.

[106] Y. V. Afanas'ev, N. N. Demchenko, O. N. Krokhin, V. B. Rosanov, Y. V. Afanas, N. N. Demchenko, O. N. Krokhin and V. B. Rosanov. Absorption and reflection of laser radiation by a dispersing high-temperature plasma. *Sov. Phys. JETP.*, 45:90, 1977.

[107] J. Nikl, M. Kuchařík, J. Limpouch, R. Liska and S. Weber. Wave-based laser absorption method for high-order transport–hydrodynamic codes. *Advances in Computational Mathematics*, 45(4):1953–1976, 2019. doi:10.1007/s10444-019-09671-3.

[108] Y. V. Afanas'ev, E. G. Gamalii, N. N. Demchenko, O. N. Krokhin and V. B. Rozanov. Theoretical study of the hydrodynamics of spherical targets taking the refraction of the laser radiation into account. *J. Exp. Theor. Phys.*, 52(3):425–431, 1980.

[109] T. Kapin, M. Kuchařík, J. Limpouch and R. Liska. Hydrodynamic simulations of laser interactions with low-density foams. *Czechoslovak Journal of Physics*, 56:B493–B499, 2006.

[110] J. Velechovský. *Modelování absorpce laserového záření v plazmatu (Modelling of laser radiation absorption in plasma)*. Bachelor project, FJFI ČVUT v Praze, 2009.

[111] A. Colaïtis, G. Duchateau, X. Ribeyre, Y. Maheut, G. Boutoux, L. Antonelli, P. Nicolaï, D. Batani and V. Tikhonchuk. Coupled hydrodynamic model for laser-plasma interaction and hot electron generation. *Physical Review E - Statistical, Nonlinear, and Soft Matter Physics*, 92(4):1–5, 2015. doi:10.1103/PhysRevE.92.041101.

[112] I. G. Lebo, N. N. Demchenko, A. B. Iskakov, J. Limpouch, V. B. Rozanov and V. F. Tishkin. Simulation of high-intensity laser-plasma interactions by use of the 2D Lagrangian code "ATLANT-HE". *Laser and Particle Beams*, 22(3):267–273, 2004.

[113] P. Nicolaï, J. L. Feugeas, T. Nguyen-Bui, V. Tikhonchuk, L. Antonelli, D. Batani and Y. Maheut. Effect of nonthermal electrons on the shock formation in a laser driven plasma. *Physics of Plasmas*, 22(4), 2015. doi:10.1063/1.4917472.

[114] M. M. Basko and I. P. Tsygvintsev. A hybrid model of laser energy deposition for multi-dimensional simulations of plasmas and metals. *Computer Physics Communications*, 214(6):59–70, 2017.

[115] J. Nikl, M. Kuchařík, M. Holec and S. Weber. Curvilinear high-order Lagrangian hydrodynamic code for the laser-target interaction. In S. Coda, J. Berndt, G. Lapenta, M. Mantsinen, C. Michaut and S. Weber, editors, *Europhysics Conference Abstracts – 45th EPS Conference on Plasma Physics*, volume 42A, page P1.2019. European Physical Society, 2018. ISBN 979-10-96389-08-7.

[116] MFEM: Modular finite element methods library. `<https://mfem.org>`. doi: 10.11578/dc.20171025.1248.

[117] E. Livne and A. Glasner. A Finite Difference Scheme for the Heat Conduction Equation. *Journal of Computational Physics*, 66(1):59–66, 1985. ISSN 00219991. doi:10.1016/0021-9991(85)90156-1.

[118] V. Dobrev, T. Kolev and R. Rieben. High-order curvilinear finite element methods for lagrangian hydrodynamics. *SIAM Journal on Scientific Computing*, 34(5):B606–B641, 2012. doi:10.1137/120864672.

[119] E. Caramana, D. Burton, M. Shashkov and P. Whalen. The Construction of Compatible Hydrodynamics Algorithms Utilizing Conservation of Total Energy. *Journal of Computational Physics*, 146(1):227–262, 1998. doi:10.1006/jcph.1998.6029.

[120] M. Kuchařík. *Arbitrary Lagrangian-Eulerian (ALE) Methods in Plasma Physics*. Doctoral thesis, FJFI ČVUT v Praze, 2006.

[121] R. Liska and M. Kuchařík. Arbitrary Lagrangian Eulerian method for compressible plasma simulations. In J. Donea, A. Huerta, J.-P. Ponthot and A. Rodríguez-Ferran, editors, *Proceedings of Equadiff 11*, pages 213–222. 2007.

[122] F. Brezzi and M. Fortin. *Mixed and Hybrid Finite Element Method*. Springer, New York, 1991.

[123] P. Lesaint and P. A. Raviart. On a Finite Element Method for Solving the Neutron Transport Equation. *Mathematical aspects of finite elements in partial differential equations*, 33:89–123, 1974.

[124] M. Kuchařík, J. Limpouch, R. Liska and J. Nikl. Hydrodynamic simulations of laser/plasma interactions via ALE methods. In *Europhysics Conference Abstracts – 46th EPS Conference on Plasma Physics*, volume 43C, page P5.2009. European Physical Society, 2019. ISBN 979-10-96389-11-7.

[125] J. A. Stamper, E. A. McLean and B. H. Ripin. Studies of spontaneous magnetic fields in laser-produced plasmas by Faraday rotation. *Physical Review Letters*, 40(18):1177–1181, 1978. doi:10.1103/PhysRevLett.40.1177.

[126] I. V. Igumenshchev, A. B. Zylstra, C. K. Li, P. M. Nilson, V. N. Goncharov and R. D. Petrasso. Self-generated magnetic fields in direct-drive implosion experiments. *Physics of Plasmas*, 21(6):062707, 2014. doi:10.1063/1.4883226.

[127] E. M. Epperlein and R. W. Short. Nonlocal electron transport in the presence of high-intensity laser irradiation. *Physical Review E*, 50(2):1697–1699, 1994. doi:10.1103/PhysRevE.50.1697.

[128] A. Marocchino, M. Tzoufras, S. Atzeni, A. Schiavi, P. D. Nicolaï, J. Mallet, V. Tikhonchuk and J.-L. Feugeas. Comparison for non-local hydrodynamic thermal conduction models. *Physics of Plasmas*, 20(2):022702, 2013. doi:10.1063/1.4789878.

[129] J. Nikl, M. Kuchařík and S. Weber. Modelling of the non-local transport of energy in laser plasmas with high-order numerical methods. In *Europhysics Conference Abstracts – 46th EPS Conference on Plasma Physics*, volume 43C, page P5.2010. European Physical Society, 2019. ISBN 979-10-96389-11-7.

[130] J. Nikl, I. Göthel, M. Kuchařík, S. Weber and M. Bussmann. Implicit reduced Vlasov–Fokker–Planck–Maxwell model based on high-order mixed elements. *Journal of Computational Physics*, 2020. Submitted.

[131] A. G. R. Thomas, R. J. Kingham and C. P. Ridgers. Rapid self-magnetization of laser speckles in plasmas by nonlinear anisotropic instability. *New Journal of Physics*, 11(3):033001, 2009. doi:10.1088/1367-2630/11/3/033001.

[132] R. Kingham and A. Bell. An implicit Vlasov–Fokker–Planck code to model nonlocal electron transport in 2-D with magnetic fields. *Journal of Computational Physics*, 194(1):1–34, 2004. doi:10.1016/j.jcp.2003.08.017.

[133] M. Shashkov and S. Steinberg. Solving Diffusion Equations with Rough Coefficients in Rough Grids. *Journal of Computational Physics*, 129(2):383–405, 1996. doi:10.1006/jcph.1996.0257.

[134] M. Gittings, R. Weaver, M. Clover, T. Betlach, N. Byrne, R. Coker, E. Dendy, R. Hueckstaedt, K. New, W. R. Oakes, D. Ranta and R. Stefan. The RAGE radiation-hydrodynamic code. *Computational Science & Discovery*, 1:015005, 2008. doi:10.1088/1749-4699/08/015005.

[135] J. Sanz, R. Betti, V. A. Smalyuk, M. Olazabal-Loume, V. Drean, V. Tikhonchuk, X. Ribeyre and J. Feugeas. Radiation hydrodynamic theory of double ablation fronts in direct-drive inertial confinement fusion. *Physics of Plasmas*, 16(8), 2009. doi:10.1063/1.3202697.

[136] P. S. Epstein. Reflection of waves in an inhomogeneous absorbing medium. *Proceedings of the National Academy of Sciences of the United States of America*, 16(10):627, 1930.

[137] J. Limpouch, V. Tikhonchuk, J. Dostal, R. Dudzak, M. Krupka, N. Borisenko, J. Nikl, A. Akunets, L. Borisenko and V. Pimenov. Characterization of the homogenization time of a plasma created by laser ionization of a low-density foam. *Plasma Physics and Controlled Fusion*, 62(3):035013, 2020. doi:10.1088/1361-6587/ab6b4d.